



5-2008

Novel Approaches to Prepare and Utilize SERS Substrates: Multiplex Microfluidics and Nanotransfer Printing

Nahla A. Abu-Hatab

University of Tennessee - Knoxville

Recommended Citation

Abu-Hatab, Nahla A., "Novel Approaches to Prepare and Utilize SERS Substrates: Multiplex Microfluidics and Nanotransfer Printing." PhD diss., University of Tennessee, 2008.
https://trace.tennessee.edu/utk_graddiss/322

This Dissertation is brought to you for free and open access by the Graduate School at Trace: Tennessee Research and Creative Exchange. It has been accepted for inclusion in Doctoral Dissertations by an authorized administrator of Trace: Tennessee Research and Creative Exchange. For more information, please contact trace@utk.edu.

To the Graduate Council:

I am submitting herewith a dissertation written by Nahla A. Abu-Hatab entitled "Novel Approaches to Prepare and Utilize SERS Substrates: Multiplex Microfluidics and Nanotransfer Printing." I have examined the final electronic copy of this dissertation for form and content and recommend that it be accepted in partial fulfillment of the requirements for the degree of Doctor of Philosophy, with a major in Chemistry.

Michael J. Sepaniak, Major Professor

We have read this dissertation and recommend its acceptance:

Ziling (Ben) Xue, Jimmy Mays, Elizabeth Howell

Accepted for the Council:

Dixie L. Thompson

Vice Provost and Dean of the Graduate School

(Original signatures are on file with official student records.)

**Novel Approaches to Prepare and Utilize Surface-
Enhanced Raman Spectroscopy (SERS) Substrates:
Multiplex Microfluidics and Nanotransfer Printing**

A Dissertation
Presented for the
Doctor of Philosophy
Degree
The University of Tennessee, Knoxville

Nahla Ahmad Abu-Hatab
May 2008

DEDICATION

This dissertation is dedicated to the soul of my mother,

Jamila A. Awadallah

Who was instrumental to my success my entire life and who devoted all
her life to my father, brothers, sister, and me

And to

My father, my two brothers, and my sister

Who supported and gave me the power to finish this work.

ACKNOWLEDGEMENTS

I want to take this opportunity to express my most sincere respect and gratitude to all the people who helped to make this work possible. First, I am incredibly thankful to God by whom all things are made possible. He is the only one who gives me the strength, power, hope, and guidance all the times. Secondly, I am indebted and thankful to my research advisor, Dr. Michael J. Sepaniak. Dr. Sepaniak has guided me through my graduate studies and I can't thank him enough, for not only accepting me when I decided to switch groups, but for supporting me during my mother's sickness and subsequent death. I wish to thank him for his professionalism, patience, wisdom, support, and encouragement throughout all the difficult research times. He taught me to think creatively and improve my problem-solving skills. It has been an honor to be part of your research group

Thirdly, I want to thank my family, without them I would be lost. They always challenged me to do my best, and any portion of my success can be directly attributed to their positive influence. They have always been there for me, and I cannot thank them enough. I thank my mother for it was she who was always available to me, gave me courage, taught me how to persevere, and provided me with valuable insights and inspiration. Mother was behind me all the time and until the last minute of her life. I ask God to reward her for being the perfect example of a mother. I want to thank my father for his strength, love and support. My sincere gratitude goes to my brothers, Dr. Mazen and Dr. Moeen, and my sister Ezdehar for their continuous encouragement, love and financial

support which made it possible to finish my undergraduate and graduate studies. I would also like to thank my two sisters' in-law Clair and Raya and my brother in-law Jamil. Special thanks go to my nephews Ahmad, Malik, Moneer, Anees, Mohand and my nieces Manar, Jamila, and Salma for putting a smile on my face during stressful times.

Fourthly, I also wish to express my most sincere gratitude to the past Sepaniak group members Marco de Jesús, Dr. Pampa Dutta, Kathleen Giesfeldt, Amber Wellman for their assistance and advice. In addition, I wish to express my gratitude for the current group members, Kasey Hill, Peter Chapman, Matthew Walworth, Jenny Oran, Joe Long, Deepak Bhandari, Dr. Maggie Connatser, and Dr. Mel Eldridge from CEB for all their friendship, suggestions and for making this experience a more enjoyable one. I would like also to thank Khaled Mriziq, Fabrice Gritti, and Tarab Ahmad for their moral support.

Thanks to the Chemistry Department's staff for their support and unconditional help during these years of study. Also I would like to express my acknowledgment, appreciation and respect to Tim Free for his amazing mechanical talent and input. I am very grateful to the electronics shop staff, specifically Bill Gurley, Johnny Jones, and Gary Wynn, for all their endless computer and electronics support. I also thank Dr. Jonh Dunlap and Greg Jones for their help with the AFM and SEM instruments.

I would also like to thank my professors and committee members for their comments, suggestions, guidance and instruction over the years.

Finally, I would also like to acknowledge Drs. Fred Schell, Jeffery D. Kovac, and Charles S. Feigerle for their guidance during my graduate experience at UT.

ABSTRACT

Over the past few decades, surface enhanced Raman spectroscopy (SERS) has garnered respect as an analytical technique with significant chemical and biological applications. SERS is important for the life sciences because it can provide trace level detection and a high level of molecular structure information. The development of quantitative, highly sensitive substrates requires control over size, shape, and position of metal nanoparticles which function as the SERS active medium. Thus, creating and successfully implementing a sensitive, reproducible, and robust SERS active substrate continues to be a challenging task. Its future development depends critically on techniques for lithography and nanofabrication. Herein, we report a novel method for SERS that is based upon using colloidal silver nanoparticles in a multiplexed microfluidics (MMFs) platform. The MMF is created in polydimethylsiloxane (PDMS) polymer material and used to perform parallel, high throughput, and sensitive detection/identification of single or various analytes under easily manipulated conditions. A facile passive pumping method is used to deliver samples into the channels under flowing conditions that are highly conducive for SERS measurements.

Also an unconventional nanofabrication approach is modified to produce efficient SERS substrates. Metallic nanopatterns of silver discs are transferred from a stamp onto PDMS to create nanocomposite substrates with regular periodic morphologies. The stamp with periodic arrays of square, triangular, and

elliptical pillars is created via Electron Beam Lithography of ma-N 2403 resist. A modified cyclodextrin is thermally evaporated on the stamp to overcome the adhesive nature of the ebeam resist and to function as a releasing layer. Subsequently, the stamp is over coated with Ag by physical vapor deposition at a controlled rate and thickness and used *directly* for nanotransfer printing (nTP). Stamps, substrates, and the efficiency of the nTP process were explored by SEM. Ag nano-disc-PDMS substrates are studied by SERS using Rhodamine 6G as the probe analyte. The SERS response of metallic nano-discs of various shapes/sizes on the original stamp is compared to the corresponding nTP substrates. We demonstrate that physical manipulation of the PDMS post nTP can be used to alter morphology. Additionally, stamps are shown to be reusable after the nTP process.

TABLE OF CONTENTS

Chapter	Page
1. Introduction to Surface Enhanced Raman Spectroscopy and Microfluidics: History, Principles, Substrates, and Instrumentation.....	1
1.1 The Discovery of the Raman Effect.....	1
1.2 Theoretical Basis for Raman Scattering.....	2
1.3 Raman instrumentation Design.....	8
Radiation Source.....	12
Sample System.....	13
Charged Coupled Devices (CCDs).....	14
Holographic Optics.....	15
Raman Microscope Instrument.....	16
1.4 Surface Enhanced Raman Spectroscopy: Background and Theory...18	
SERS Physical Picture.....	19
An Overview of SERS Substrates.....	24
1.5 An Overview of Microfluidics.....	28
1.6 Statement of the Problem	32
2. Multiplex Microfluidic-Surface Enhanced Raman Scattering	34
2.1 Introduction.....	34
2.2 Experimental.....	38
Surface Enhanced Raman Spectroscopy.....	38
Instrumentation for Colloid Characterization.....	40

Preparation of Ag Colloid and Ag Cubic Nanoparticles.....	41
Reproducibility, Irradiation Time, and Microscope objective Studies...	42
Anion Studies.....	42
pH Studies.....	43
Calibration Studies.....	43
2.3 Results and Discussion.....	43
General Performance Studies.....	44
Multiplex Performance & Optimization Studies.....	48
Multiplex Performance for Quantitative & Qualitative Studies.....	53
3. Introduction to Nanofabrication Methods and Attempted Approaches to Nanotransfer Printing.....	57
3.1 Introduction.....	57
3.2 Overview of Photolithography and Electron Beam Lithography.....	58
3.3 Overview of Unconventional Nanofabrication Methods.....	62
Hard Molds or Stamps.....	62
Soft Molds or Stamps.....	63
Step-and-Flash Imprinting Lithography (SFIL).....	63
Nanoimprint Lithography (NIL).....	66
3.4 Nanofabrication by Printing.....	68
Introduction.....	68
Nanotransfer Printing.....	69
3.5 Attempted Approaches for <i>Direct</i> Nanotransfer Printing (nTP) to Create Substrates for SERS.....	72

Introduction.....	72
Experimental.....	76
Preparation of Stamps.....	76
Preparation of SERS Substrates.....	78
Results and Discussion.....	79
Initial Results for Macro-Transfer Printing.....	80
Initial Results for Nanotransfer Printing.....	82
Initial Approaches to Control Pressure for nTP.....	84
Initial Approaches to Overcome the Adhesive Nature of the Resist..	89
4. SERS Substrates Created Via Electron Beam Lithography	
and Nanotransfer Printing	115
4.1 Introduction.....	115
4.2 Experimental.....	118
Surface Enhanced Raman Spectroscopy Instrumentation.....	118
Preparation of the Stamp Substrates.....	119
Preparation of SERS Substrate.....	120
Sample Preparation.....	121
Data Acquisition and Analysis.....	122
4.3 Results and Discussion.....	122
Description of the Technique.....	122
Optimization and Performance.....	123
SERS Response and the Comparison Studies.....	130
5. Concluding Remarks.....	139

References	144
Vita	165

LIST OF TABLES

Table		Page
3.1	Resolution of Conventional and Unconventional Nanofabrication Techniques.....	73
4.1	EBL-created patterns and dimensions.....	125

LIST OF FIGURES

Figure		Page
1.1	Numbers of publications involving Raman, resonance Raman spectroscopy and surface enhanced Raman spectroscopy by decade.....	3
1.2	Schematic energy level diagram describing Rayleigh scattering, Stoke and anti-Stoke Raman spectroscopy. E is the energy of the photon, h is the Plank's Constant, ν is the frequency, and ΔE is the difference in energy for the vibration.....	4
1.3	Schematic energy level diagram describing RRS and Fluorescence....	9
1.4	Comparison of Rhodamine 6G spectra by fluorescence (top) and Raman (bottom) spectroscopy.....	10
1.5	Schematic of confocal Raman microscope.....	17
1.6	A) Schematic diagram of the SERS effect where molecules are in close proximity to metal nanoparticles. B) Illustation of metallic nanoparticles and the generation of LSPR and the electromagnetic field enhancement around the metallic nanoparticles.....	21
1.7	(A-C) Examples of Microfluidic systems that have been developed in Soper group for collecting certain cells from from mixed population. (D) An example of commercially available MF (from Dolomite website).....	32
2.1	Schematic representation of the instrument apparatus used for MMF-SERS.....	39
2.2	Spectral profiles of 1×10^{-7} M solution of crystal violet in Ag colloids as a function of microscope objective. Each bar represents the area of the 1175 cm^{-1} band of crystal violet as a function of objective and average velocities.....	45
2.3	Spectral profiles of 1×10^{-4} M 4-ABA in Ag colloids as a function of irradiation time with a laser power of 4.5 mW.....	47
2.4	Reproducibility of the MMF-SERS signal of a 1.0×10^{-6} M crystal violet in Ag colloids in each of the microfluidic channels (overall N = 20).....	49

2.5	(A) Change in the SERS spectra of 1×10^{-4} M 4-ABA in Ag colloids upon the addition of different anions (1×10^{-2} M) to Ag colloids. (B) Influence of pH changes on the SERS spectra of caffeine.....	50
2.6	(A) Optical extinction curves of Ag nanocubic colloids with their scanning electron micrographs. (B) Representative SERS spectra of 5×10^{-6} crystal violet using different Ag cubic nanoparticles obtained via MMF-SERS. The weight percent of nanocubes is approximately 0.2 %.....	52
2.7	(A) Working curves of crystal violet and (B) mitoxantrone using MMF-SERS and passive pumping ($-R = \text{HO}-(\text{CH})_2-\text{NH}-(\text{CH})_2$). The spectra are for 5×10^{-9} M crystal violet and 1×10^{-12} M mitoxantrone.....	54
2.8	MMF-SERS spectra of pesticides at different pH; (A) Dinoseb, (B) Dithianon, and (C) Monuron.....	56
3.1	Schematic illustration of the fabrication of patterns by conventional methods: photolithography and Electron Beam Lithography.....	59
3.2	Schematic illustration for the steps of fabrication by Step-and-Flash Imprinting Lithography.....	65
3.3	Schematic illustration of steps for Nanoimprinting Lithography.....	67
3.4	Schematic illustration for steps to fabricate patterns by Nanotransfer printing.....	70
3.5	(Top) White light illumination of the original mask with dimension of squares being $200 \mu\text{m} \times 200 \mu\text{m}$. The bottom is the white light illumination of the macro-Ag pillars transferred onto PDMS.....	81
3.6	White light illumination of 35 nm Ag disc transferred from SU-8 stamp onto PDMS substrate. Ag disc is roughly $480 \mu\text{m} \times 480 \mu\text{m}$	82
3.7	(a) Scanning electron micrographs illustrating the PDMS substrate and the resist stamp after the nTP process using Ag.....	84
3.7	(b) Scanning electron micrographs illustrating the PDMS substrate and the resist stamp after the nTP process using Ag.....	85
3.8	Scanning electron micrographs of: A) 15 nm transferred Au onto PDMS B) Shows 25 nm Au transferred onto PDMS C) Shows the resist stamp after the transferring process.....	87

3.9	White light illumination showing: (Top) The mask covering the patterns. (Bottom) Shows the patterns after depositing 60 nm Ag and removing the mask.....	88
3.10	(Top) Shows the white light illumination of the stamp after depositing Cal[4] and before the transfer process. (Middle) shows SEM image of stamp after the transfer process. (Bottom) Shows SEM image of PMDS after nTP.....	90
3.11	(Top) Shows white light illumination of the stamp (200nm Ag was deposited as a ledge) after the transferring process, where there is no indication of silver on the discs was transferred. (Bottom) Shows white light illumination image of the PDMS substrate without any indication that Ag nano discs are being transferre.....	91
3.12	A) Shows chemical structure of methacrylate (ma-N2403) resist. The top white light illumination image shows the resist stamp on macroscale before the transfer process. Middle image shows the stamp after the transfer process and the Al layer can be seen. The bottom image shows Ag disc on PDMS substrate with small amount of Al being transferred at the same time.....	93
3.13	(a) Scanning Electron Micrographs of the stamp and the PDMS substrate. Here, 15-20nm Al was used to cover ma-N2403 resist. The left column shows the PDMS substrate and the right column shows the resist stamp.....	95
3.13	(b) Scanning Electron Micrographs of the stamp and the PDMS substrate. Here, 15-20nm Al was used to cover ma-N2403 resist. The left column shows the PDMS substrate and the right column shows the resist stamp.....	96
3.14	SEM micrographs of: (a) the negative ma-N2403-EBL stamp with square wells being created instead of discs. (b) the first nanotransfer trail with this stamp. This small area is where the Ag nano-discs were transferred onto the PDMS substrate.....	97
3.15	(a) SEM micrographs of PDMS substrate shows that some discs were transferred but not sufficient for SERS application (b) SEM micrographs of EBL stamp of ma-N2403 resist after developing the patterns.....	98
3.16	SEM micrographs of a nTP trial results with EBL nano-wells stamp. Left column shows PDMS substrate after the nTP process, using 10 nm Al to cover the traces of resist. Right column shows the EBL nano-wells stamp.....	100

- 3.17** (A) SEM micrographs of HSQ resist stamp that was exposed to 1100 $\mu\text{m}/\text{cm}^2$ EBL dose. (B) SEM micrographs of PDMS substrate exhibits a continuous transfer of Ag film 102
- 3.18** Atomic Force Microscopy (AFM) image of HSQ resist EBL stamp. Exposure dose was 1100 $\mu\text{C}/\text{cm}^2$. (Top) Shows an area of 2.5 μm X 2.5 μm that was mapped. Middle shows a three dimensional AFM image for the pattern. Bottom shows the height of the discs which was approximately 20 nm..... 103
- 3.19** AFM image of HSQ resist EBL stamp. Exposure dose was 1600 $\mu\text{C}/\text{cm}^2$. (Top) Shows an area of 2.5 μm X 2.5 μm that was mapped. (Bottom) Shows the height of pillars which is approximately 10 nm..... 105
- 3.20** AFM image of HSQ resist stamp. Exposure dose was 700 $\mu\text{C}/\text{cm}^2$ and the height of the pillars is approximately 15-20 nm..... 106
- 3.21** (Top) AFM image of HSQ resist stamp. Exposure dose was 100 $\mu\text{C}/\text{cm}^2$ and the height of the pillars is approximately 60 nm. (Bottom) The exposure dose was 150 $\mu\text{C}/\text{cm}^2$ and the thickness is approximately 80nm..... 107
- 3.22** (Top) AFM image of HSQ resist stamp. Exposure dose was 200 $\mu\text{C}/\text{cm}^2$ and the height of the pillars is approximately 80 nm. (Bottom) The exposure dose was 250 $\mu\text{C}/\text{cm}^2$ and the thickness is approximately 50nm.....108
- 3.23** AFM image of HSQ resist stamp. Exposure dose was 500 $\mu\text{C}/\text{cm}^2$ and the height of the pillars was approximately 30 nm..... 109
- 3.24** (Top) Shows SEM images of HSQ resist pattern where the exposure dose was 150 $\mu\text{C}/\text{cm}^2$ and the height of the pillars is approximately 80 nm. (Bottom) Shows SEM image of PDMS substrate after the nanotransfer process and without any discs being transferred..... 111
- 3.25** SEM micrographs image of PDMS substrate after the nTP trial. Ellipses, 100x250 nm in size were transferred from ma-N2403 stamp that was coated first with 50nm H-B-CD followed by 40nm Ag..... 113
- 3.26** (Top) Shows the SEM images of PDMS substrate after the nTP trial with the usage of H-B-CD to cover the adhesive resist. Squares, 100 nm- 500 nm in size were transferred to the PDMS substrate. (Bottom) Shows SERS spectrum of 1×10^{-5} M Rhodamine 6G..... 114

4.1	Schematic illustration of procedures for using nTP to fabricate nano-disc SERS substrates.....	124
4.2	Scanning electron micrographs of the E63_1 pattern (A) nano-disc arrays transferred from a stamp under optimal conditions; 50 nm H-β-CD followed by 50 nm Ag and (B-D) nano-disc arrays transferred from a stamp under non optimal conditions; (B) 50nm Cal-4 followed by 50 nm Ag, (C) 20 nm H-β-CD followed by 50nm Ag, (D) 50 nm H-β-CD followed by 20 nm Ag.....	127
4.3	Scanning electron micrographs of a 50 nm H-β-CD followed by 50 nm thick Ag evaporated on the stamp (left column), stamp after nTP (middle column), and PDMS substrates showing integrity of the nanotransfer printing (right column).....	129
4.4	Scanning electron micrographs of the (A) S200_1 nano-disc arrays transferred from a stamp and after being stretched. The arrow denotes the stretching direction.....	131
4.5	Comparison of R6G (1×10^{-6} M) SERS spectra for E63_1 pattern from a stamp (50 nm Ag discs) (black) and upon nTP of the nano-disc array onto PDMS (red).....	133
4.6	Comparison of the 767 cm^{-1} band area SERS signal of R6G (1×10^{-6} M) for stamp and nTP substrate as a function of the geometric pattern.....	134
4.7	SERS spectra of R6G (1×10^{-6} M) using the same nano-disc nTP stamp onto three different PDMS substrates	136
4.8	Spectra of crystal violet (A) and Mitoxantrone (B) at 10^{-8} M and 10^{-9} M, respectively.....	138

ABBREVIATIONS AND SYMBOLS

AFM	Atomic Force Microscopy
$A(\nu)$	field enhancement factor
4-ABA	4-Aminobenzoic acid
α	molecular polarizability constant
α_0	the polarizability of the bond of a molecule at equilibrium
Cal-4	4- <i>tert</i> -Butylcalix[n]arene
CCD	charged coupled devices
CV	crystal violet
ϵ_m	the dielectric constant of the metal composing the sphere.
ϵ_0	the dielectric constant of the local environment around the sphere.
E	magnitude of the incident electromagnetic field
E_0	amplitude of the electromagnetic wave (electric portion)
EBL	Electron Beam Lithography
E_1	energy of the first state
E_2	energy of the second state
EG	ethylene glycol
EDCs	endocrine disrupting chemicals
H- β -CD	Heptakis(6- <i>O-tert</i> -butyldimethylsilyl-2,3-di- <i>O</i> -acetyl)- β -CD
HSQ	Hydrogen silsesquioxane
IR	infrared spectroscopy
k	Boltzmann's constant
LOC	lab-on-a-chip
LSPR	localized surface Plasmon resonance
MF	microfluidic
MMFs	Multiplexed Microfluidics
μ CP	Microcontact Printing
3-MPTMS	(3-Mercaptopropyl)trimethoxysilane

μ	electric dipole moment
N_1	number of molecules in the lower energy state
N_2	number of molecule in the excited state
NA	numerical apertures
NIL	Nanoimprint Lithography
nTP	Nanotransfer printing
ν_0	frequency of the incident laser beam
t	time
PDMS	Polydimethylsiloxane
PVP	poly(vinyl pyrrolidone)
PMMA	Poly(methyl methacrylate)
PVD	Physical Vapor Deposition
QCM	quartz-crystal microbalance
r	bond length at any instant
r_{eq}	equilibrium bond length
r_{max}	maximum separation distance between atoms relative to their equilibrium position
RIE	Reactive Ion etching
RF	radio frequency
RRS	Resonance Raman Scattering
R6G	Rhodamine 6G
SERS	Surface enhanced Raman spectroscopy
SFIL	Step-and-Flash Imprinting Lithography
SAM	self-assembled monolayer
SEM	Scanning Electron Microscope
T	Temperature (kelvin)
ν_j	vibrational frequency

CHAPTER 1

Introduction to Surface Enhanced Raman Spectroscopy and

Microfluidics:

History, Principles, Substrates, and Instrumentation

1.1 The Discovery of the Raman Effect

It was the inquisitiveness of Lord Rayleigh about the color of the sky that led him to generate a classical theory of light scattering without change in frequency (Rayleigh 1871). Then in 1922, after observing the color of the sky and the Mediterranean Sea, Chandrasek Venkata Raman showed experimentally that the color of the sea resulted from intrinsic light scattering by water molecules. Raman and his student, Krishnan, continued to study a number of liquid, organic vapor, gases, and some crystal solids. Their observation and what is known as the Raman effect were reported and published in *Nature* in 1928 [1].

Since then, Raman spectroscopy has ascended through several stages. In the early stages, mercury arc was used as an excitation source and spectra were collected over very long periods of time to achieve reasonable signal intensities. In the 1960s, Raman Spectroscopy took another step forward as a result of the development of lasers as an intense monochromatic light source. The application of Raman spectroscopy in real practical chemical analysis started around 1985 with the advent of Fourier transform(FT)-Raman, charge-

coupled devices, small computers, and visible and near-infrared lasers [2-4]. Figure 1.1 shows the number of publications involving Raman spectroscopy by decade [5]. As one can see, the dramatic increase in number of publications in the last ten years implies that Raman spectroscopy is developing quickly into a routine spectroscopic technique for many applications.

1.2 Theoretical Basis for Raman Scattering

When monochromatic light of certain energy interacts with sample (gas, solid, or liquid), most of the light from the incident photons is scattered elastically with no change in the frequency (Rayleigh scattering). However, a small fraction of the incident photons are scattered inelastically (Raman scattering) toward either lower frequencies (Stokes scattering) or higher frequencies (anti-Stokes scattering) [3]. Figure 1.2 shows the schematic energy level diagram for Rayleigh, Stokes and anti-Stokes Raman scattering.

Classical electromagnetic theory can sufficiently explain the molecular polarization that occurs with Raman scattering. The incident light contains both an oscillating electric and magnetic field, though it is the interaction of the electric field with the electron cloud that produces an electric dipole moment (μ) and a net polarization of the molecule [6]. The strength of the dipole moment is given by:

$$\mu = \alpha E \quad (\text{Eq. 1.1})$$

Where:

α = molecular polarizability constant

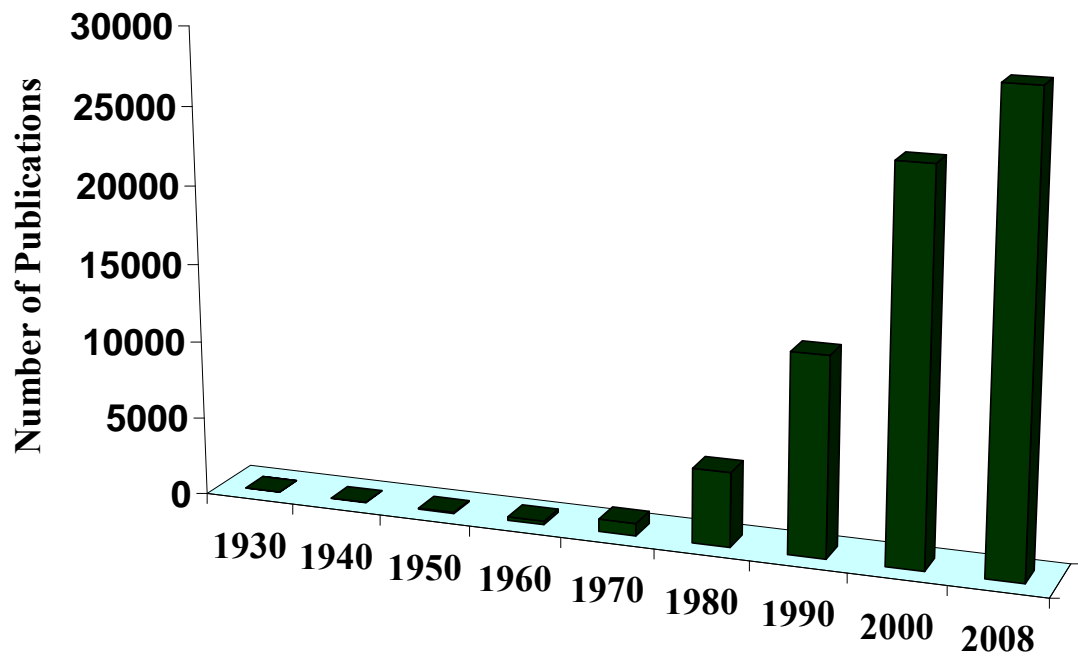


Figure 1.1 Numbers of publications involving Raman, resonance Raman spectroscopy and surface enhanced Raman spectroscopy by decade.

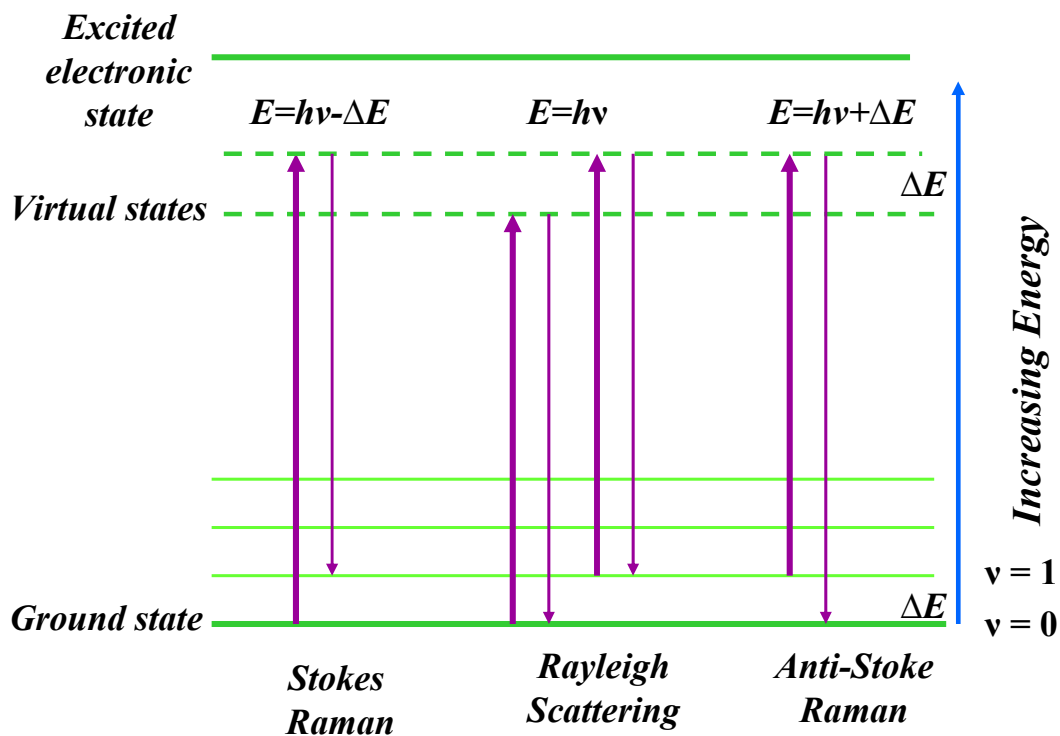


Figure 1.2 Schematic energy level diagram describing Rayleigh scattering, Stokes and anti-Stokes Raman spectroscopy. E is the energy of the photon, h is Planck's constant, ν is the frequency, and ΔE is the difference in energy for the vibration.

E = magnitude of the incident electromagnetic field

The virtual states shown in Figure 1.2 are not true quantum states but they can be explained as being a very short lived distortion of the electron clouds of the molecule caused by the oscillating electric field of the light.

The classical description of Raman spectroscopy is based on equation 1.1 and the incident electromagnetic field (E) that surrounds the analyte is governed by Equation 1.2:

$$E = E_0 \cos(2\pi\nu_0 t) \quad (\text{Eq. 1.2})$$

Where:

E = magnitude of the electromagnetic field

E_0 = amplitude of the electromagnetic wave (electric portion)

ν_0 = frequency of the incident laser beam

t = time

The relationship between the induced dipole moment and the incident electromagnetic field is formed by combining Equations 1.1 and 1.2:

$$\mu = \alpha E_0 \cos(2\pi\nu_0 t) \quad (\text{Eq. 1.3})$$

However, the polarizability changes with molecular vibration motion according to Equation 1.4.

$$\alpha = \alpha_0 + (r - r_{eq}) \left(\frac{\partial \alpha}{\partial r} \right) \quad (\text{Eq. 1.4})$$

Where:

α_0 = the polarizability of the bond of a molecule at equilibrium

r = bond length at any instant

r_{eq} = equilibrium bond length

The difference between bond length and equilibrium bond length varies as a function of vibrational frequency (ν_j) as follow:

$$r - r_{eq} = r_{max} \cos(2\pi\nu_j t) \quad (\text{Eq.1.5})$$

Where r_{max} is the maximum separation distance between atoms relative to their equilibrium position. Substituting Equation 1.5 into 1.4 will yield:

$$\alpha = \alpha_0 + \left(\frac{\partial\alpha}{\partial r}\right)r_{max} \cos(2\pi\nu_j t) \quad (\text{Eq.1.6})$$

Substituting Equation 1.6 into Equation 1.3 will give:

$$\mu = \alpha_0 E_0 \cos(2\pi\nu_0 t) + E_0 r_{max} \left(\frac{\partial\alpha}{\partial r}\right) \cos(2\pi\nu_j t) \cos(2\pi\nu_0 t) \quad (\text{Eq.1.7})$$

By using the trigonometric identity $\cos a \cos b = [\cos (a+b) + \cos (a-b)]/2$,

Equation 1.7 can be expressed as follow:

$$\mu = \alpha_0 E_0 \cos(2\pi\nu_0 t) + \frac{E_0}{2} r_{max} \left(\frac{\partial\alpha}{\partial r}\right) \cos[2\pi(\nu_0 - \nu_j)t] + \frac{E_0}{2} r_{max} \left(\frac{\partial\alpha}{\partial r}\right) \cos[2\pi(\nu_0 + \nu_j)t]$$

(Rayleigh)

(Stokes)

(Anti-Stokes)

(Eq.1.8)

This Equation demonstrates that light will be scattered at three different frequencies. The first term is the Rayleigh scattering which occurs at the same frequency of the laser and has a magnitude proportional to the α_0 , the polarizability of the molecule. The second and third terms refer to the Stokes Raman scattering and Anti-Stokes Raman Scattering, respectively. Further

examination of Equation 1.8 yields certain useful insights such as the linear behavior of the Rayleigh and Raman scattering intensities with laser intensity and the importance of molecular selection rules; a vibration will be Raman active only if the polarizability changes during molecular vibrational motion. Another result of Equation 1.8 is the fact that the Raman energy shift can be both positive and negative. The intensity of the anti-Stokes Raman depends on the population of the first vibrational excited state whose temperature dependence is described by the Boltzmann's distribution (Eq. 1.9):

$$N_1 / N_2 = e^{\frac{(E_2 - E_1)}{kT}} = e^{\frac{h\nu}{kT}} \quad (\text{Eq.1.9})$$

Where:

N_1 = number of molecules in the lower energy state

N_2 = number of molecule in the excited state

E_1 = energy of the first state

E_2 = energy of the second state

k = Boltzmann's constant

T = Temperature (Kelvin)

Based on Equation 1.9, the population of the lowest vibrational state at room temperature is much greater than the excited vibrational states. Quantum mechanical analysis of the Raman effect shows that the intensity-ratio of the Stoke and the anti-Stokes bands is a function of Boltzmann's distribution (Eq.1.10).

$$\frac{I_{anti-Stokes}}{I_{Stokes}} = \frac{(v_0 + v_j)^4}{(v_0 - v_j)^4} e^{-\left(\frac{hv_j}{kT}\right)} \quad (\text{Eq.1.10})$$

This equation also shows that the intensity of the Stokes Raman bands is much greater than the anti-Stokes Raman bands. Nevertheless, Raman scattering is a very weak effect since it suffers from extremely small cross section, typically 10^{-30} - 10^{-28} cm²/molecule, indicating that at least 10^8 molecules are required to generate Raman signal [7]. The need for a large sample size can be alleviated by Resonance Raman Scattering (RRS) [8-10]. RRS occurs when the excitation laser wavelength is coincident (or near coincident) with an electronic absorption band of the analyte molecules; as a result the analyte molecule is excited to a higher electronic vibrational state and immediately returns to one of the vibrational level of the electronic ground state by emission of Stokes Raman photon as shown in Figure 1.3. RRS can lead to a 10^2 - 10^8 enhancement in the Raman signal compared with the non-resonant case.

RRS is closely related to fluorescence, since both phenomena are caused by the absorption of a photon. However, the lifetime for both phenomena is different. In fluorescence, the molecule is promoted to any vibrational level during electronic excitation process, and then it relaxes first to the vibrational ground state of S_1 via internal conversion and vibrational relaxation. Afterwards, the molecule emit fluorescent photon as it returns to any of the vibrational levels of the electronic ground state [11], as seen in Figure 1.3. The lifetime of fluorescence is on the order of nanoseconds. RRS, on the other hand, occurs immediately when the molecule relaxes without any radiation-less decay to the

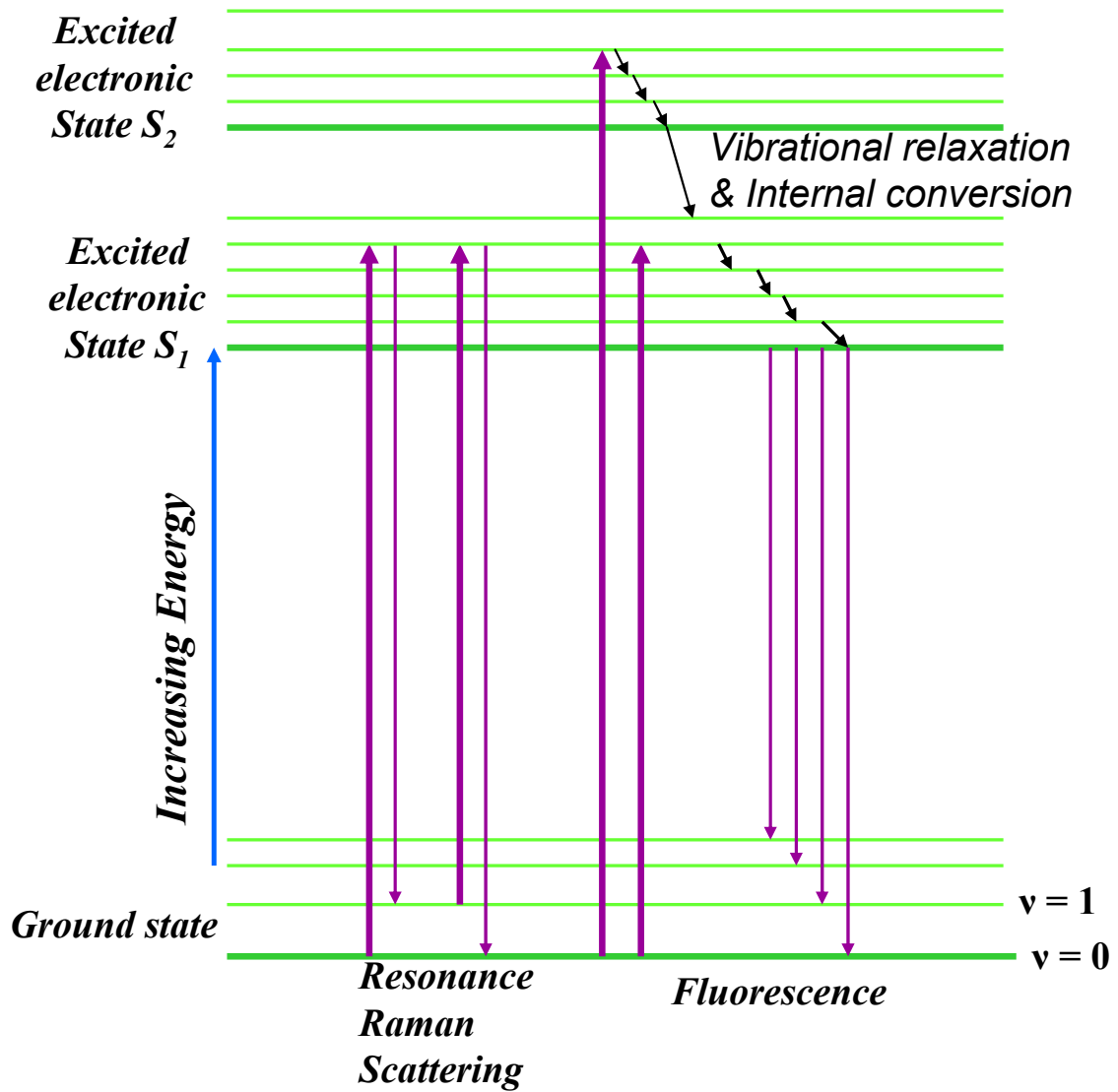


Figure 1.3 Schematic energy level diagram describing RRS and Fluorescence.

vibrational levels of the electronic ground state. As a result, interference from fluorescence is often a problem with RRS. The shapes of the fluorescence spectra of analytes are usually broad-banded and poorly structured, whereas in Raman and RRS, the bands are sharp, well defined with fingerprint properties. Figure 1.4 represents a comparison of Rhodamine 6G spectra measured by fluorescence and Raman spectroscopy. The fluorescence background can easily overwhelm the RRS spectrum and can be amplified further if the analyte or sample contains trace amounts of fluorophores. Therefore, suppression of fluorescence is the main concern in RRS.

1.3 Raman Instrumentation Design

Raman spectroscopy suffers from the low intensity of inelastic scattering and the high intensity of Rayleigh scattering. This has placed several restrictions on the improvement of Raman Spectroscopy and the development of effective instrumentation. In the early experiment, Raman and Krishnan used strong sunlight to provide a powerful beam of radiation. This beam passed through an initial filter to produce a monochromatic beam that in turn passed into a liquid benzene sample. The weak inelastic scattering was detected and separated from the intense elastic scattering by placing a second optical filter before the scattered light struck the detector. Initially, detector was the human eye and later it was replaced by photosensitive plate [12].

Most of the early research was focused on improving the radiation sources, with one of the biggest developments being the invention of sufficiently

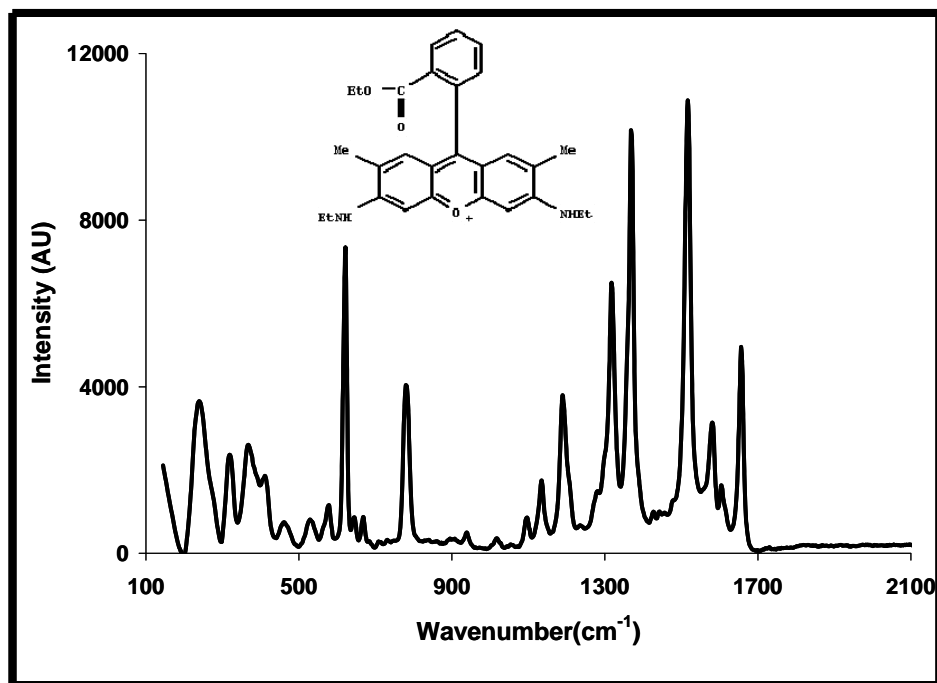
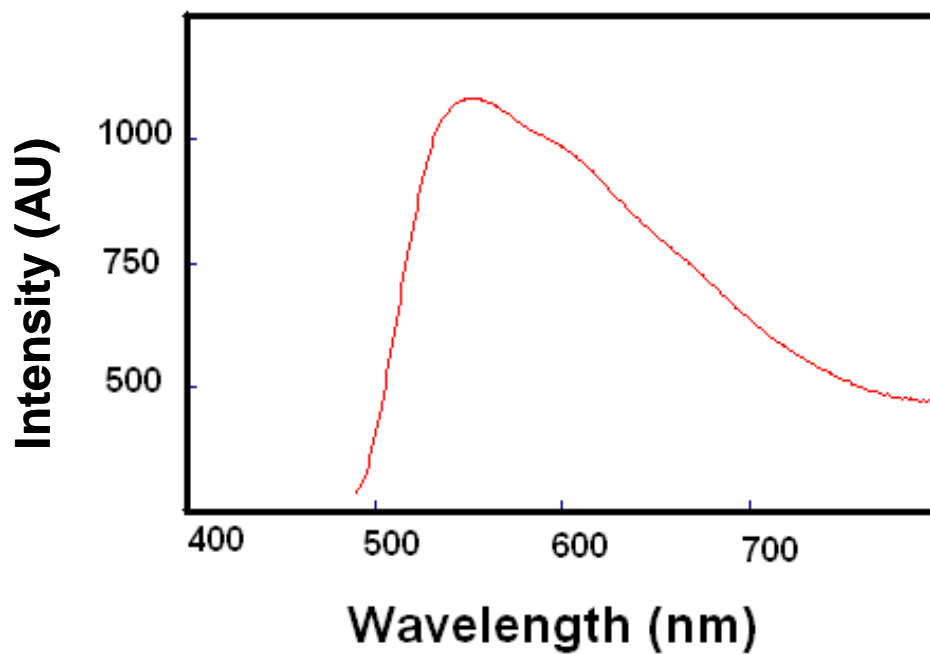


Figure 1.4 Comparison of Rhodamine 6G spectra by fluorescence (top) and Raman (bottom) spectroscopy.

intense and monochromatic optical sources in the 1960s. The introduction of the laser provided a major break through not only for its intensity, but also for the narrowly collimated beam that was easy to focus into sampling optics. However, difficulty in eliminating the intense Rayleigh signal at the detector still remained, until the relatively recent availability of holographic notch filters, multiple-stage monochromators or spectrograph. These were necessary to separate the Raman signal from the intense laser signal. Lasers are also capable for focusing onto very small samples, thereby, minimizing the amount of time required to obtain excellent spectra from materials in short supply.

Over the last forty-five years, there has been substantial progress in designing lasers that are more efficient, more stable, and more durable. Problems and interference from fluorescence background, photodecomposition of analytes encountered in many samples measured by Raman spectroscopy can be eliminated with the availability of variable laser wavelengths from the visible to the infrared region.

As mentioned previously, Raman spectroscopy has always had complications due to the intense level of Rayleigh scattering. Initially, the solution was to fit the monochromator with two or three dispersion stages to reduce the high level of elastic scattering. By 1940, the double monochromator was incorporated into spectrophotometer and commercially available on the market. The recent advances in technology (over the last 15 years) have resulted in the development of high efficiency holographic notch filters capable of removing over 99.5% of the laser background line. High quality photomultiplier tubes were

universally used as the detector of choice until the advent of array detectors in 1990. Instrument configurations were first modified by using the photodiode array and later the highly sensitive charged coupled devices (CCD) detectors. These silicon detectors arrays, with up to 80% quantum efficiency, superseded the sensitive photomultipliers. They also enabled improved signal processing techniques to be employed for spectral analysis. The following section provides a summary of each of the major components of a Raman instrument.

Radiation Sources: Lasers started to be the excitation sources for Raman spectrometers in the 1960's, since lasers provided intense, stable radiation in the appropriate spectral region for Raman. Raman spectrometers generally employed lasers such as Argon ion (488 and 514.5 nm), Krypton ion (530.9 and 647.1 nm), Helium/Neon (632.8 nm), diode (782 and 830 nm), and Nd/Yag (1064 nm). Until the late 1980's, most of the Raman spectrometers were used with Argon and Krypton ion due to that fact that Raman scattering intensity varies as the fourth power of the laser frequency and both lasers are lower wavelength sources. The wavelengths for these sources are in the visible region and, in fact, the Argon and Krypton sources can generate Raman responses that are three times more intense than other sources, such as Helium/ Neon laser (at the same electrical power rating). The only drawback with these lasers is that the use of higher energy radiation may result in higher fluorescence emission by the analytes and sometimes promote photodecomposition as well [13]. Starting in the late 1980's and early 1990's, radiation sources that emit near the infrared such as diode and Nd/YAG lasers have been more frequently used as excitation

sources. Those lasers do not have enough energy to cause analyte fluorescence emission and do not cause analyte or sample matrix photodecomposition or thermal damage (which is a big concern when working with biologically sensitive samples, polymers or other photolytically sensitive materials) [6]. Other aspects evolving Raman systems compensate for the lower Raman intensity at the longer excitation wavelengths.

Sample System: Sample preparations for Raman spectroscopy are much simpler than those for infrared spectroscopy (IR). Any small size (micrometer scale) of solid or liquid material can be easily probed with very basic preparation. In addition, any cell-window material such as glass and quartz can be used for liquid and gaseous samples. There are also many other cells that can be used, such as fiber optics and capillary tubes. A major advantage for sample system in Raman spectroscopy is the fact that water exhibits very weak Raman scattering (water is almost present in all biological samples). This allows for direct analysis of aqueous samples with minimum background interferences and is especially advantageous for biological samples; consequently, Raman spectroscopy is a more appropriate technique than IR [6].

Charged Coupled Devices (CCDs): Since the mid 1980s, CCDs had been the most commonly used detectors in Raman systems, since they are rugged, stable, and reliable. A CCD two –dimensional array is comprised of a large number of small individual square silicon photosites (elements or pixels) on a single chip. Each pixel has two conductive electrodes separated by a thin insulating layer of silica that isolates them from the n-doped silicon substrate and

each pixel surrounded by a non-conductive barrier. This array of electrodes provides local potential wells below the surface and attracts the electrons generated as a result of the incoming Raman photons. The potential at these electrodes can be controlled and used to shift the photogenerated electrons along the chip and allow them to be counted. When the acquisition is completed, the number of electrons generated in each pixel or data can be recorded via the control electronics and computer to give a Raman spectrum [12]. CCDs are characterized by having the ability to simultaneously collect the entire spectrum, low noise, and high quantum efficiency. CCDs have the additional multi-channel advantages of simultaneous and rapid measurement of a substantial portion of the Raman spectrum (on average $\sim 1000\text{ cm}^{-1}$ wide).

Holographic Optics: There are several holographic optics or wavelength selectors that the laser line passes through. The laser line passes through a narrow line band pass filter to remove all unwanted laser lines. These filters are present at both the absorption and interference stages: absorption filters (used since the early stages of Raman spectroscopy) absorb all unwanted laser lines and transmit specific laser lines of interest, while interference, or laser line filters, reject the unwanted laser lines/wavelengths and transmit the desired bands of laser wavelengths in the visible, NIR, and mid-IR regions. A pinhole spatial filter is then used to improve the spatial properties of the laser beam.

Another filter used is the holographic notch filters which are made by creating a volume phase hologram within the matrix of a photosensitive gelatin: two coherent laser beams record a periodic interference pattern in the gelatin

thereby producing an approximate sinusoidal variation in the refractive index throughout the thickness of the polymer. The period of this spatial modulation is selected such that the unwanted laser wavelength is partially reflected by successive modulations in the refractive index. The efficiency of transmission depends on the number of modulations (i.e. the thickness of the film) and the uniformity of the modulation spacing [6].

Raman Microscope Instrument: Figure 1.5 shows a schematic of the JY Horiba LabRam instrument, the confocal Raman microscope system used in the work presented here. This system contains an optical microscope with five-position nosepiece that allows several objectives to be incorporated (each objective has its numerical aperture (NA), magnification, and focal length). A major advantage of this system is the presence of a CCD video camera, where the white light source and the Raman mapping images can be compared. The laser source for this instrument is a Helium/Neon (He/Ne 632.8 nm) with a power output less than or equal to 9 mW. The laser beam passes through a narrow band pass filter to reject the unwanted laser lines. The power of the laser beam is regulated by using neutral density filter, after which it then passes through a pinhole spatial filter to improve the spatial properties of the laser beam. The laser beam then passes through holographic notch filter where the beam will be redirected to the microscope objective. The microscope objective will cause the beam to be focused into very small spot at the sample and will increase the power density of the beam, thereby increasing the intensity and the spatial resolution at the sample. The light returning from the sample (comprised of both

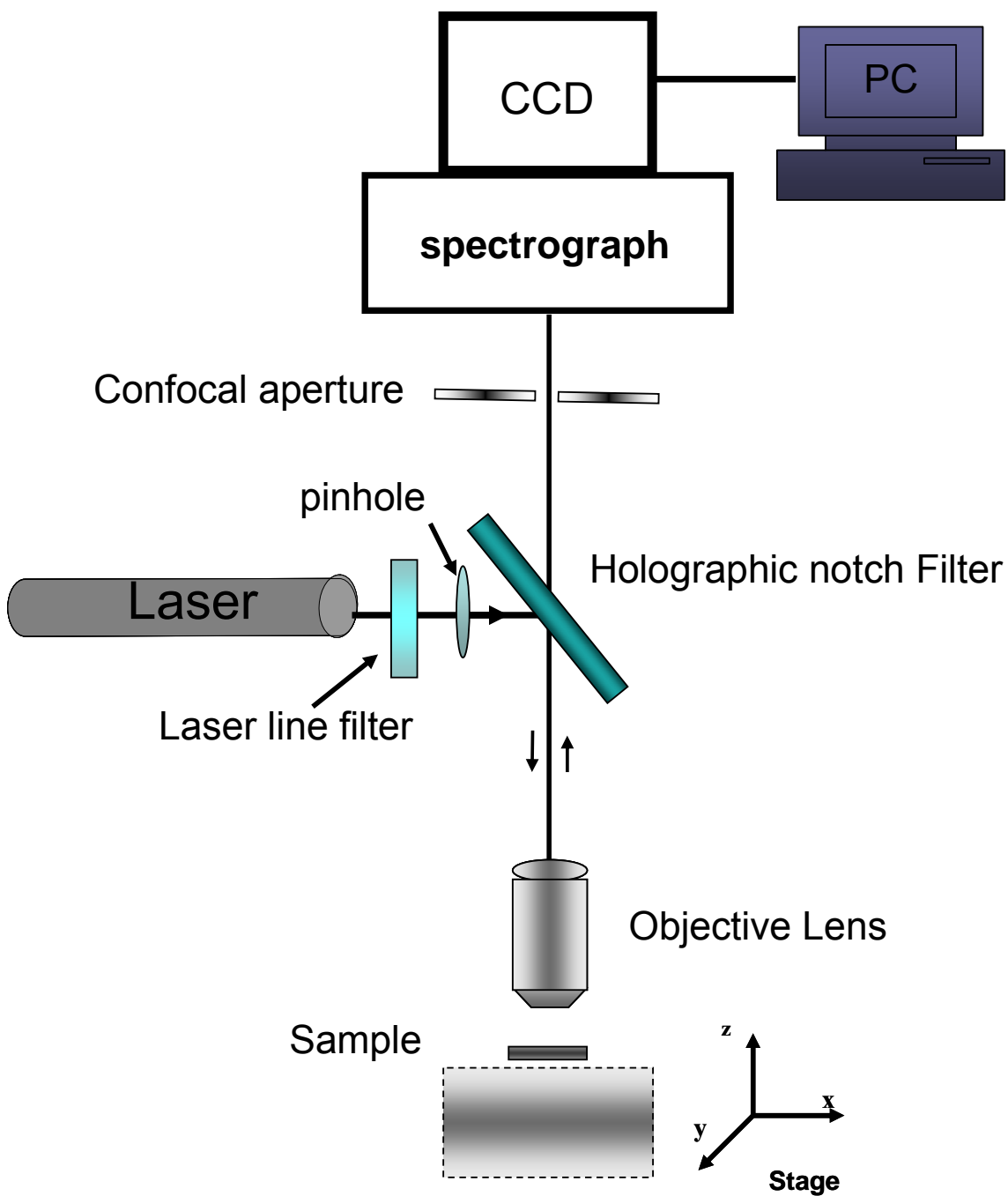


Figure 1.5 Schematic of confocal Raman microscope.

Raman and Rayleigh scattering light) is collected by the objective in a 180° backscattering geometry. Typically, one uses microscope objectives with large numerical apertures (NA) to increase the intensity of the Raman signals, since NA is a measure of light collection ability as discussed in 2.3.

The light then passes again through the holographic filter to remove the Rayleigh scattering. The Raman scattering photons are dispersed by high throughput single-stage spectrograph and redirected to the CCD and the data is processed by the software to display the corresponding Raman spectrum. Raman microscopy is characterized by being high sensitive and data can produce high resolution Raman spectra of a sample [14].

1.4 Surface Enhanced Raman Spectroscopy, Background and Theory

Surface enhanced Raman spectroscopy SERS was discovered in 1974, when Fleischmann et al. observed unexpectedly intense Raman signal from pyridine sub-monolayers on roughened (Ag) electrode [15]. Then in 1977, Jeanmaire et al. demonstrated that the increase in Raman scattering intensity of up to 10^5 - 10^6 orders of magnitude was due to the surface properties of roughened electrode [16]. When the localized surface Plasmon resonance of nanoscale roughness features on a noble-metal substrate such as silver, gold, or copper is excited by the photons in the visible light spectrum, strong local electric fields are generated [17]; if an adsorbed Raman scattering molecule is subjected to these intensified electromagnetic fields, the magnitude of the inelastic scattering increases [18-20].

Since this discovery, SERS has progressed from being from simple system studies of pyridine on roughed Ag electrode to a spectroscopy surface method with practical sensor applications [21-27]. The technique proved to be not only effective for sensitive and selective molecular identification, but also a tool for ultrasensitive trace detection. This is due to the high effective SERS cross section 10^{-18} cm²/molecule which allows for detectable Raman signal from just a few molecules. In the thirty-three years since the discovery of SERS, the spectroscopy technique has developed to be the state-of-art for surface science and nanotechnology [22,28-30]. The development of nanotechnology and nanofabrication methods, spectroscopic instrumentation, theoretical modeling has increased the interest in using SERS as a potential effective analytical tool [18,31,32].

SERS Physical Picture: The mechanism of SERS enhancement remains or continues to be an active and interesting research topic. However, two major mechanisms are proposed and accepted widely: charge transfer or chemical enhancement and electromagnetic enhancement [33-37]. Over the years, it was proven that SERS is not so much a “surface effect” but instead a “nanostructure effect” [35]. Since particle absorption and scattering depends on the size, shape, type of noble metal nanoscale roughness features, SERS intensities and specifically electromagnetic mechanism are influenced by these factors. This is because these characteristics determine the resonant frequency of the conduction electrons in the metallic nanostructure. Figure 1.6 shows a schematic representation of the SERS effect and the interaction between the nano-metal

particles and the analyte. When the incident light irradiates the metallic nanostructure, it excites the conduction electrons of the metal into collective oscillation, and results in localized surface Plasmon resonance (LSPR). Excitation of the LSPR will result in the generation of large electromagnetic field at the surface of the nanometallic roughness feature [18-20,38,39]. Extensive theoretical modeling has been done by Hinde, Kahl, Van duyne, Kneipp, and Schatz and others to provide an insight into electromagnetic enhancement by noble-metal nanoparticles [34,35,40-52]. The physical deposition process, roughed electrodes surfaces, and colloidal solution preparations create randomly spaced and sized nanoparticles in a statistically determined wide distribution of sizes and shapes. In most of these models, surface morphology has been simplified to an isolated and simple-shaped nanostructure. The simplest example is a single isolated nanosphere, where the effective electric field E at the surface of a sphere is given by:

$$E^2 = E_0^2 \left| \frac{\epsilon_m - \epsilon_0}{\epsilon_m - 2\epsilon_0} \right|^2 \quad (\text{Eq.1.10})$$

Where:

E_0 = the incident field magnitude

ϵ_m = the dielectric constant of the metal composing the sphere.

ϵ_0 = the dielectric constant of the local environment around the sphere.

This indicates that when the wavelength dependent dielectric constants have the relationship $\epsilon_m = -2\epsilon_0$, the most intense surface plasmon resonance

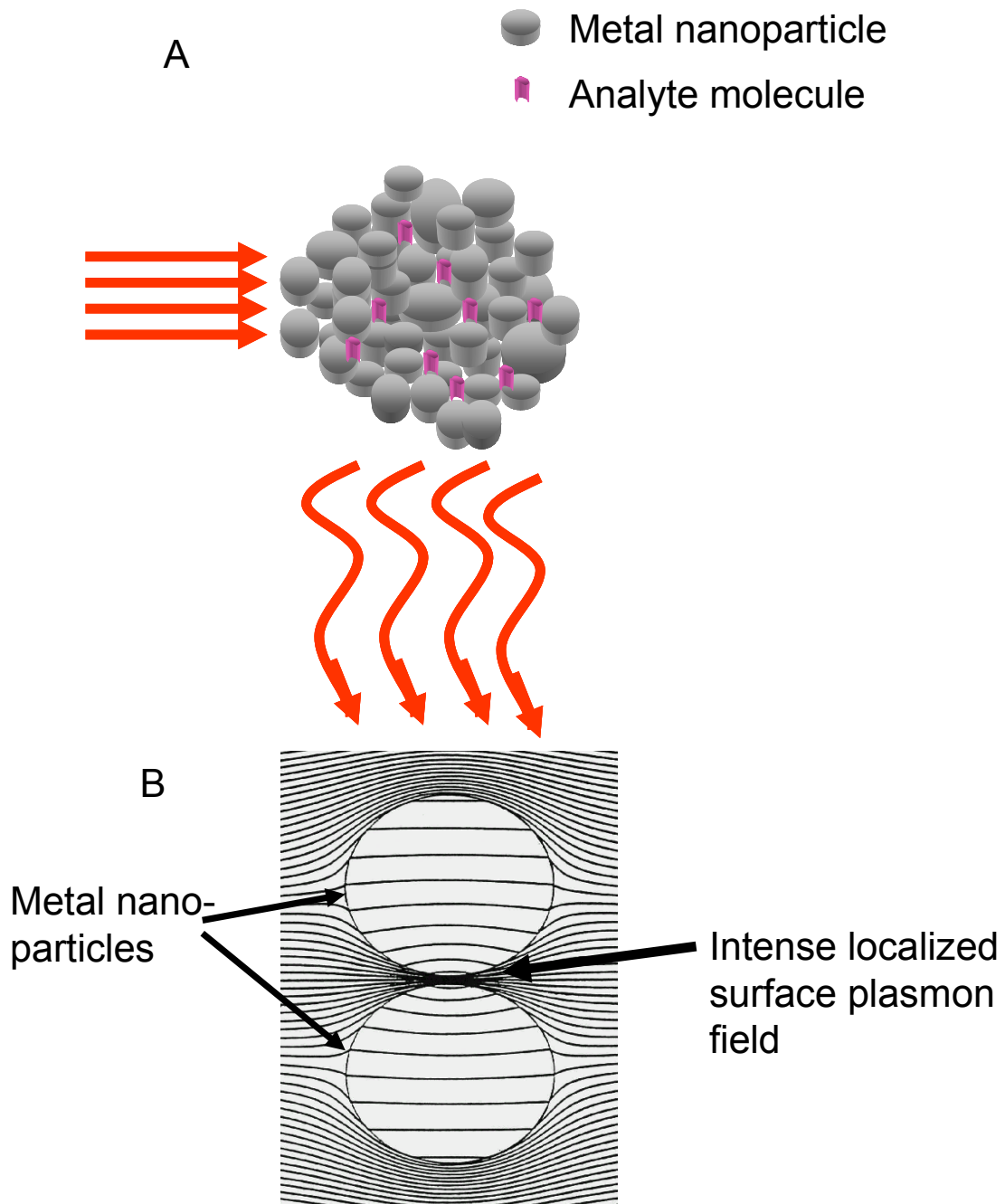


Figure 1.6 A) Schematic diagram of the SERS effect where molecules are in close proximity to metal nanoparticles. B) Illustration of metallic nanoparticles and the generation of LSPR and the electromagnetic field enhancement around the metallic nanoparticles.

occurs and the magnitude of the electric field at the surface of the sphere becomes very large. The interaction of light with the metallic nanosphere depends on the value of the complex dielectric function, and thus the type of metal play an important role. Metal such as silver and gold can achieve the above conditions at certain wavelengths in the visible and near-IR [18,34,48]. Silver is used in the present work, because it is the most efficient SERS metal due to its dielectric properties. The excitation of the nanospheres is strongly influenced by the dielectric constant of the environment surrounding the sphere.

When the analyte molecule is brought close to the surface of the metal nanosphere, it experienced a field E_M which is the superposition of the incoming incident field and the field induced at the surface of the nanosphere(LSPR). The field enhancement factor $A(\nu)$ is the ratio of the field at the position of the molecules and the incoming field as given by:

$$A(\nu) = \frac{E_M(\nu)}{E_0(\nu)} \approx \frac{\epsilon_m - \epsilon_0}{\epsilon_m + 2\epsilon_0} \left(\frac{r}{r+d}\right)^3 \quad (\text{Eq.1.11})$$

Where:

r = radii of the metal nanoparticles

d = distance from the molecule to the surface of the metal nanoparticle

The enhancement factor for the electromagnetic mechanism is on the order of 10^6 - 10^7 ; therefore, the electromagnetic enhancement mechanism is largely responsible for the enhancement of Raman scattering [49]. Theory and modeling studies predict stronger enhancement factor up to 10^{11} for sharp features and particles separated by gap of 1 nm (hot sites) [50-52]. Theoretical

predictions also indicate that dimer pairs of metal particles can produce exponentially increased fields between them, illustrating the importance of particle spacing [53-55]. In order to exploit such long range effects in both the substrates available now and those developed in the future, one must find methods to favorably position analyte molecules within locations of highest enhancement [56]. Electromagnetic SERS enhancement does not require contact between Raman active molecule and metal, but it strongly decreases as $1/r^3$ from the surface.

In addition to the electromagnetic enhancement which focuses on the E-term in Eq.1.1, the chemical mechanism, also known as the “first-layer effect” is thought to contribute an average enhancement factor of $10-10^2$. This mechanism depends on the chemical nature of the molecule and selectivity of the molecule in terms of its interaction with the enhancing metal nanostructure, its spatial orientation and polarization properties [33,34,48,57]. It is referred to as the “first layer effect” since it requires direct contact between molecule and metal and the molecule must be chemisorbed on the metal substrate; clearly, this effect is limited to the first layer of adsorbed molecules. The presence of the metal nanostructure permits specific interactions between the metal and adsorbate molecules. As a result, an adsorbate-surface complex is formed and the Raman cross section of the adsorbed molecule is increased. These interactions also increase the possibility of a charge transfer transition from the highest occupied molecular orbital (HOMO) of the adsorbate molecule to the Fermi level of the metal nanostructure or it can cause a charge transfer from the Fermi level of the

metal nanostructure to the lowest unoccupied molecular orbital of the adsorbate molecules. Since this process is site-specific, the molecule must be directly adsorbed to the roughened noble metal surface to experience this mechanism; the “first layer effect”, however, is analyte dependent.

An Overview of SERS Substrates: SERS is becoming an accepted analytical technique. However, the main challenge to its application in quantitative analysis is the lack of a reliable and reproducible SERS substrate and technique. Researchers have been focusing on developing techniques to prolong SERS substrate lifetime, provide stable and optimized enhancement factors, and permit SERS studies in diverse environments [58,59].

There are variety of SERS substrates available today, with the most common SERS substrates being those with the desired experimental and optical properties; those substrates include (but are not limited to) electrochemically roughened electrodes, metal island films, colloidal nanoparticles, and surface confined nanostructures. Silver electrode was the first substrate to exhibit the SERS enhancement by Fleischmann et al [15]. SERS active Ag electrodes substrates are prepared by roughening the Ag electrode by the oxidation-reduction cycle in an electrochemical cell containing an appropriate solution of a silver salts. Silver and gold electrode substrates were exploited in the initial SERS studies and they have the advantage of adjusting the electrode potential, allowing one to study charge transfer phenomena between the analyte molecule and the metal surface and molecular orientation at the surface.

Metal island films prepared by vacuum deposition have a long and extensive research history for their optical properties [60-65]. They are easy to fabricate, high in purity and LSPR wavelength can be tuned by varying the film's thickness (mass thickness of 5-20nm is usually used for SERS substrates) [60], deposition rates, temperature of the substrate during deposition, and substrate roughness [60]. Continuous and discontinuous metal film substrates can be prepared, where continuous film is prepared by depositing on different materials: continuous film is prepared by depositing on quartz, glass, poly(dimethylsiloxane) (PDMS) [61-65], while discontinuous metal film is prepared by depositing on coated dielectric nanoparticles such as silica particles. Discontinuous metal films hold an advantage over continuous films, since one can control the particle size and optical properties.

The process of physical vapor deposition involves evaporation of the metal to be deposited or to be transported to the substrate. This can be accomplished by heating or by using an energetic beam of electron, photons, or positive ions under high vacuum conditions. The deposition rate is a critical parameter for SERS substrates, since it influences the film properties [61,66]. The contamination of the thermal evaporation source and the deposition system are also issues to be considered in the evaporation and deposition processes. Controlling all the above parameters is necessary to produce a thin metal film with reproducible properties. Metal island films are among the most reproducible substrates for SERS application and Ag vapor deposited substrates exhibits more stability over time [67].

Colloidal conventional nanoparticle substrates are easy to prepare and do not need complicated instrumentation for fabrication and are well suited to solution-phase SERS studies; colloidal nanoparticles substrates are also used for single-molecule SERS experiments [68-72]. The most commonly used SERS substrates are clusters of colloidal silver and gold particles in the 10-80 nm size range [73]. There are a large number of methods for the preparation of colloidal nanostructures with different shapes for SERS and their preparation continued to be very active field of research [68,74-80].

The colloidal substrates are prepared by either chemical reduction process or by laser ablation procedures. In the chemical reduction process, a starting metal salt is reduced by a chemical agent to produce colloidal suspensions with nanoparticles of variable size (depending on the method of production) [81]. The distribution of sizes and shapes can be partially controlled by controlling parameters in the preparation method such as the reducing reagent, the temperature, the stabilizing agents and the metal ion concentration [77]. A common problem with the metal colloids is the surface contaminants from the reducing agents that are sometimes reduced by the addition of inorganic salts such as sodium chloride. Sodium chloride will also promote the aggregation of colloidal particles and reduce the background in SERS signal [73,82-86]. Metal colloids are also prepared by laser ablation procedure which involves irradiating a cleaned metal film, immersed in deionized water in a quartz cell, with a laser beam with certain parameters. With this method, chemically clean colloidal surfaces can be obtained [87]. The size of the colloidal particles

produced by this method is roughly 20 nm and the size distribution is broad and asymmetric [77,88].

The most interesting SERS substrates are the surface confined nanostructures which can be produced by numerous fabrication methods, including nanosphere lithography [20,56,89-91], and electron beam lithography [92-97]. Nanosphere lithography begins with the self-assembly of size-monodisperse nanospheres of a certain size to form a two-dimensional colloidal crystal deposition mask. A metal is then deposited at specific rate and thickness and the nanosphere mask is removed, leaving behind surface confined triangles nanoparticles. These nanoparticles have been used to tune the absorption of nanostructure for maximum electromagnetic enhancement and SERS [31]. Producing surface confined nanostructures using Electron Beam Lithography (EBL) involves the exposure of a thin layer of a photoresist to high energy electrons, followed by the chemical development of this resist and the deposition of noble metals. EBL provides control over inter-particles spacing (to a limit) and can fabricate arbitrary shapes; this technique can then be used to explore the magnitude of enhancement factor as the inter-particle spacing is varied. Unfortunately, EBL is an expensive and slow serial form of lithography [31]. Metal feature size, shape and spacing have been controlled with these methods to allow detailed analysis of the optical properties of the nanoparticle arrays. In addition, the wavelength corresponding to the extinction maximum of the surface plasmon resonance of the particles arrays (fabricated by the nanofabrication methods) can be tuned.

1.5 An Overview of Microfluidics

Microfluidics technology, or “lab-on-a-chip (LOC)”, is a major modern theme in the chemical analysis and synthesis of molecules. It is based on the idea of using channels with the dimensions of tens to hundreds of micrometers to manipulate small amount of fluids [98,99] (these are also known as a micrometer-scale total analysis system, μ -TAS). The first applications of microfluidic (MF) technologies have been in chemical analysis, since they offer a number of useful capabilities such as the ability to have precise spatial control over samples and reagents, the ability to carry out separations and detections with high resolution and sensitivity, low cost, fast analysis time, small footprints for the analytical devices [100,101]. MF also exploits characteristics of fluids in microchannels, such as laminar flow and it offers fundamentally new capabilities in the control of concentrations of molecules in space and time.

The origin of MF lay in analytical methods such as gas-phase chromatography (GPC), high-pressure liquid chromatography (HPLC) and capillary electrophoresis (CE). By combining these methods with the power of the laser in optical detection, it is possible to simultaneously achieve high sensitivity and high resolution using very small amount of sample [102]. The success of these methods has encouraged the development of more compact format for microscale applications in biotechnology, chemical synthesis and analytical chemistry [103-107]. Another factor that stimulated the development of the MF methods was the advanced photolithography technologies that would be

directly applicable to microfluidics and permits flexibility of design. These technological advances have made it possible to build miniaturized devices with complex networks of channels, valves, pumps and other methods of fluidic encapsulation and manipulation.

MF can be manufactured from many different materials at relatively low cost. The earlier works involving microfluidics used silicon and glasses, but soon they were replaced by different types of elastomers, since they were more appropriate for many applications. For example, silicon is an expensive material and optical detection system cannot be used with it, since silicon is opaque to visible and UV light. Elastomers, in contrast, are relatively inexpensive and much easier to be fabricated into channels and have almost all the properties required for any system - even for biological samples and living mammalian cells [108]. MF systems also provide the capability of integrating a series of multiple tasks such as preparation, mixing, and separation in both serial and parallel schemes on a single LOC platform. Most of the research in MF has been carried out with PDMS polymer. Along with being relatively inexpensive, PDMS is a nontoxic, optically transparent, soft elastomer that is permeable to gases such as oxygen/carbon dioxide [109,110]; polycarbonate or polyolefin are examples of other polymers that have been used in microfluidic research [111,112].

MF systems should have at least three components: a method for introducing reagents and sample as fluids; a method for moving these fluids through the channel or around the chip and for combining/mixing these fluids; and a method for detection. The development of soft lithography allowed

researchers to use PDMS for fabricating prototype devices and to fabricate pneumatically activated valves, mixers, and pumps in relatively short times compared to silicon technology.

MF devices offer several analytical and operational advantages over many other conventional macroscale systems. Microfluidic systems are amenable to many different detection schemes and fluids flowing in microsystems have some useful characteristics such as electro-osmotic flow (EOF). When an ion-containing fluid such as water is placed in a PDMS or silicon dioxide microchannel and an electrical potential is applied along the channel, the fluid moves as a plug—effectively minimizing any broadening of a sample and yields a very high resolution separation of ionic species [99,105].

Microfluidic systems have been applied to many situations such as screening conditions for protein crystallization (such as pH, concentration, composition) [99], DNA microchip electrophoresis separation [113], separation coupled to mass spectroscopy [114,115], screening in drug discovery [104,116,117], bioanalyses studying and manipulating samples consisting of single cells or single molecules [118]. Along with being used for high-efficiency, two-dimensional chromatographic separations of tryptic protein digest [119], microfluidics have also been used to create a total cell analysis system for culturing, sorting, trapping, and lysing cells and separating the content of single mammalian cells [120]. Figure 1.7 shows examples of relatively sophisticated MFs that have been constructed in Soper's group to collect low-abundant cells from a mixed population [111,113,114,116]. Two additional examples of microfluidic

applications are complex metallic microstructures in three dimensions for building flexible electronic circuits¹⁰⁹ and multi-channels microfluidic chip electrophoresis devices [112]. The work presented here uses lab-on-a-chip technology to perform SERS analyses under flowing condition to yield more reproducible results.

1.6 Statement of the Problem

In the last thirty-three years, SERS has grown to be a promising technique. SERS has trace analytical capabilities which allows molecular identification down to the single molecule level in some cases. In addition, SERS is a method for detecting and identifying molecule without any labeling. However, the lack of reliable and reproducible substrates and approaches or techniques to perform SERS measurements has been, and continued to be a major hurdle in its wider use. This research will consider the application of a simple and fast technique for SERS measurements. It is based on multiplexed microfluidics system with a passive pumping method to optimize SERS response and the figures of merit. Through this approach, achieving high reproducible experimental conditions is possible. This method can be easily employed for different kinds of samples and can result in high sensitivity spectra with out damage to the samples.

Size, shape, proximity, and inter-particle spacing of Ag nanoparticles are all important factors that determine SERS electromagnetic enhancement. Theory

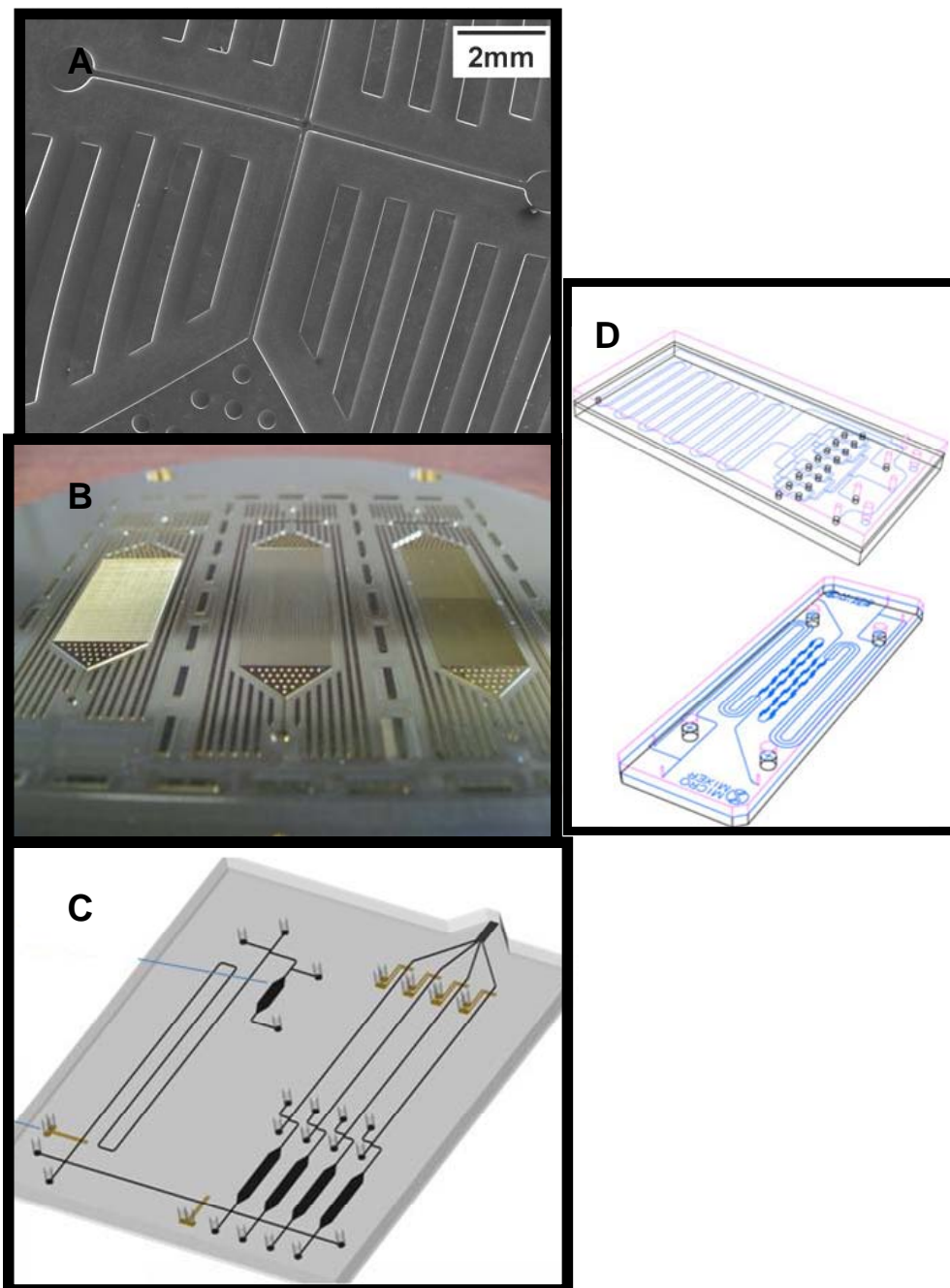


Figure 1.7 (A-C) Examples of Microfluidic systems that have been developed in Soper group for collecting certain cells from mixed population. (D) An example of commercially available MF (from Dolomite website).

and modeling studies have been extensively applied to examine the effect of spacing and gap on SERS electromagnetic enhancement factors. The lack of reliable techniques for controlling the properties of the local electrical field at the nanostructural metal surface has been a major experimental limitation in the quantification and understanding SERS.

With EBL, experimental studies are limited by resolution of electron beam and the resist. An unconventional nanofabrication technique with EBL is presented *herein to scale up the production of SERS substrates and improve cost effectiveness*. EBL-nanotransfer printing substrates may offer a means to design substrates so as to close the gap and produce substrate with high electromagnetic field across them – while Ag-nanodiscs transfers will permit the interrogation of the particles proximity by physical manipulation of PDMS.

CHAPTER 2

Multiplexed Microfluidic - Surface Enhanced Raman Spectroscopy

2.1 Introduction

Since the observation of Surface Enhanced Raman Spectroscopy (SERS) signal from pyridine adsorbed on a roughed Ag electrode [121], SERS has become a powerful analytical technique for chemical and biological sciences as it can provide selective structural information [122], chemical identification [123], as well as provide useful quantitative information by sensitive detection of polarizable molecules [90,124]. In special cases, there have been reports of Raman enhancement factors up to 10^{14} [7]. SERS potential for low detection limits, in combination with the capability of Raman spectroscopy to provide structural information, has made it a very promising to be applied in various experiments that include, but are not limited to: trace detection of pesticides [125], toxins [126], explosives [127], biomolecules [128,129], and nuclear waste [130], in some cases down to a single molecule level [7,57,131-134]. In the last fifteen years, there have been extensive research efforts to investigate and determine the source of enhancement seen in SERS. As discussed in section 1.4, two mechanisms for enhancement have been accepted widely; one is the chemical mechanism which is due to specific interactions or coupling effects between the active metal surface and adsorbate molecule and the other is an

electromagnetic mechanism that arises from the excitation of localized surface plasmon resonances (LSPRs) of metal nanoparticles by visible and near-IR light that constitute large Raman exciting electromagnetic fields near the metal surface [34]. SERS can be an effective surface-based analytical technique, however, it often suffers from poor reproducibility from experiment to experiment and a very limited dynamic range. SERS response or/and intensity depends on analyte intrinsic properties such as analyte polarizability, the effects of pH on the analyte, and its ability to compete with other sample components for the active metal surface. In addition there are analyte extrinsic properties that largely pertain to the effectiveness of the SERS substrate and instrumental factors. Several processes and methods have been proposed by various researchers to address the effects of these factors on SERS [135-144]. The instrumental approach or technique that we describe in this chapter is aimed at rapidly assessing these factors.

In Chapter 1, it was mentioned that MFs has emerged as a new technology for optics, biological analysis, and chemical synthesis and analysis [145]. MF technology is based on manipulating small amount of fluids in channels with width/depth dimensions of micrometers. As mentioned in section 1.5, MF technology enables the development of small, faster, more cost-effective, and more powerful instruments [145,146]. MF technology also permits the reduction in sample volume and reagent usage, improves control of fluid mixing and heating, gives the ability to run reaction and analysis faster, and gives an excellent reproducibility and consistency of results. Many MF devices are

made with the elastomer Polydimethylsiloxane (PDMS); a material that is easily molded, optically transparent, and exhibits low permeability to water [145-148]. All of the above-mentioned advantages for MF systems indicate that the technology will continue to be a major theme in analytical sciences.

Silver colloids have optical properties, including LSPRs, that depend on the colloidal nanoparticles size, shape, and aggregation state. Silver colloid solutions have been widely used for SERS due to several reasons, such as ease of preparation by different methods (see section 1.4), their stability, the convenience of characterizing the colloids by visible absorption spectroscopy, and a limited ability to control and vary the particle size and shape by the preparation methods [76]. Typically, when performing SERS experiments using Ag colloids, a large amount of colloid is used and spectra are collected under static (non-flowing) conditions where analyte is continually irradiated by the laser beam. This can promote the rapid decomposition or fragmentation of both the sample analyte and SERS substrate, altering the observed spectral bands (which may lead to a misinterpretation of the analytical data) and affecting the reproducibility of the observed signals [149]. In addition, thermal diffusion of colloid and associated analyte out of the illuminated region of the sample can contribute to poor reproducibility.

Lee *et al.* reported the use of a single MF channel for quantitative SERS detection. In their study, an alligator-teeth-shaped PDMS microfluidic channel was used for mixing analyte and colloids before detection [150,151]. Conversely, we are utilizing individually addressable Multiplexed Microfluidics (MMFs)

technique for high throughput qualitative and quantitative SERS studies. MMF-SERS technique will permit rapid parallel Raman analysis not only of multiple samples under one set of experimental conditions, but also a single test sample under variable experimental conditions to optimize these conditions. Our MMF-SERS devices are made out of PDMS and sealed to a glass slide surface. Each device has five parallel channels (many more channels are possible) which makes parallel SERS detection of separate/different samples or analytes possible. Samples colloidal substrates are passively pumped through the channels [152], which minimizes the effect of laser irradiation. This method of pumping utilizes the surface energy in a drop of liquid and two ports on the channel (reservoir port and pumping port). The large drop of sample is placed over the reservoir port of a sample filled channel while the small drop of sample is used to pump the sample through the channel. Passive pumping method only requires a device capable of delivering small drops such as a syringe or pipette. Therefore, this method is easy, efficient, and semi-autonomous.

In this chapter, we first discuss and demonstrate the general performance of MMF-SERS technique through several studies. We compare the performance of different microscope objectives in the instrument set-up, sample flow rate, and laser irradiation time. Next, we demonstrate the efficiency and applicability of the MMF-SERS approach by studying and reporting channel to channel spectral reproducibility, effect of different anions on the Ag colloid, and effect of pH on selective sorption of analyte to the colloids (as reflected in SERS signals). In

addition, Ag nanocube samples are synthesized with sizes ranging from approximately 45 nm to 120 nm and studied in the MMF-SERS system. Working curves of crystal violet and Mitoxantrone are obtained and reported with low LODs. Dinoseb, Dithianon, Monuron are three different pesticides that are studied and SERS spectra obtained at different pH values using the system.

2.2 Experimental

Surface Enhanced Raman Spectroscopy: A schematic of the instrumental set-up used for MMF-SERS is depicted in Figure 2.1. All SERS spectra were acquired using a LabRam Spectrometer from JY-Horiba. The instrumental arrangement has been described in detail in chapter 1 (section 1.3). In general, most experiments were performed using an Olympus ULWD MSPlan80X microscope objective with 80X (0.75 NA, ∞ , $f = 180$, WD 7.0mm) objective for the instrument, except for the study done to compare microscope objectives where three other objectives were used. In that study, the following objectives were used (1) Olympus BX-40 with a 10X (0.25 NA, ∞) objective, (2) Olympus LWD CDPlan 20X PL with a 20X (0.40 NA, ∞) objective, (3) Nikon 50X with a 50X (0.45 NA, ∞ , WD 13.8mm) objective. All microscope objectives deliver up to 9 mW of the 632.8 nm line from an electrically cooled He-Ne laser. The laser spot size in these studies ranged from approximately 5 to 25 μm when going from the 80X-to-10X objectives. All spectra were acquired in a 180° scattering geometry with a 2936 cm^{-1} spectral window centered at 1747 cm^{-1} . The scatter was dispersed with a 600 groove/mm grating, imaged with a 1024 x 256

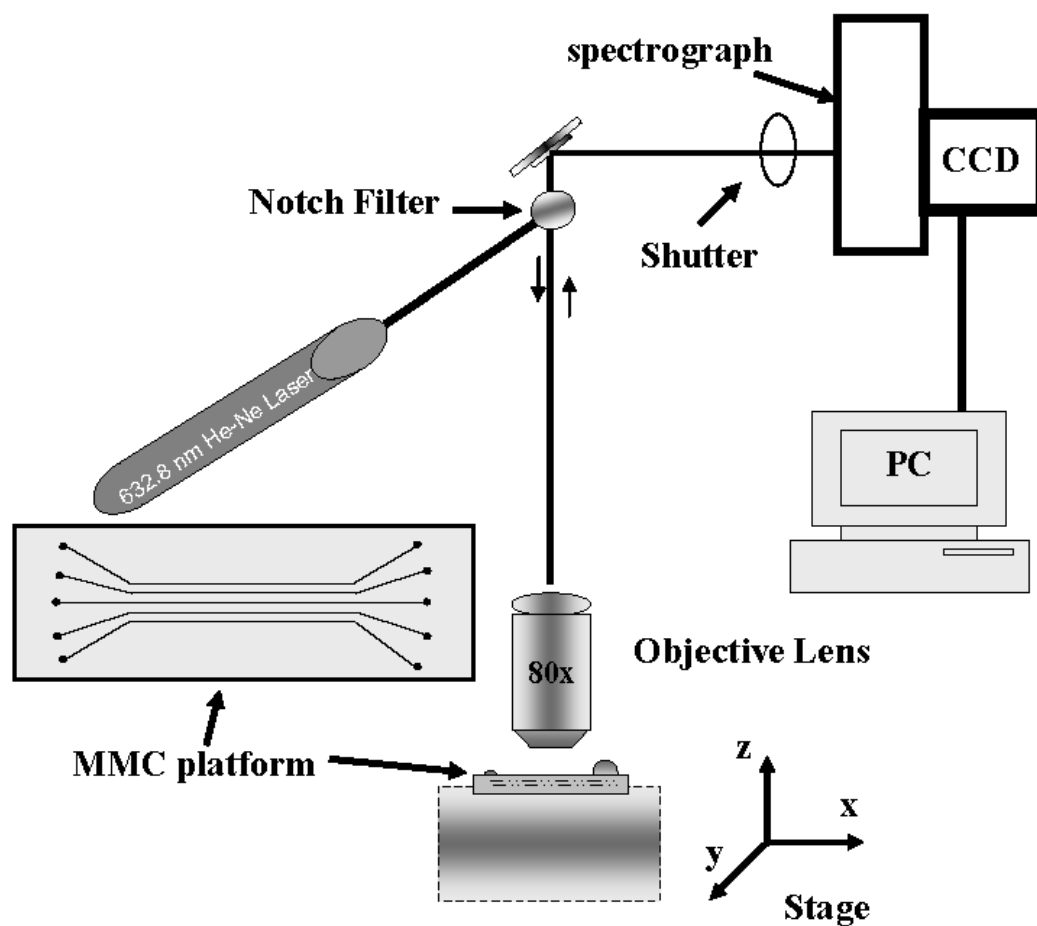


Figure 2.1 Schematic representation of the instrument apparatus used for MMF-SERS.

thermoelectrically cooled CCD camera, and processed with Labspec 4.03 software. A computer controlled x-y-z stage was used to adjust the focusing of the objective and position of the laser spot in the MMF channels.

The MMF platform was fabricated from PDMS (Sylgard 184, Dow-Corning, Midland, MI) using a previously published procedure with the exception of the use of a transparency in place of an aluminum photomask [153]. The channels were approximately 400 μm wide, 200 μm deep and 6.5 cm long. Analytes and Ag colloids were mixed together before they were introduced into the channels with sufficient time to establish equilibrium with the SERS-active media. A passive solution pumping method was employed for delivering the sample that simply involved adjustment of the volume level at the channel terminating pumping port while keeping the reservoir port volume constant. The point of maximum SERS signal in each channel was obtained by fine-focusing of the microscope objective. Once the signal was brought into focus, the SERS spectra of the sample were acquired. Different average velocities of samples were determined based on adjusting the drops sizes placed on the pumping port and recording the times required for the drop to diminish from the port through the channel. Since flow rates are changing during these experiments the volumetric flow rates are reproducibly attained but only approximate as reported herein.

Instrumentation for Colloid Characterization: Extinction spectra of colloids were collected from 300 to 800 nm on a Thermospectronic Biomate 5 UV-Visible spectrometer. All SEM images were collected using a LEO 1525 scanning electron microscope with a field-emission gun operating at 15 kV. Images were

obtained in secondary electron detection mode. These operating conditions were applied to reduce the sample damage and the build up of charge while producing high-resolution images of Ag cubic nanoparticles.

Preparation of Ag Colloid and Ag Cubic Nanoparticles: The conventional Ag colloid was prepared using the chemical reduction procedure according to the description by Lee and Meisel [135]. 85 mg of AgNO₃ (99+% Sigma) was dissolved in 500 mL deionized water (18ΩBarnstead E-pure) and heated to boiling. 10 mL of 1% w/v trisodium citrate (Fisher) was then added drop by drop with vigorous stirring, and the solution was kept stirring at the boiling point for an hour. The solution color was yellowish and the colloids are stable for several months. Conventional Ag colloids were used in all MMF-SERS experiments with the exception of the nanocubes size study.

Metallic particles synthesized with uniform, special morphologies have been showed to exhibit unique optical properties [154-156]. The Ag nanocubes were prepared with modification from Xia's regular synthetic procedure where silver nitrate is reduced by ethylene glycol in the presence of poly(vinyl pyrrolidone) (PVP) and HCl [154]. In this synthesis, 5 mL of ethylene glycol (EG) (Fisher) was heated in an oil bath at 144 °C for 1h to remove trace amount of water. 1 mL of 3 mM HCl was then added and after 10 min, 3 mL of 94 mM AgNO₃ and 3 mL poly(vinyl pyrrolidone) (PVP) were simultaneously added. When the reaction was completed (reaction time influences nanocubes size), the solution was washed twice with acetone and several times with ethanol and water to remove most of the EG and PVP. During the washing process the

suspension was centrifuged at 3400 rpm for 30 to 40 min. Finally, the sample was dispersed in 2 mL water for characterization. For SERS experiments, 50 μL of the Ag nanocube samples were diluted to 1 mL with deionized water (18 Ω Barnstead E-pure).

Reproducibility, Irradiation Time and Microscope Objective Studies: Stock solution (1×10^{-4} M) of crystal violet (Fisher) was prepared in deionized water (18 Ω Barnstead E-pure). The colloidal solution sample for the reproducibility study was mixed with crystal violet as follows: 10 μL of 1×10^{-4} M crystal violet was mixed with 1 mL Ag colloid to yield a final concentration of 1×10^{-6} M. For the microscope objective study, 100 μL of 1×10^{-6} M crystal violet was mixed with 1 mL Ag colloid to yield a final concentration of 1×10^{-7} M. In these and most other studies small amounts of NaCl (solutions made $\sim 1 \times 10^{-6}$ M) were added to enhance the SERS signal by aggregation. For the irradiation time study stock solution 1×10^{-2} M 4-Aminobenzoic acid 4-ABA (Sigma) was prepared in deionized water (18 Ω Barnstead E-pure). Then, 10 μL of 1×10^{-2} M 4-ABA was mixed with 1 mL Ag colloid to yield a final concentration of 1×10^{-4} M.

Anion Studies: Stock solutions (1×10^{-2} M) of sodium chloride, sodium nitrate, sodium fluoride, sodium iodide, sodium bromide (Sigma) were prepared in deionized water (18 Ω Barnstead E-pure). 10 μL (1×10^{-2} M) of each anion was added to 1 mL of the colloidal solution. Each colloidal solution sample was mixed with 4-ABA as follow: 10 μL of 1×10^{-2} M 4-ABA was mixed with 1 mL Ag colloid to yield a final concentration of 1×10^{-4} M. These samples were used to study the effect of different metal anions on the MMF-SERS signal of 4-ABA.

pH Studies: 20 μL of 5×10^{-2} M caffeine (98.5% Acros organics) solution were added to 1 mL Ag colloids to yield a final concentration of 1×10^{-3} M. Small amount of 1×10^{-6} M NaCl was added to enhance the SERS signal by aggregation. 0.1 M HCl (Fisher) and NaOH (Fisher) were used to adjust the pH within the pH range of 2-10. In addition, three pesticides samples were obtain from AccuStandard as follow: (1) Dinoseb 100 $\mu\text{g}/\text{ml}$ in MeOH, (2) Dithianon 100 $\mu\text{g}/\text{ml}$ in Acetone, (3) Monuron 100 $\mu\text{g}/\text{ml}$ in MeOH. All three samples were prepared in Ag colloids to yield a final concentration of 5×10^{-5} M. HCl and NaOH (0.1 M) were used to adjust the pH.

Calibration Studies: Two stock solution (1×10^{-4} M) of Mitoxantrone dihydrochloride (sigma) and crystal violet (Fisher) were prepared with deionized water (18 Ω Barnstead E-pure). These stock solutions were used to prepare a series of calibration standards within the 5×10^{-6} to 1×10^{-15} M range for Mitoxantrone dihydrochloride and 1×10^{-4} to 9.5×10^{-9} range for crystal violet with deionized water (18 Ω Barnstead E-pure).

2.3 Result and Discussion:

SERS is a powerful vibrational spectroscopy technique since its spectrum provides much more detailed information about molecular structure than other spectroscopic techniques such as fluorescence. Analytical applications of SERS are expanding due to reduced cost of modern lasers, development of different substrates and methods, introduction of fiber-optic probes, and fast instrumental development. We demonstrate in this chapter the potential benefits of using

MMF-SERS to perform parallel, high throughput, and sensitive detection/identification of single or various analytes under easily manipulated conditions.

General Performance Studies: Microscope objectives are characterized by several parameters such as numerical aperture (NA), magnification, working distance, depth of focus and throughput; all may alter SERS performance. Correlations between these parameters are often observed; e.g., higher magnification objectives that are commercially available generally exhibit larger NAs and shorter working distances and depths of focus. However, high magnification can come with conveniently long working distances in very expensive objectives (two such are employed in this work). While the smaller focus spots of high magnification can facilitate the use of small and/or intricate MF platforms and produce higher laser excitation intensities, the impact on MMF-SERS are not great. For example, the increase in excitation intensity with tight focusing is equivalently compensated in terms of SERS signals by the smaller area of substrate (and sample) that is interrogated. Conversely, the other parameter changes that accompany increasing magnification can be substantial and are the motivation for the study presented in Figure 2.2.

The ordering of SERS signals observed in the figure is roughly consistent with the quadratic dependence on NA for the objectives (NA = 0.75, 0.45, 0.40, 0.25 from the largest to smallest signals). Moreover, the combination of SERS and MMF fortuitously negates the deleterious effects of tight focusing with traditional high-magnification objectives. The MMF flow creates the equivalent of

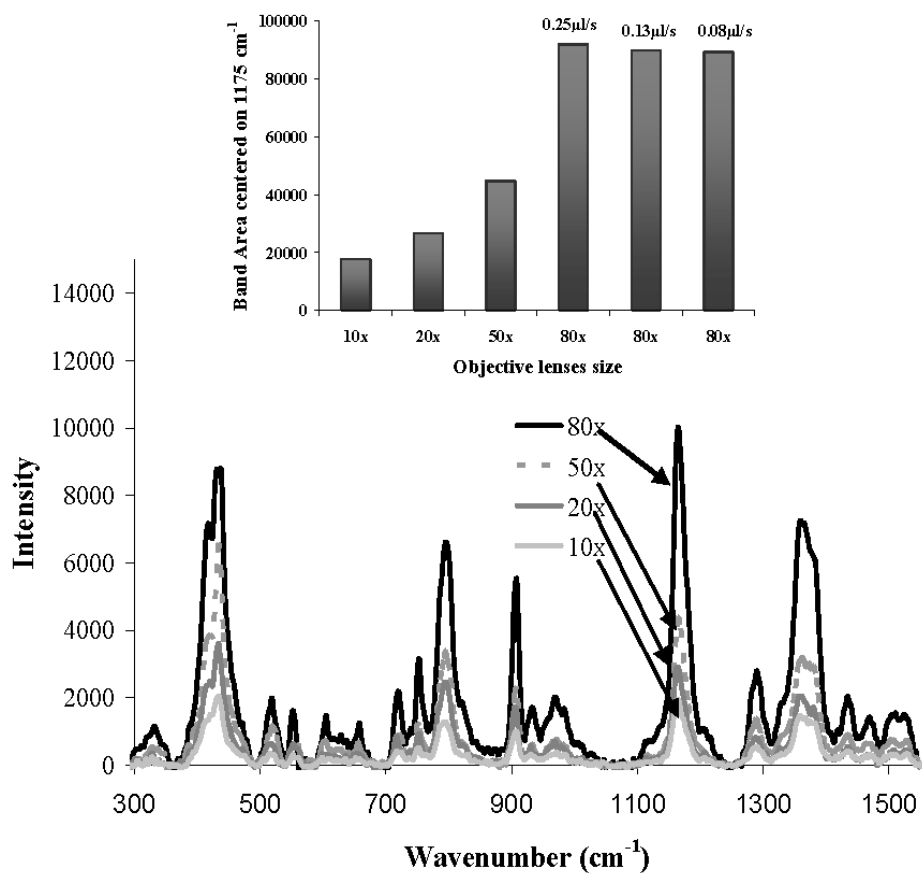


Figure 2.2 Spectral profiles of 1×10^{-7} M solution of crystal violet in Ag colloids as a function of microscope objective. Each bar represents the area of the 1175 cm^{-1} band of crystal violet as a function of objective and average velocities.

sample translation [34] and this minimizes or eliminates photothermal and photolytic problems that cause poor reproducibility in many SERS experiments, particularly with high excitation photon densities. Also the large working distances of the 50X and 80X objectives work well with the MMF platform, and the depth of the channels in the platform render translation between channels possible without the mis-alignment that would occur when mating short focusing depths with planar SERS substrates. Using the 80X long working distance objective resulted in very high collection efficiency and overall the highest SERS signal. The 1175 cm^{-1} band area bars of crystal violet (CV) in the inset of Figure 2.2 show the microscope objective lens and average velocity comparison in MMF-SERS. The average velocity comparison indicates that there was no significant effect on SERS response upon the variation of the average velocity, so long as a modest flow exists ($0.25\text{ }\mu\text{L}/\text{sec}$ was used for most SERS measurements).

Laser power and irradiation time are important parameters in SERS. Continuous irradiation with high laser power can cause photochemical changes in the sample and an irreversible decrease in the SERS signal [131,149]. Figure 2.3 shows a comparison of the SERS signal of $1\times 10^{-4}\text{ M}$ 4-ABA in Ag colloids in the MMF-SERS as a function of irradiation time. The laser power was substantial (4.5 mW) and the average velocity was $0.25\text{ }\mu\text{L}/\text{sec}$. One can see a high band resolution in SERS spectra with no changes in the spectral features even with an irradiation time of 10 sec under these flow conditions. The flow also serves to average out variations in substrate activity.

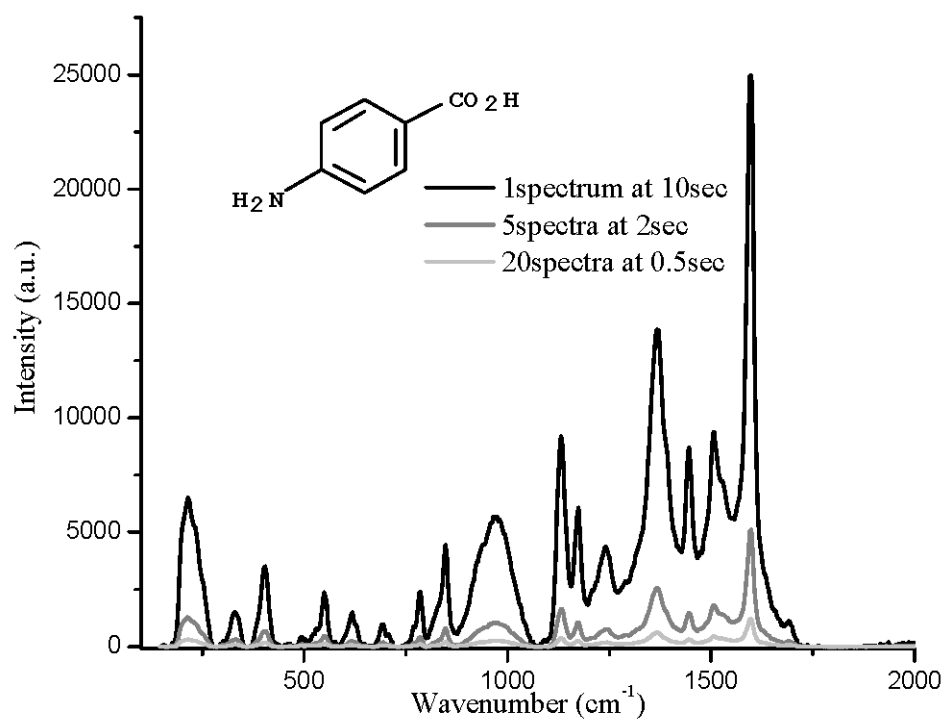


Figure 2.3 Spectral profiles of 1×10^{-4} M 4-ABA in Ag colloids as a function of irradiation time with a laser power of 4.5 mW.

Multiplex Performance and Optimization Studies: A lack of reproducible substrates in SERS has been a limiting factor for its application in quantitative analysis. The first multiplex performance study was to determine the reproducibility of MMF-SERS. This was done by acquiring SERS spectra of 1×10^{-6} M crystal violet by fine-focusing at a spot that is 2.5 cm from the reservoir port for each channel ($N = 20$ for each channel). Figure 2.4 shows the reproducibility for each channel and the overall reproducibility. The overall RSD was found to be 6.4 % and this ascertains the efficacy of this MMF-SERS approach. The time to acquire spectra across entire array of MMF channels for an aligned platform can be well under one minute.

Anions are often used in SERS studies with Ag colloids as signal enhancers. The mechanism for this enhancement is still under investigation, but it is sometimes thought that the anions cause Ag colloid to aggregate as a result of the loss of electrostatic repulsion. The LSPR for these aggregated particles can give rise to large electromagnetic fields (hot spots) and an overall improvement in SERS signal [142,143]. Therefore, a study of the changes in the SERS signal of 4-ABA in the presence of different anions was performed in the MMF to demonstrate how optimization studies can be performed rapidly and effectively. It was observed (Figure 2.5A) that the addition of 1×10^{-2} M sodium nitrate resulted in fast oxidation of the silver colloids.

The addition of 1×10^{-2} M sodium fluoride had no effect on the SERS signals of the analyte, while the addition of 1×10^{-2} M chloride, iodide and bromide anions quenched the SERS signal. This could be due to the competitive

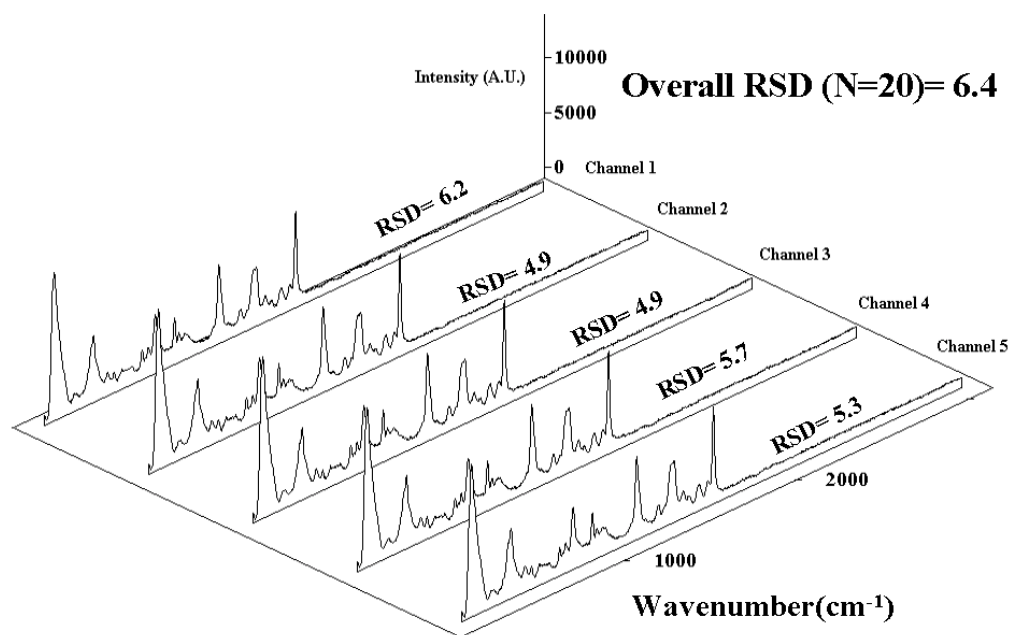


Figure 2.4 Reproducibility of the MMF-SERS signal of a 1.0×10^{-6} M crystal violet in Ag colloids in each of the microfluidic channels (overall N = 20).

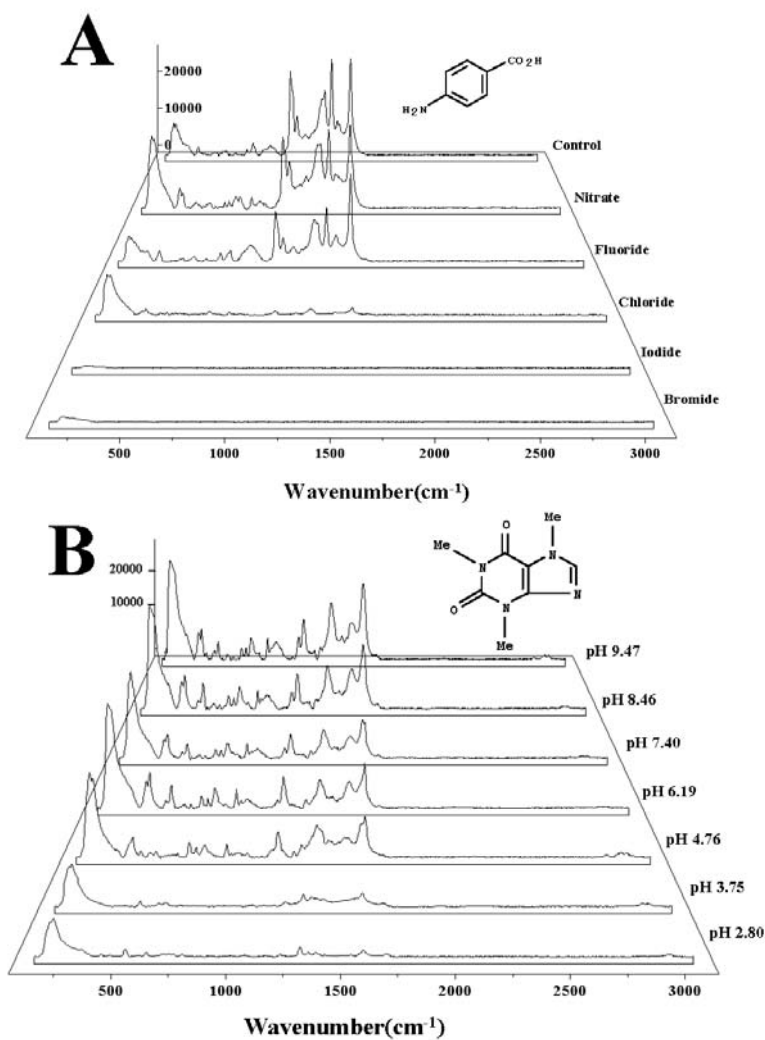


Figure 2.5 **(A)** Change in the SERS spectra of 1×10^{-4} M 4-ABA in Ag colloids upon the addition of different anions (1×10^{-2} M) to Ag colloids. **(B)** Influence of pH changes on the SERS spectra of caffeine.

adsorption between 4-ABA and the anions to Ag colloid surfaces at high electrolyte concentrations [140,141]. A similar study could have been performed for a lower range of electrolyte concentrations, perhaps with enhanced signals rather than the effects seen in Figure 5A.

pH studies were also done in the MMF; Figure 2.5B shows the spectral profile of caffeine in Ag colloid at different pH values in the range of 2-10. Pavel *et al.* explained the changes in the SERS intensity and peak positions by the presence of different caffeine adsorbed species and the reorientation of the molecule to the Ag surface [157]. According to their study, caffeine can accept one proton in an acidic environment and can not lose any in a basic environment. They speculate in neutral and basic environments caffeine is adsorbed through the π electrons and lone pair of the nonmethylated N atom, whereas in acidic environments caffeine is adsorbed through one or both oxygen atoms. The spectral profiles in Figure 2.5B reflects these changes which are in good agreement with the data reported previously [157].

The size and shape of Ag nanoparticles is an interesting topic for determining their unique optical properties and blending theory with experiment. These morphological characteristics determine the LSPRs of the Ag nanoparticles. Figure 2.6A shows the UV-Vis extinction spectra for three different sizes of Ag cubic nanoparticles with their SEM images. Cubic nanoparticles in the 45-60 nm size range show sharp band at 450nm, whereas particles in the 80-90 nm size range show a broader and blue-shift of the band; all consistent with prior reports for these cubic particles [38,76]. Figure 2.6B

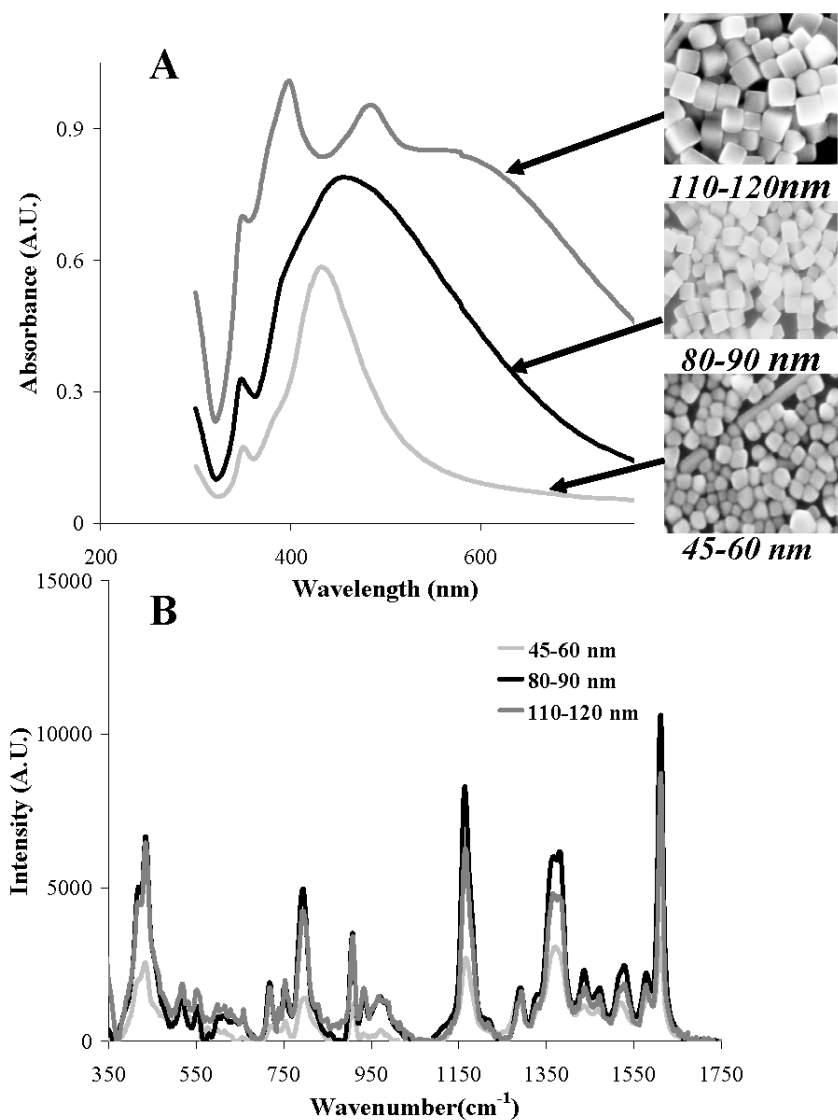


Figure 2.6 **(A)** Optical extinction curves of Ag nanocubic colloids with their scanning electron micrographs. **(B)** Representative SERS spectra of 5×10^{-6} M crystal violet using different Ag cubic nanoparticles obtained via MMF-SERS. The weight percent of nanocubes is approximately 0.2 %.

shows that cubic nanoparticles ranging from 80-90 nm in size provide the greatest SERS activity when excited using 632.8 nm light and in the dielectric environment of this study. Overall the results of these anion, pH, and colloid-type studies show the applicability of the MMF platform for parallel SERS optimization studies.

Multiplexed Performance for Quantitative and Qualitative Analysis: We have explored the validity of the MMF-SERS approach for quantitative studies. Figure 2.7A shows the calibration curve for crystal violet dye, which is a non-resonant SERS case at the excitation wavelength used. As demonstrated in the figure, linearity of the analytical curve in the range from 5×10^{-9} M up to 1×10^{-6} M (solutions in different channels of the MMF platform) is obtained with $R^2=0.993$. The spectrum of the lowest concentration obtained shows that most SERS peaks are observable with $S/N > 10$ (thus LODs should be below one nM). At higher concentration the deviation from linearity could indicate the saturation of the analyte to the silver colloids solution.

The second analyte tested was Mitoxantrone, a compound belonging to a general group of drugs known as antineoplastics (structure shown in Figure 2.7B). It is used to treat some kinds of cancer and forms of multiple sclerosis. Mitoxantrone has an absorption maximum at ~ 650 nm [158] rendering this a resonance SERS case. A linear response is obtained in the range of 1×10^{-13} M up to 1×10^{-9} M with correlation coefficient of 0.982. Above 1×10^{-9} M the analyte saturates the Ag colloids, and above 5×10^{-5} M intense fluorescence quenches the SERS signal. Details of the mitoxantrone spectrum and bands assignment were

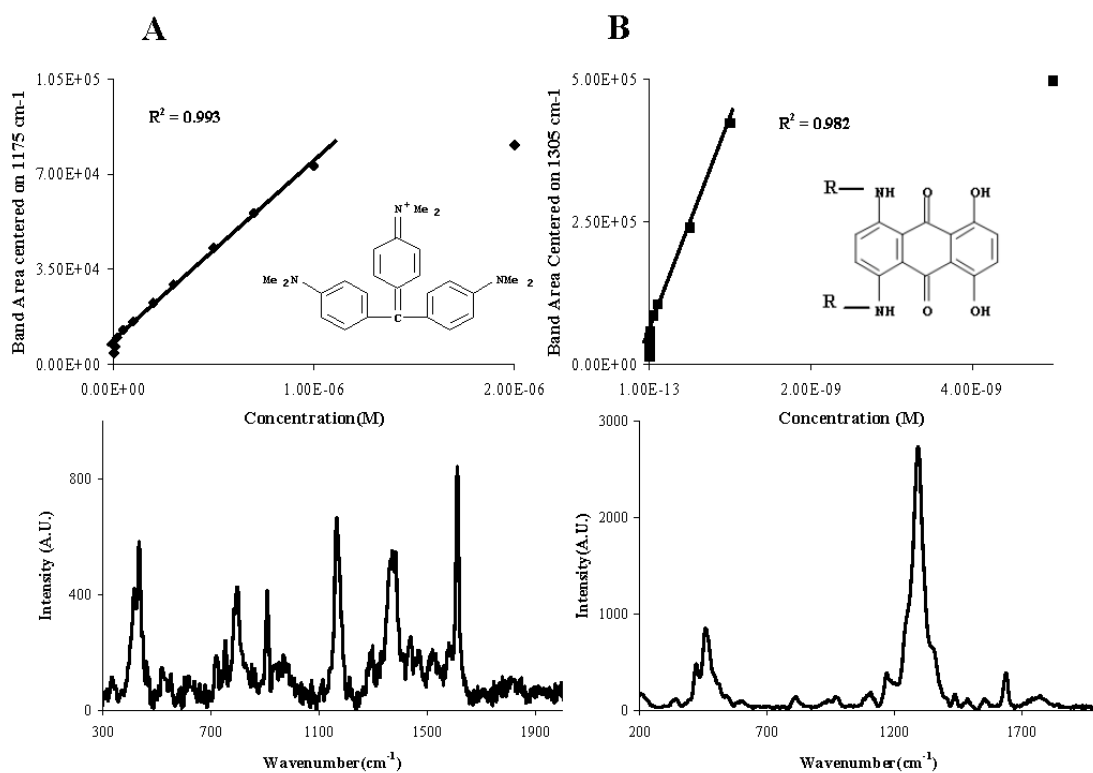


Figure 2.7 **(A)** Working curves of crystal violet and **(B)** mitoxantrone using MMF-SERS and passive pumping ($-R = \text{HO}-(\text{CH})_2-\text{NH}-(\text{CH})_2$). The spectra are for 5×10^{-9} M crystal violet and 1×10^{-12} M mitoxantrone.

reported elsewhere and are consistent with the spectrum shown in Figure 7B [159]. The sensitivity achieved with the MMF-SERS approach is better than reported previously for this compound [160].

Pesticides are organic compounds that are used in agriculture. The full health risks associated with pesticides are not accurately known. However, they can cause short-term severe health effect such as rashes, blisters, blindness, nausea, dizziness, and diarrhea. They can also cause chronic effects such as cancers, birth defects, immunotoxicity, and actions as endocrine disrupting chemicals (EDCs). There is a pressing need to analyze a wide rang of environmental matrices for pesticides and other EDCs in high-throughput and with methods possessing both quantitative and qualitative capabilities.¹⁶¹ Figure 2.8 shows the SERS spectra of three different pesticide compounds, (A) Dinoseb, (B) Dithianon, and (C) Monuron), measured at different pH with MMF-SERS. In general, the results demonstrate that each individual SERS spectrum can be used as a “fingerprint” for each compound and that conditions can be optimized for their measurement using this high-throughput platform. In principle this can be used to generate spectral libraries that allow the identification of the agent of interest.

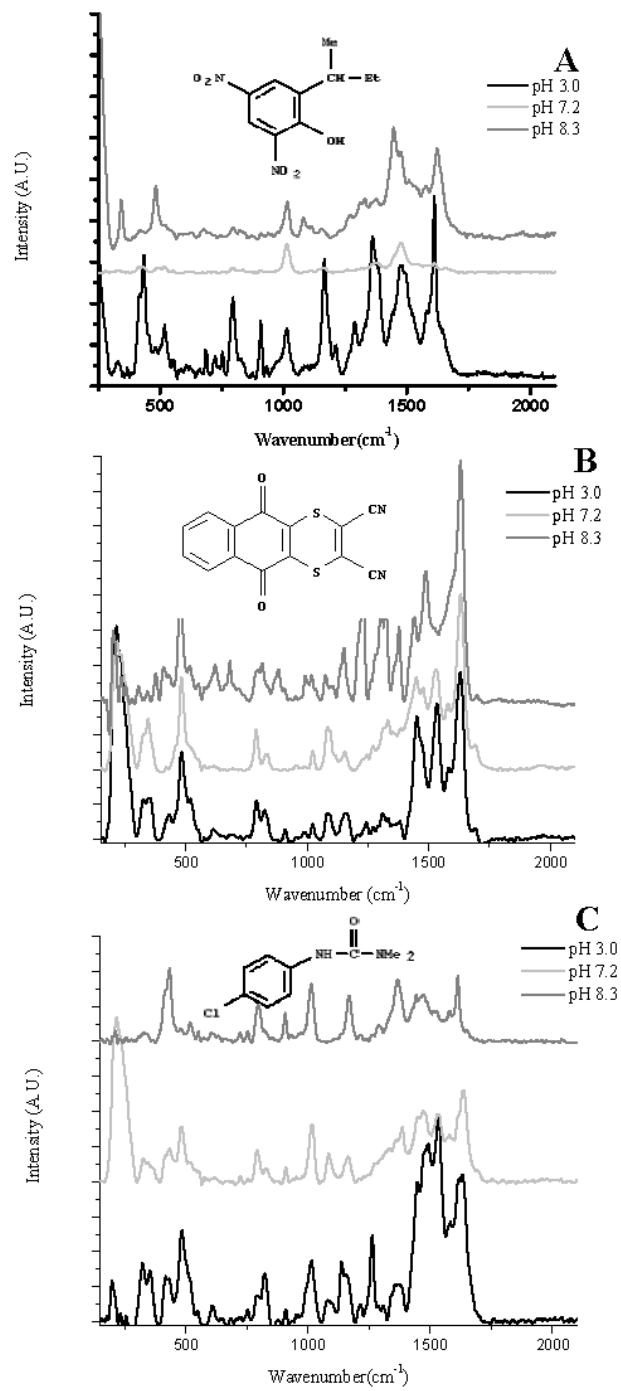


Figure 2.8 MMF-SERS spectra of pesticides at different pH; **(A)** Dinoseb, **(B)** Dithianon, and **(C)** Monuron.

CHAPTER 3

Introduction to Nanofabrication Methods and Attempted Approaches to Nanotransfer Printing

3.1 Introduction

Nanofabrication is the process of generating certain structures with patterns having dimensions in the nanoscale and is an extension of microfabrication. Nanofabrication research and development has been driven by the needs of microelectronic devices. The motivations for Microelectronic devices have developed massively as a result of the commercial implementation of nanofabrication. Historically, photolithography and electron beam lithography have been an excellent well suited for tasks that involved creating structures of radiation sensitive materials, such as photoresist or electron beam resist on semiconductor surfaces [162,163]. These conventional methods are highly developed and optimized for semiconductor fabrication, but the cost of purchasing, installing, and maintaining the tools they require limit their application in areas other microelectronics. These methods also expose substrates to corrosive etchants and high-energy radiation. As a result, applying these methods to areas of research that require unusual materials and structures such as bioscience or plastic electronics is a challenging task. Consequently, much research has been done to develop alternative methods to photolithography based on nanofabrication.

The ability of any method or technique to overcome the limitations of

conventional methods, and to fabricate microscale and nanoscale structures rapidly and inexpensively using common laboratory facilities, will influence the acceptance of that method. Unconventional methods have the potentials to be very useful for nanofabrication. These unconventional methods include molding, embossing, and printing. These methods have demonstrated a high potential for nanofabrication and some of the techniques have achieved widespread use in academic and industrial laboratories. They are useful for fabricating devices such as diodes, photoluminescent porous silicon pixels, organic light-emitting diodes, and thin-film transistors. Other examples of unconventional nanofabrication applications are compact disc (CDs), digital versatile discs (DVDs), diffraction gratings and holographic gratings for identification markings on credit cards and currencies, and plastic parts [164].

3.2 Overview of Photolithography and Electron Beam Lithography (EBL)

Figure 3.1 shows a schematic illustration of the steps involved in conventional Photolithography and EBL. Photolithography is based on projecting collimated light through a quartz plate that supports a patterned mask on a photoresist coated planar substrate for a period of time (these planar substrates are usually semiconducting silicon wafers) [165,166]. Photoresists are based on organic polymer whose chains are cross-linked, degraded, or forced to go through molecular rearrangements when exposed to high energy particles such as UV photons light. Photoresists are divided into two types: positive photoresist - where the resist is exposed to light whenever the underlying part is to be

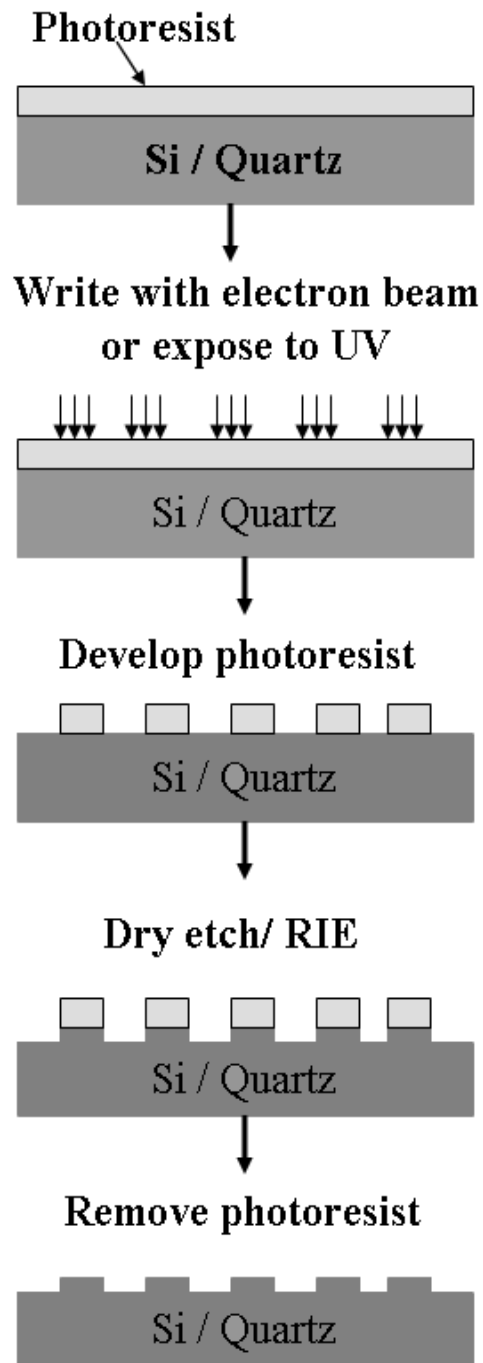


Figure 3.1 Schematic illustration of the fabrication of patterns by conventional methods: photolithography and Electron Beam Lithography.

removed and negative photoresist - where the exposed part is polymerized and becomes harder to be removed [167,168]. Photolithography is well suited for many fabrication tasks, but sometimes, it is not the best option for the application. For example, it provides a limited control over the surface functionality, since it can only be applied to directly pattern certain functional materials such as photoresist. The resolution of photolithography technique with the current capabilities is approximately 90 nm [162].

EBL is a slower process compared to photolithography, but it is capable of generating high resolution features with arbitrary patterns and, in fact, has become a standard tool for writing arbitrary patterns for many technological and scientific applications [169,170]. EBL is based on using a tightly focused beam of electrons, instead of light, to scan across the surface of a photoresist and generate high resolution patterns [171]. The resolution of electron beam lithography is controlled by the choice of resist, the spot size of the beam, high energy secondary electrons and by scattering of electrons from the primary beam within the resist. The resolution of EBL with the current capabilities is approximately 20 nm [163]. It is also important to mention the proximity effect, since it effects the resolution of the patterns where the parasitic exposure of an unwritten area by scattered electrons has an effect on resolution (due to both forward and backward scattering of electrons in the exposure beam) [172]. The forward scattered electrons give rise to a broadening of the beam as it penetrates the resist, whereas backward scattered electrons from substrate give rise to an exposure halo of radius much greater than the beam diameter; decreasing the

resist thickness can minimize the forward scattering contribution to the proximity effect. In addition, increasing the resolution requires decreasing the diameter of the beam. This, in turn, decreases the current of the beam and makes the beam unstable, increasing the time required to achieve the correct dose. Using a very sensitive resist will eliminate this issue, since it requires a low dose of electrons. The ability of the developer to distinguish between exposed and unexposed regions effect the resolution of the system. An example of electron beam resist is Poly(methyl methacrylate) (PMMA), a well known resist for EBL that has appeared in a large number of works [173-177].

Photolithography and EBL processes are followed by Reactive Ion etching (RIE). It is a dry etching technique used to generate deep trench structures on silicon substrate. It has several advantages compared with wet etching. RIE includes smaller undercut (allowing smaller lines to be patterned) and higher anisotropy (allowing high-aspect-ratio vertical structure). In this technique, radio frequency (RF) energy is used to excite ions in a gas (i.e. CF_4 or SF_6) to an energetic state. The energized ions supply the necessary energy to generate physical and chemical reactions on the exposed area of the substrate, which start the etching process [162]. RIE can generate strong anisotropic (directional etch that stops on certain crystal planes in the substrate which results in holes and lines to have straight, vertical sides), as well as isotropic profiles (nondirectional etch that results in undercutting of the resist mask by the same distance as the etch depth). The resolution of RIE depends on the gases used,

the condition of plasma, and the applied power [162]. As illustrated in Figure 3.1, RIE process is followed by the removal of the resist.

3.3 Overview of Unconventional Nanofabrication Methods

Molding and embossing of nanostructures can be performed with hard and soft (elastomeric) molds. Molding is the process of curing a precursor such as a monomer and prepolymer against a topographically patterned substrate, whereas embossing is the process of transferring a mold with certain structure topography into an initially flat polymer film by pressing a mold into the surface [168,178-180]. These processes are mainly used by techniques with the names “step and flash imprinting lithography” and “nanoimprint lithography”, respectively.

Hard Molds or Stamps: Hard molds are used in different techniques to transfer specific patterns or features in the macro- and nanoscale level into a monomer, polymer, or prepolymer [181]. The nanostructure hard molds are usually prepared by first creating photoresist nanostructures with EBL and then transferring the patterned photoresist onto a hard substrate such as quartz or silicon via reactive ion etching (RIE) or wet chemical etching. Hard molds offer several advantages for nanofabrication. They are rigid, yielding minimum distortions of the molds as result of the pressure applied during the nanofabrication processes. Hard molds are also thermally stable at high temperatures and this stability allows for their usage in different nanofabrication process. Hard mold surfaces are usually covalently linked to a fluorosilane

releasing agent such as $\text{CF}_3(\text{CF}_2)_7(\text{CH}_2)_2\text{SiCl}_3$ to facilitate the separation of the mold from the substrate and to minimize the high defect level associated with most of nanofabrication techniques [182,183].

Soft Molds or Stamps: Soft molds are created by casting liquid polymers (usually elastomers) precursors against a topographically patterned master. Polydimethylsiloxane (PDMS) is the most popular implemented elastomer for nanofabrication. This material is un-reactive to most materials being molded or patterned. In some cases, the process of curing the PDMS against a hard master can result in the adhesion of PDMS to the exposed regions of the silicon wafer; to prevent this adhesion, the master surface must be passivated by a gas phase deposition of the fluorosilane releasing agent. PDMS has useful properties for nanofabrication such as being durable and transparent above a wavelength of approximately 280 nm. PDMS is inexpensive, so creating a large number of stamps, molds or substrates is not a problem. Polyurethane is another example of elastomer used in nanofabrication.

Step-and-Flash Imprinting Lithography (SFIL): Step-and-Flash Imprinting Lithography (SFIL) is based on replicating a specific topography of rigid mold using a low-viscosity photo-curable prepolymer solution as the molded material [184-190]. SFIL is an alternative technique to photolithography that efficiently generates high aspect-ratio patterns in resist materials. The resolution of the SFIL with current capabilities is approximately 20 nm, and this number decreased steadily with improvements in fabricating molds or masters [162]. Figure 3.2 illustrates the steps for patterns fabrication by SFIL.

In this technique, the photo-curable liquid or solution is a low viscosity molecular weight monomer and a photo-initiator that fills the void spaces of the quartz mold. When this solution is exposed to UV light through the transparent quartz mold, it will polymerize, solidified, and harden the precursor while in contact with the mold; furthermore, the use of transparent mold allows for mold optical alignment. When the mold is removed a topographically patterned inverse replica substrate is obtained. SFIL techniques avoid incomplete mold filling by using low viscosity prepolymer solution. However, hydrodynamic forces prevent complete displacement of the fluid by the mold, leaving a residual layer of cured material between patterned features. An important fact is that the substrate must be parallel to the mold and thoroughly flat to ensure that the residual layer is uniform in thickness over the entire imprinted area and that the residual layer can be removed by RIE.

SFIL uses a rigid, transparent mold to print features at a constant low temperature of approximately 22°C and low applied pressure - meaning that distortions caused by thermal expansion or flexing of the mold or substrate are not an issue; additionally, a constant temperature technique speeds throughput by eliminating temperature cycling steps. The lifetime of the mold is an important consideration in all nano-molding techniques. It is important to use a releasing layer that is covalently linked to the surface of the mold to reduce the surface free energy of the mold and minimize the adhesion of the cross-linked polymer to the mold; a fluorinated silane is a common releasing layer used in all nano-molding

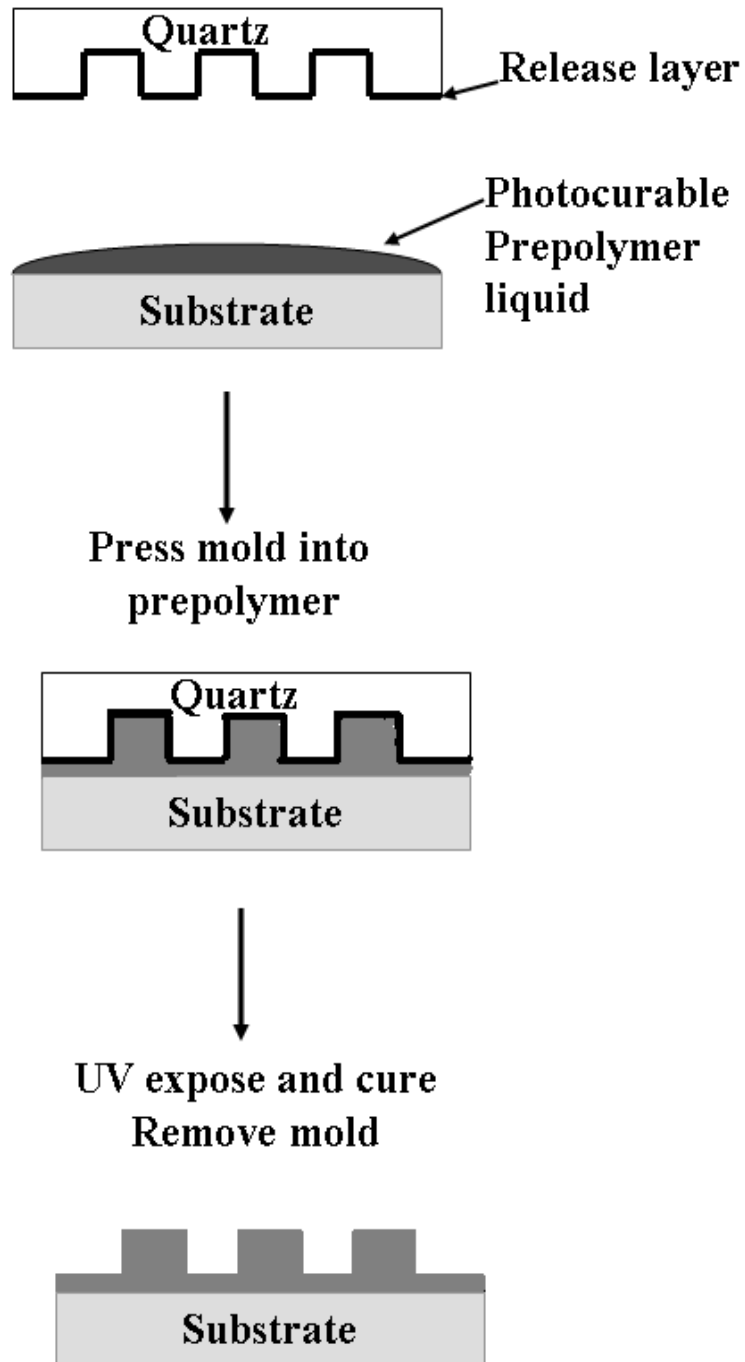


Figure 3.2 Schematic illustration for the steps of fabrication by Step-and-Flash Imprinting Lithography.

techniques. SFIL technique is “self cleaning” because any particulate matter on the surface of the rigid mold is captured mechanically in the photo-curable prepolymer solution during polymerization.

Nanoimprint Lithography (NIL): Nanoimprint Lithography (NIL) is based on pressure-induced transfer of a topographic pattern from a rigid silicon mold into a thermoplastic (deformable) polymer film heated above its glass transition temperature [191-200]. NIL is a physical process that does not use any energetic beams and it is under rapid development to meet the needs of the new generation of applications extended into the nanoscale arena. The resolution of NIL with the current capabilities is similar to SFIL. Figure 3.3 shows the steps for NIL. This method is also known as “hot embossing” since it requires heating the thermoplastic polymer above its glass transition temperature, where the resist can become a viscous liquid to flow and deformed into the shape of mold [201]. The mold is pushed into the polymer under high pressure and removed after cooling below the glass transition temperature. This step usually is followed by a transfer step where an anisotropic process such as reactive ion etching (RIE) is used to remove the residual resist in the compressed area; an example polymer is PMMA which needs to be heated above 110 °C for NIL. Materials that have been patterned with NIL method include conducting polymers, block copolymer, fluorescently labeled polymers, and biomolecules [202,203].

The lifetime of the mold is an important issue for NIL, since the procedure requires heating, cooling, and applying pressure during embossing, which, in turn, results in an increased stress on the mold [204,205]. The hard mold and

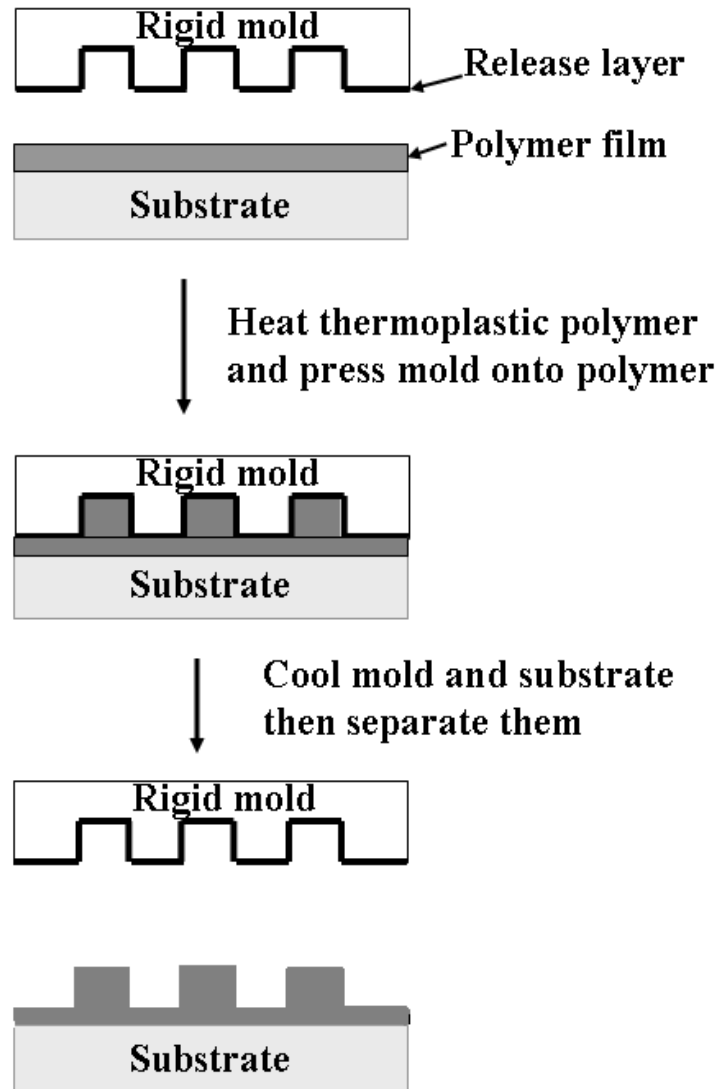


Figure 3.3 Schematic illustration of steps for Nanoimprinting Lithography.

the spin-coated thin film polymer must be parallel and the pressure applied must also be uniform across the hard mold [206,207]. NIL has been used to pattern Fresnel lenses and electrical contacts for nanowires [208,209].

SFIL and NIL are the most widely techniques for unconventional nanofabrication. These techniques have been used to pattern functional structures for microelectronics and optics devices. The resolution of nanofabrication by SFIL and NIL is controlled by several factors such as the ability to fabricate masters with nanometer features, the ability of a material to mold the features of the master, the distortion of features in the transferred pattern, and the ability of the molded material to fill the mold completely.

3.4 Nanofabrication by Printing

Introduction: Nanofabrication by printing is an additive approach that involves transferring material or an “ink” onto a substrate by printing from a topographically patterned stamp. This process, known as “Microcontact Printing” (μ CP), transfers molecules from a patterned stamp to a substrate by the formation of covalent bonds and was invented by the Whitesides group at Harvard University [210-214]. This method requires a stamp with relief features in the geometry of the desired pattern, a method to deposit the solid material on the stamp, a means to bring the stamp in to physical contact with the substrate and surface chemistry to prevent adhesion of deposited material to the stamp and to promote its adhesion to the substrate [162,181,185].

μ CP is a useful technique for generating patterns of functional organic surfaces over large area. The procedure starts by using a solution of molecules such as alkanethiol to ink the surface of the stamp and form a self-assembled monolayer (SAM). Then the stamp is brought into conformal contact with an appropriate substrate that consists of a thin layer of gold, silver, or palladium [215-219]. The molecules are transferred in a pattern defined by the topography of the stamp via chemisorption or physisorption. μ CP has patterned a number of materials other than SAM such as catalyst, dendrimers, polymers, biomolecules, and colloidal particles [210,220-225]. Nanotransfer printing (nTP) is an extension technique from μ CP that is studied and applied in the author's research.

Nanotransfer Printing (nTP): Nanotransfer printing (nTP) is a more recent straightforward method that refers to the process of transferring solid film or layer from a stamp with patterned features to a substrate with nanometer resolution [226-228]; the stamps are either made from soft or hard material, such as PDMS and silicon, respectively [229,230]. Figure 3.4 illustrates the procedure for nTP. First, the stamps are typically coated with a continuous layer of metal (e.g. Au, Al) without any adhesion layer between the metal and the stamp. The stamp is then brought into contact with the substrate coated with SAM and the exposed thiol group covalently bond to the metal layer in the regions of contact. Separating the stamp from the substrate yields the metal layer, on the raised regions of the stamp,

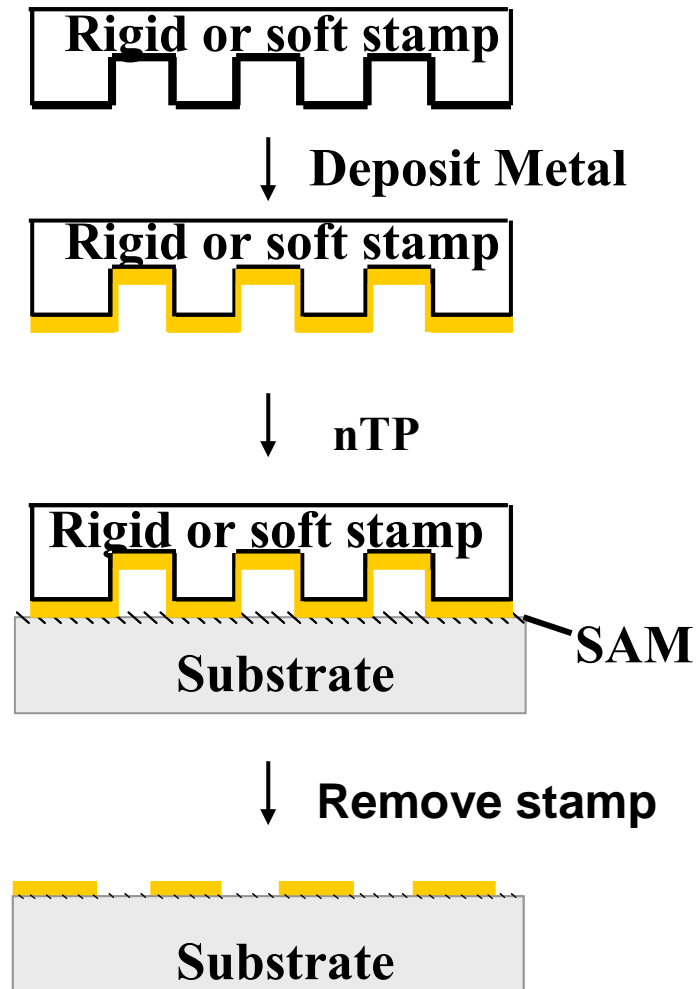


Figure 3.4 Schematic illustration for steps to fabricate patterns by Nanotransfer printing.

bounded to the SAM and the underlying substrate. Another method of releasing the structured film relies on condensation reactions between surface-bound silanols (Si-OH) [231]. This technique can generate complex patterns of two and three-dimensional structures with nanometer resolution over large area in a single process step [232-234]. Examples of the structures fabricated by nTP are organic thin film transistors and electrostatic lenses. nTP simplifies nanofabrication by eliminating the need for developers and etchants during pattern transfer and by rectifying the need to expose the substrate to harsh material such as acids and bases. In addition, transferring metal film to a fragile substrate can be performed without exposure to the high temperatures common in other techniques.

nTP resolution with the current capabilities is approximately 30 nm. The smallest feature that can be printed with minimum defects is determined by several factors [235,236] minimum size and depth of features in the stamp, lateral dimensions and resolution of the transferred material, and the degree of adhesion of the printed material to the second surface. The minimum size of features in the stamp is determined by resolution of the master or the mold created with photolithography or EBL. It is also determined by the ability of the mold or stamp to retain nanoscale features. A stamp can be distorted while in contact with the substrate surface which limits the minimum size of the transfer patterns. Lateral dimensions and resolution of the transfer material depends on the interaction of the transferred material with the substrate surface. The

resolution and the minimum feature size of the material transferred by nTP depend also on the nature and integrity of the transferred materials [162,181,185]. Table 3.1 summarized the resolutions of the conventional and unconventional methods for patterning nanostructures.

3.5 Attempted Approaches for *Direct* Nanotransfer Printing (nTP) to Create Substrates for SERS

Introduction

In Chapter One, it was shown that the main contribution to SERS effects arises from the huge enhancement of the local electromagnetic field close to the surface. This is due to the excitation of localized surface plasmon resonance, leading to hot spots around nano-sized metal particles, the excitation of the molecule, and the amplification of the Raman scattered light. It is necessary that the molecule be situated in the vicinity of a structured metal surface, preferably one that supports an electromagnetic resonance at the excitation and emission wavelength involved in the Raman scattering process. Extensive theoretical studies prove that the conditions for surface plasmon resonance and the subsequent SERS enhancement of analyte signals depend critically on shape, size, inter-particle spacing and the dielectric constants of the substrate, surrounding medium, and analyte. These separate dielectric constants combine to form a unique dielectric environment to such an extent that the individual dielectric constants cannot be decoupled from one another. Over the years, there have been several lithographic techniques as well as improvements to

Table 3.1 Resolution of Conventional and Unconventional Nanofabrication techniques

Technique	Resolution	Pattern
Photolithography	90 nm	Parallel generation of arbitrary patterns
Electron Beam Lithography	20 nm	Serial writing of arbitrary patterns
Step-and-Flash Imprinting Lithography	20 nm	Parallel formation of arbitrary patterns
Nanoimprint Lithography	20 nm	Parallel formation of arbitrary patterns
Nanotransfer Printing	30 nm	Parallel formation of arbitrary patterns

classical wet chemistry methods employed for the production of more uniform and controllable SERS substrates exhibiting large homogeneous electromagnetic field – a feature that is almost impossible to achieve in traditional substrates or system such as metal island films, electrochemically roughed electrodes, and metal colloids. The random, complex nature of these substrates is difficult to study and understand, as is modeling the SERS effect. Some of the interesting possibilities with the lithographic approaches are to control the size, shape, and inter-particle spacing in hopes of developing more suitable SERS substrates for improving our understanding of the mechanisms involved in the SERS effect.

Periodic nano-patterned substrates fabricated by nanosphere lithography are limited in terms of structures and the future of SERS depends on methods for nanofabrication. EBL with lift-off and RIE techniques have been shown to produce highly ordered periodic nano-particle SERS substrates and can potentially produce well defined geometry and spatial arrangements; however, EBL lift-off and RIE techniques are associated with high capital and operational cost that are impractical for SERS applications. One of the challenges in characterizing the electromagnetic mechanism is the difficulty associated with preparing nano-particles structures with controllable inter-particle gaps, and with all existing methods, theoretical predicted gaps for high electromagnetic field cannot be achieved.

One of the aims of this research is to fabricate substrates for SERS using EBL and nTP approaches, so as to produce *highly efficient SERS substrates and addresses the scaling limitation of EBL*. While the nTP technique has become one

of the virtually routine methods in the semi-conductor industry, it has not, to our knowledge, been applied to the fabrication of SERS substrates. The goal is to transfer metallic nano-patterns of silver EBL stamp *directly* onto the elastomer PDMS to create SERS nano-composite substrates with regular periodic morphologies. As discussed in chapter 1, PDMS polymer has some unique properties such as its comprisal of a saturated silicone-oxygen backbone with high resistance to degradation from temperature, ozone, radiation and high voltage ionization [61]. PDMS also has a unique phase separated layer with high tensile strength and potential for elongation [149]. This is particularly useful to create SERS substrates and to control the gap size simultaneously, under one set of conditions in a SERS experiment.

In the remainder of this chapter, preliminary partially successful and unsuccessful results from different approaches for *direct* nano-transfer of the metallic discs to PDMS substrate will be shown and discussed. Results will be discussed concerning the challenging task of direct usage of a stamp created with EBL and applied without any major modification such as using RIE. Results from different experimental conditions such as the type of resist, thickness of metal, type of metal, pressure applied, etc. will also be presented and discussed. Discussion will be organized as follow: First, initial results on the macroscale will be discussed. Next, the initial results on the nanoscale using ma-N 2403 resist stamp and the approaches attempted to control the pressure during the nTP process will be demonstrated. In addition, the approaches attempted to overcome the adhesive nature of the EBL resist stamp will also be discussed.

Results from EBL exposure doses studies of hydrogen silsesquioxane (HSQ) resist to create non-adhesive resist stamp will then be also discussed. Heptakis(6-*O-tert*-butyldimethylsilyl-2,3-di-*O*-acetyl)- β -CD (H- β -CD) and 4-*tert*-Butylcalix[n]arene (Cal-4) phases will be studied and presented herein to coat the adhesive resist layer. These preliminary studies ultimately led to the published successful work presented in chapter 4

Experimental

Preparation of Stamps: A set of two-dimensional models of different structures such as square, triangles, and elliptical nano-arrays were designed in AutoCAD 2005. Pattern size varied between 100-300 nm in diameter with an inter-particle spacing of 50-200 nm. Following that, each drawing was converted to GDS-II format by using the LinkCAD conversion program. The files were then transferred and programmed into the EBL computer. **For the ma-N 2403 resist,** a 300 nm film of ma-N 2403, a methacrylate-based negative e-beam resist, was uniformly applied to the surface of a new 2" wafer (Wafer World, FL) by spin coating at 3000 rpm for 30 seconds. The coated wafer was then baked at 90°C in a conventional oven for 60 seconds and placed into the EBL system. Film thickness of the ma-N 2403 resist was estimated from a chart provided by the manufacturer and is based on spin rate. **For the ma-N2403 macro stamp,** the stamp that was created by spin coating ma-N2403 resist at 300 rpm for 30 second. A mask was then placed onto of the uniform resist coating and irradiated with UV light for 4 minutes, then developed in alkaline ma-D 332 developer for 6 second and rinsed in deionized water (18M Ω Barnstead E-Pure) for 3 minutes.

After development, the samples were carefully dried using low-flow streams of N₂ gas. **For Hydrogen silsesquioxane (HSQ) resist**, HSQ is a negative electron beam resist (FOX-14® from Dow-Corning, Midland, MI), the HSQ was spin coated at 3700 rpm for 50 second, and then baked at 120 °C for 120 seconds and followed by a second bake at 200 °C for 120 seconds. The thickness of the resulting HSQ film was measured using F20 Advanced spectrometry thin-film measurement system (FILMETRICS; San Diego, CA). **For the SU-8 photoresist stamp**, the stamp was created by spin coating SU-8 negative photoresist polymer (Microchem; Newton, MA) at 4000 rpm onto a Si wafer, after which a transparency mask was placed on top of the smooth resist coating. UV irradiation for 3 min was used to crosslink SU-8 only in the expose pattern cut into the mask; the remaining un-crosslinked SU-8 was subsequently rinsed off with propylene glycol methyl ether acetate.

A Jeol JBX-6000 FS/E electron beam lithography system with a 50keV thermal field-emission gun was used for the nanofabrication of the stamp. The ma-N 2403 resist film was exposed to 170 $\mu\text{C}/\text{cm}^2$, yielding an array of nano-patterns. The HSQ resist film was exposed to 100-1600 $\mu\text{C}/\text{cm}^2$ for different studies. Each array is approximately 40x40 μm in size with 500 μm spacing in the x direction and 100 μm spacing in the y direction between each uniquely patterned array. Once exposed, the ma-N 2403 patterns were developed in alkaline ma-D 332 developer for 6 seconds and rinsed in deionized water (18M Ω Barnstead E-Pure) for 3 minutes. After development, the samples were carefully dried using low-flow streams of N₂ gas. The HSQ patterns were

developed by immersion in a solution of the tetramethyl ammonium hydroxide (TMAH) developer (MF-322 from Shipley) at 22 °C for 70 second, followed by a bath in 1:9 TMAH:DI for 10 seconds; they were then rinsed for 10 seconds in pure deionized water. After development, the samples were carefully dried using low-flow streams of N₂ gas.

In some studies, the stamps were then prepared for nanotransfer printing as follow: an in-house physical vapor deposition system was used to vapor deposit Squalane (Sigma), Poly-ethylenimine (PEI) (Sigma), Heptakis(6-*O-tert*-butyldimethylsilyl-2,3-di-*O*-acetyl)- β -CD (H- β -CD) (was prepared using the method of Stoddart et al [78]) and 4-*tert*-Butylcalix[n]arene (Cal-4) (Lancaster, Pelham, NH). This system uses light source for heating and operates at roughly 10⁻² Torr. Average mass thickness and deposition rates were measured for each film with a Maxtec quartz-crystal microbalance (QCM) mounted adjacent to the arrays. A Physical Vapor Deposition (PVD) chamber from Cooke Vacuum Products, Inc was used to vapor deposit Ag. Samples were mounted 25 cm above and normal to the effusive source. The ma-N 2403 arrays were coated with different thickness of 99.999% Ag (Alfa Aesar, MA) under high vacuum conditions (1x10⁻⁶ torr). Once prepared, stamps were stored in a vacuum dessicator held at 10⁻⁴ Torr in the dark prior to use.

Preparation of the SERS Substrate: A 2" Si wafer was cleaned with ethanol (HPLC, Fisher). PDMS was then prepared by the addition of Sylgard 184 curing agent (Dow Corning) and its elastomer in a 1:10 mass to mass ratio. The two compounds were combined and then degassed under high vacuum condition for

15 minutes. The PDMS film was either spin coated at 200 rpm for 30 second or poured onto Si wafer, then cured in the oven at 70°C for one hour and finally, stored at room temperature until it gained full strength. PDMS was peeled off and the side facing the Si wafer was treated with 1×10^{-5} M (3-Mercaptopropyl)trimethoxysilane, (95%, Aldrich)(dissolved in Acetone) for 24 hours and then rinsed with deionized water (18M Ω Barnstead E-Pure) for 1minute. The stamps were placed on top of the treated PDMS and left in a vacuum dessicator held at 10^{-4} Torr in the dark for 1 hour to transfer the patterns. All SEM images were collected using LEO Scanning Electron Microscope with a field-emission gun operating at 1-22kV. Images were obtained in secondary electron detection mode. These operating conditions were applied to reduce the sample damage and the charge builds up, while producing high-resolution images of stamp and the PDMS substrate surfaces.

Results and Discussion

The transfer of metal from a stamp created by EBL to a PDMS substrate allows the mass production of regular arrays as SERS substrates. It also presents an opportunity to explore nano-particles' proximity via the elastomeric properties of PDMS, i.e., by the stretching and relaxation of the PDMS substrate, along with facilitating the rapid generation of homogeneous SERS substrates. Several approaches were attempted and, with continued modifications to these approaches, a method for direct nTP from an EBL stamp to PDMS substrates was developed to create high performance SERS substrates.

Initial Results for Macro-Transfer Printing: The first step in this project was to optimize the conditions for μ -transfer printing (μ TP) before attempting to transfer to the nanoscale. This was done by vapor depositing 100 nm Ag through a macro mask and onto a Si wafer to create a stamp with silver μ -pillar arrays. The PDMS substrate was brought into contact with the Si wafer and a pressure of 500g/cm^2 was applied to transfer the pattern. The top image in Figure 3.5 shows the white light image of the mask and its dimensions, while the Ag discs transferred onto PDMS are shown in the bottom image. One can see that there are some changes in the dimensions of the Ag discs which may be due to the high pressure applied in the process. μ TP was accomplished using a large piece of Si wafer as a stamp. The next step was mimicking the conditions of the stamp created with EBL. When attempts were made to use ma-N 2403 as a photo-resist to create μ -pillars, undistinguished pillars were obtained in all trials.

The stamp was created using an SU-8 photo-resist (not an electron beam resist and used here to create distinguished μ -pillars) and it consisted of square pillars with the dimensions of roughly $480 \times 480 \mu\text{m}$. These pillars were then coated with 35 nm Ag, and subsequently, the stamp was used to transfer discs onto the PDMS substrate. Only a few of the discs were transferred; one such disc can be seen in Figure 3.6. The reason for the transfer of only a few discs may be attributed to the surface needing treatment with fluoro-chlorosilanes to alter the hydrophobicity of the surface and act as a releasing agent. When this experiment was repeated with an SU-8 photo-resist stamp treated with Heptadecafluoro-1,1,2,2-tetrahydrodecyl trichlorosilane, none of the discs were



Figure 3.5 (Top) White light illumination of the original mask with dimension of squares being $200\ \mu\text{m} \times 200\ \mu\text{m}$. The bottom is the white light illumination of the macro-Ag pillars transferred onto PDMS.



Figure 3.6 White light illumination of 35 nm Ag disc transferred from SU-8 stamp onto PDMS substrate. Ag disc is roughly 480 μm x 480 μm .

transferred. A possible explanation for the different result is that SU-8 consists of epoxy base with methyl and aromatic groups. Additionally, this fluorosilane reacts with the free silanol group on the surface of the stamp to form a surface with low interfacial energy, but the chemical structure of SU-8 resist is not like the Si wafer surface.

Initial Results for Nanotransfer Printing: In order to successfully complete the nTP process, certain initial conditions were necessary: the depths of the relief (or pillars) had to be more than 250 nm for patterning metal film with thickness less than 75 nm [228]. The vertical, collimated flux of metal from the source ensures uniform deposition only on the raised and recessed region of relief (pillars) [228], meaning that the stamp should be oriented perpendicular to the Ag boat during the physical vapor deposition to avoid deposition on the sidewalls of the relief (pillar).

A series of preliminary experiments in the nanoscale were performed using ma-N 2403 resist stamp with nano-pillars of different structures such as squares, hexagonal, ellipses, and stars. The pillars were vapor deposited with 70 nm Ag. After the nTP process, it is evident from the scanning electron microscope (SEM) micrographs of the PDMS substrate and the EBL stamp in Figure 3.7(a) and (b) that Ag in between the pillars was transferred (negative of the stamp). The SEM images led to a conclusion that the process of bringing the stamp and the substrate into contact with one another was not efficient and/or the applied pressure (weight) was not optimized. Another possibility is that three-dimensional discs or structures were transferred because the Ag thickness was

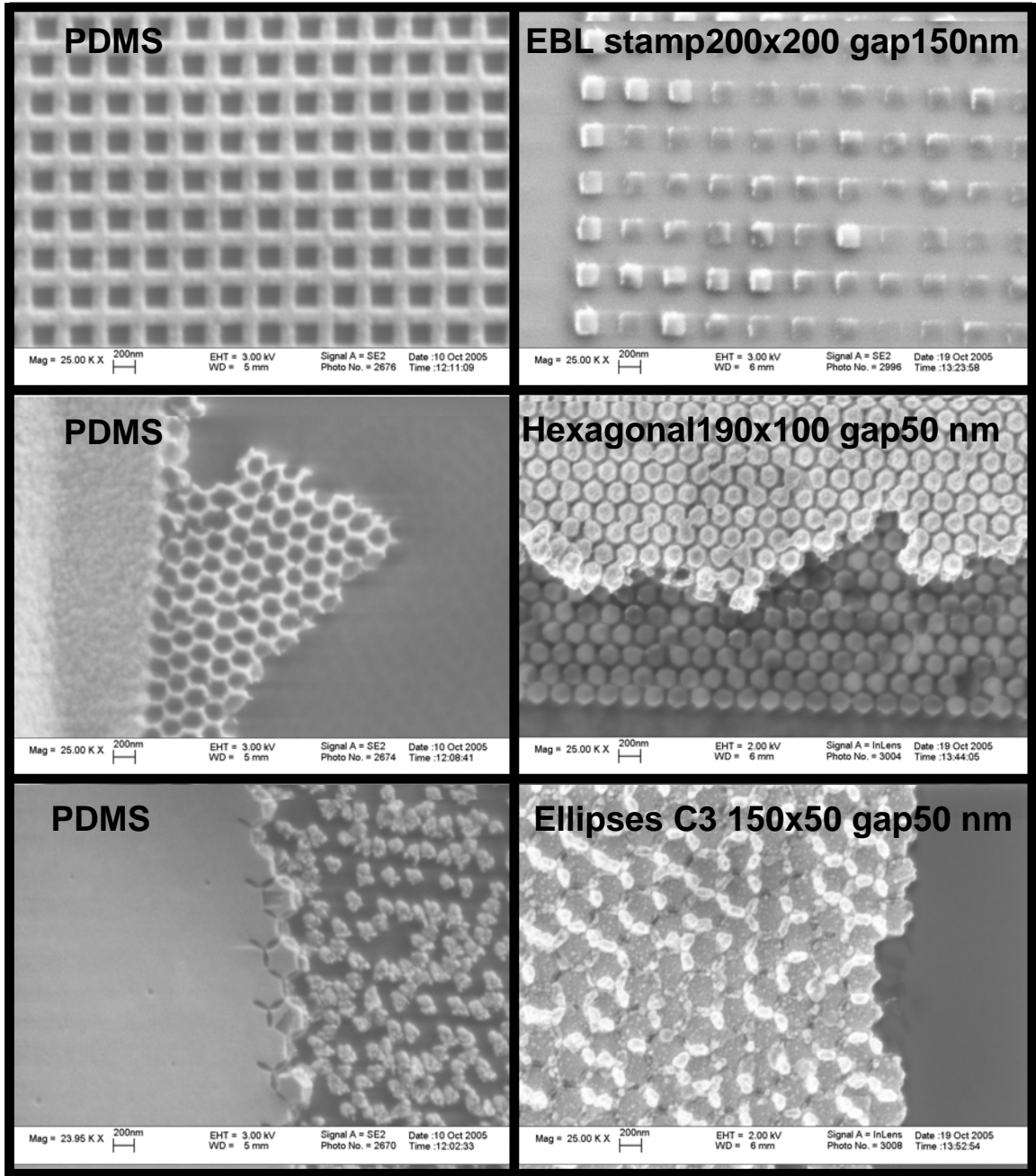


Figure 3.7(a) Scanning electron micrographs illustrating the PDMS substrate and the resist stamp after the nTP process using Ag.

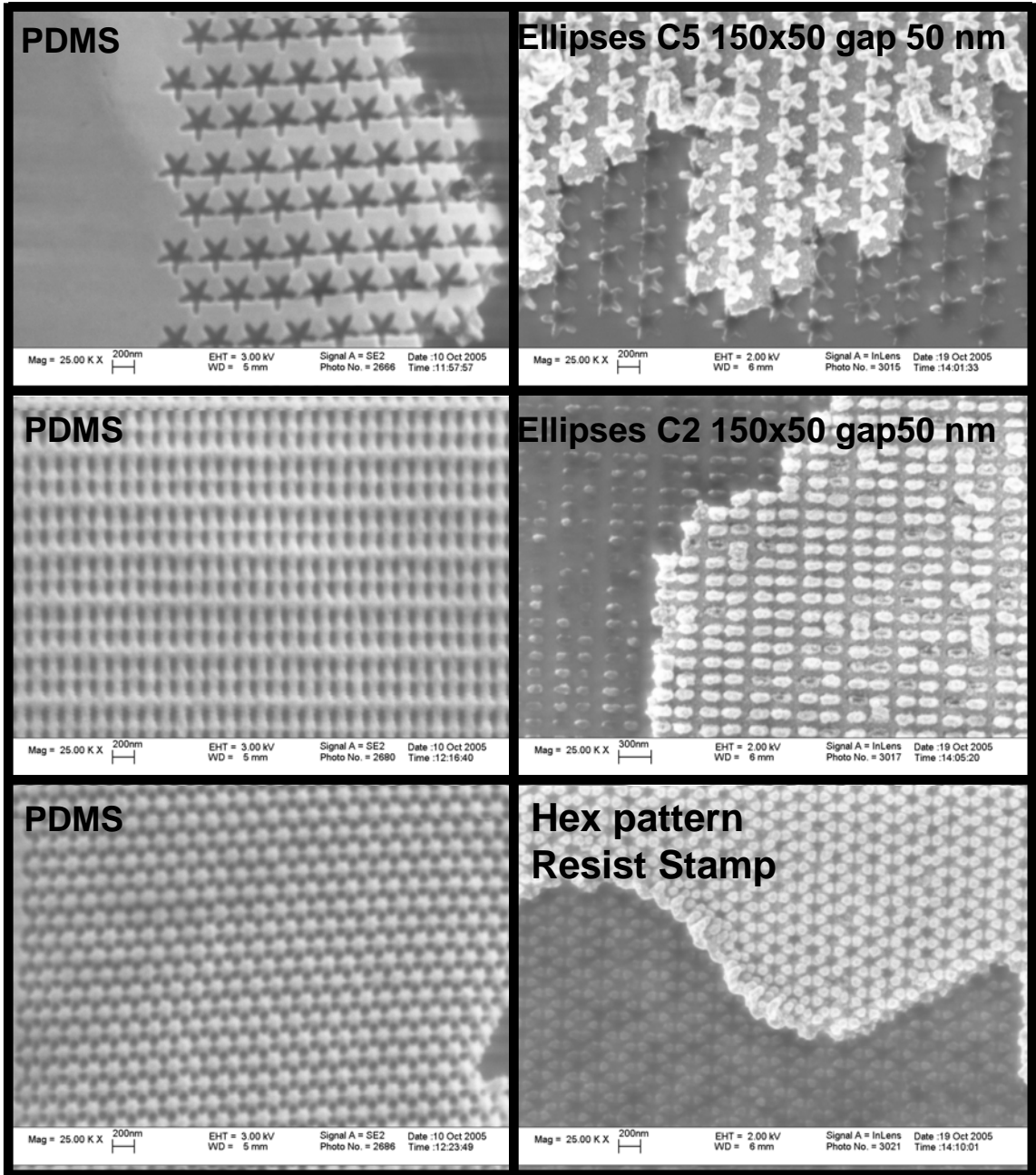


Figure 3.7(b) Scanning electron micrographs illustrating the PDMS substrate and the resist stamp after the nTP process using Ag.

too high and the flux of the metal was not collimated or oriented perpendicular to the stamp during the vapor deposition step.

In a different attempt, two stamps were vapor deposited with 15 nm and 25 nm Au to see if the type of noble metal or thickness variation would make any difference. Upon investigating the PDMS substrate and stamp after the transfer process, SEM images proved that a continuous film was being transferred, as opposed to isolated pillars (see Figure 3.8). Again, these results led to the conclusion that the process of bringing the stamp and substrate into contact and the attendant applied pressure were not optimized. Furthermore, this lack of optimization was the main reason for the inability to transfer isolated discs.

Initial Approaches to Control Pressure for nTP: In a subsequent attempt, a mask that had a width of 200 μm was created to cover the whole column of patterns. This was done so that a phase of polymer or metal could be deposited on the regions surrounding the patterns to create something like a groove or a ledge and that when pressure was applied, only isolated discs would be transferred instead of continuous film. The first task was to test if any material would diffuse under the mask and onto the patterns during the physical vapor deposition step.

Figure 3.9 shows the white light illumination images of the mask and the EBL stamp after 60 nm of Ag was vapor deposited and removing the mask without any indication that Ag diffused under the mask. The mask was then aligned on the patterns using the CCD camera of the LabRam and 250 nm Cal-4 were vapor deposited on the regions surrounding the patterns. The mask was

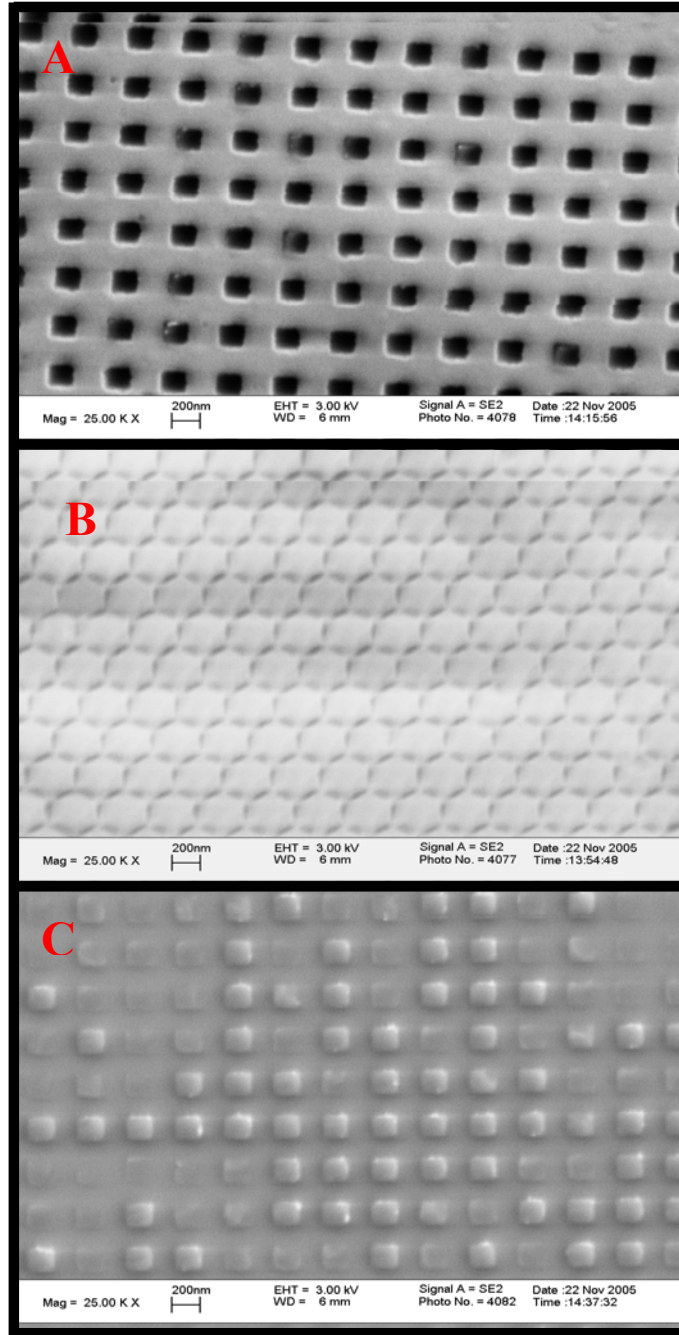


Figure 3.8 Scanning electron micrographs of: A) 15 nm transferred Au onto PDMS B) Shows 25 nm Au transferred onto PDMS C) Shows the resist stamp after the transferring process.

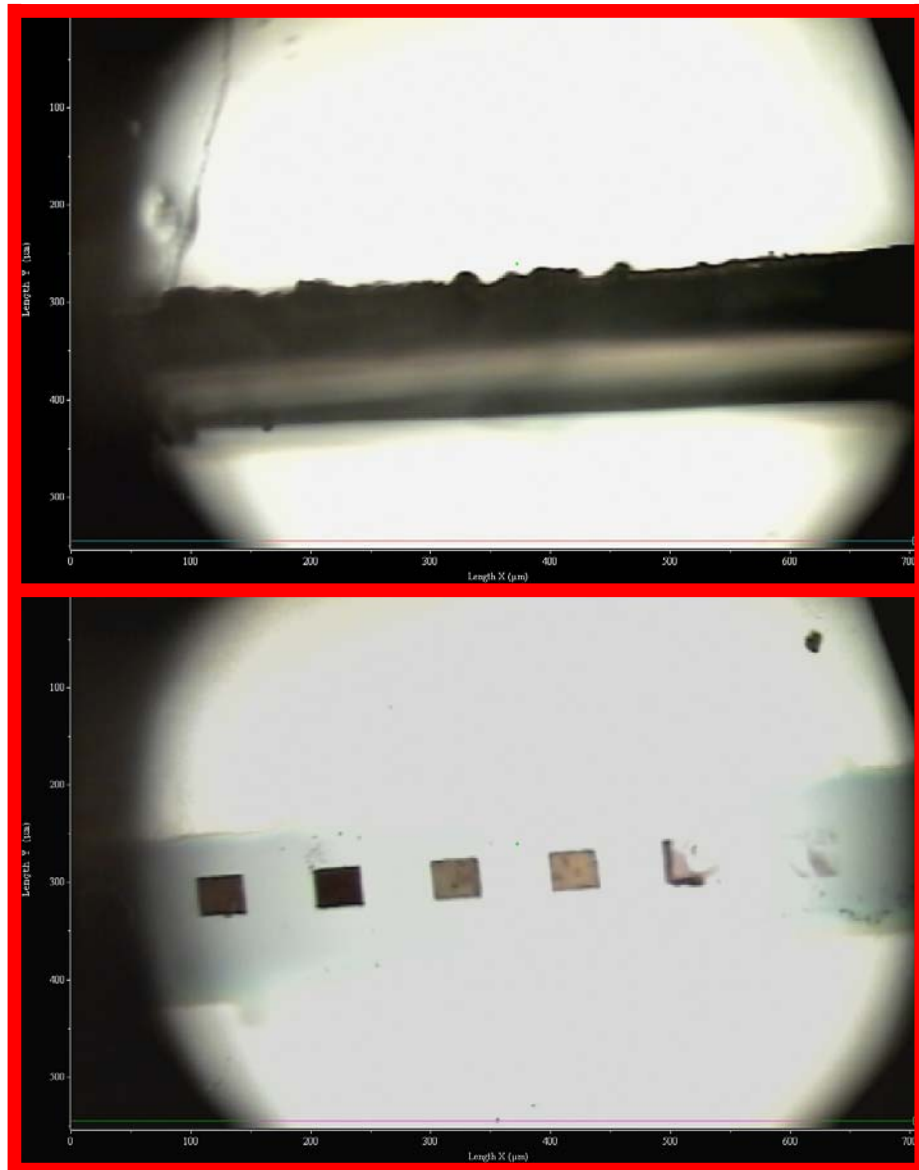


Figure 3.9 White light illumination showing: (Top) The mask covering the patterns. (Bottom) Shows the patterns after depositing 60 nm Ag and removing the mask.

then removed and 70 nm Ag was vapor deposited on the patterns. After the nTP was completed, SEM images of the PDMS substrate (seen in Figure 3.10) showed that none of the discs were transferred; the white light illumination and SEM images of the stamp also showed that traces of Cal-4 phase had diffused underneath the mask. In the next attempt, a ledge was created using Ag instead of a polymer phase. In this case, 70 nm Ag was deposited first and then the mask was used to cover the patterns where 200 nm Ag had been deposited again to act like a ledge during the transfer process. The stamp and substrate were brought into contact together slowly with the usage of a rod (diameter of 3/64 inches) attached to four split shots (a total weight of 20 g was applied to the 1 cm² surface). White light illumination from the CCD camera images showed no evidence that any patterns were transferred. Figure 3.11 shows these images of the stamp and PDMS substrate.

Initial Approaches to Overcome the Adhesive Nature of the Resist: Despite the various attempts at transferring the discs, there was little success in doing so. One of the main reasons attributed to this transfer problem was the adhesion of the resists. Thus, in another attempt, 70 nm Ag was vapor deposited through a mask onto cured and developed ma-N2403 resist to determine if any pattern would be transferred; as with previous attempt, none of the patterns were transferred. It then became clear that Ag has more affinity towards the resist, even when the temperature was raised to 40 °C during the transfer process. The same results were also obtained when an attempt was made to fluorinate the surface of the resist with the releasing agent Heptadecafluoro-1,1,2,2-

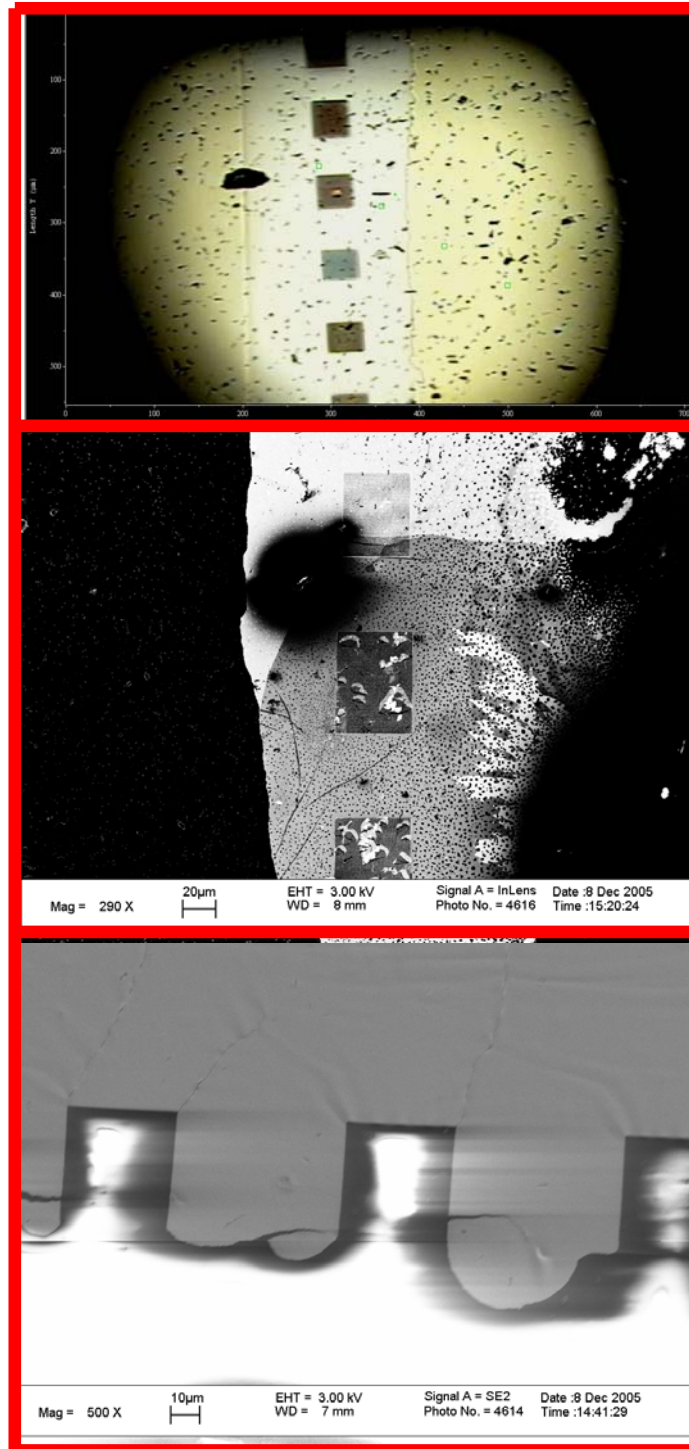


Figure 3.10 (Top) Shows the white light illumination of the stamp after depositing Cal[4] and before the transfer process. (Middle) Shows SEM image of stamp after the transfer process. (Bottom) Shows SEM image of PMDS after nTP.

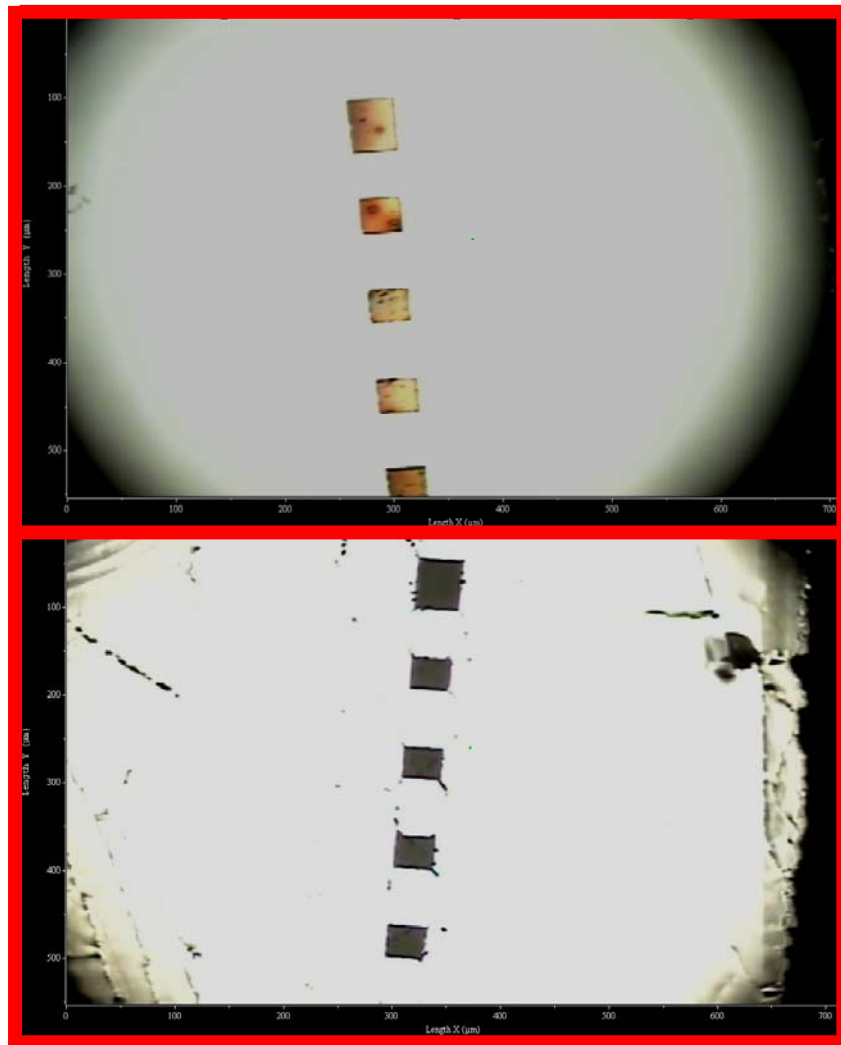


Figure 3.11 (Top) Shows white light illumination of the stamp (200nm Ag was deposited as a ledge) after the transferring process, where there is no indication of silver nano-discs was transferred. (Bottom) Shows white light illumination image of the PDMS substrate without any indication that Ag nano discs are being transferred.

tetrahydrodecyl trichlorosilane. Trying to investigate the chemical composition of the resist was not an easy task, since there was little information provided by the manufacturer (based on the manufacturer's information, the resist is a methacrylate).

Examination of the resist structure (shown in Figure 3.12(a)) suggests that the Ag will be more attracted to the resist as Ag is vapor deposited since Ag is known to interact with olefin. As a result, several attempts were made to investigate the Ag affinity to the resist. In one attempt, a 10-20 nm hydrophobic layer such as squalane was deposited on the resist before depositing the 70 nm Ag and still, no pattern was transferred. In another attempt, the thickness of the deposited squalane was increased to 50 nm to ensure the coverage of the resist, but none of the discs were transferred. A third attempt involved the use of a different phase, Poly-ethylenimine (PEI), but the results were the same. The failure to transfer discs under these conditions may be attributed to either squalane diffusing into the resist or Ag having an affinity to squalane. The resist was then covered with metal having a low affinity to Ag. In the first trial, 22 nm Al was initially vapor deposited on the resist stamp, followed by 70 nm Ag; the transfer process was carried out on the macroscale first to determine the performance of this method. Figure 3.12 show the results of the first trial where Ag discs were transferred from the resist stamp onto the PDMS substrate with some traces of Al (though most of it was left on the stamp). This trial was repeated to test the reproducibility of this method and showed positive results, indicating the method was promising in the nanoscale.

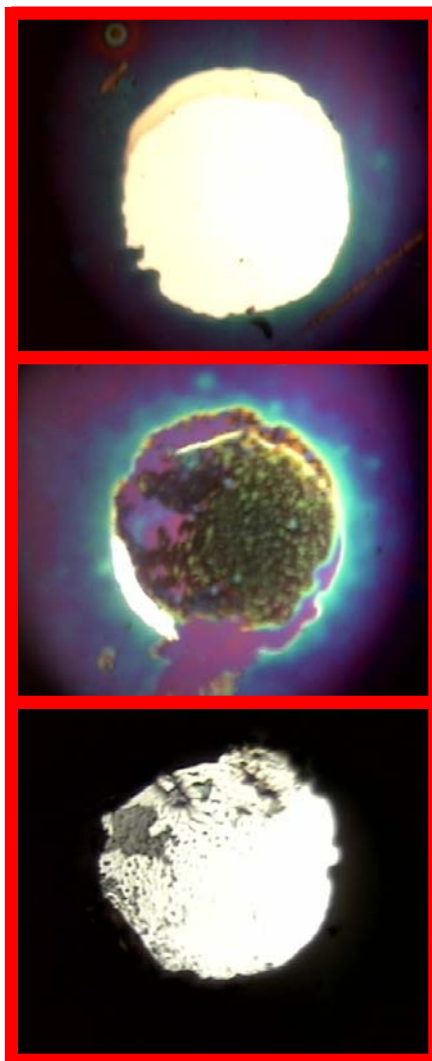
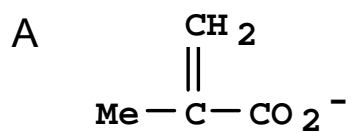


Figure 3.12 A) Shows chemical structure of methacrylate (ma-N2403) resist. The top white light illumination image shows the resist stamp on macroscale before the transfer process. Middle image shows the stamp after the transfer process and the Al layer can be seen. The bottom image shows Ag disc on PDMS substrate with small amount of Al being transferred at the same time.

The work on the nanoscale started by vapor depositing Al, then Ag onto the EBL stamp; the stamp was used immediately afterwards for the nanotransfer process to prevent and minimize the oxidation of the sample. SEM images of the PDMS substrates in Figure 3.13(a) and (b) showed in two separate trials, that the negative of the patterns was transferred without any distinguish discs being transferred.

The next proposed approach was to create the squares and hexagonal wells with EBL. This means that ideally after developing the patterns, one would get wells that were free of the ma-N2403 resist adhesive. Figure 3.14(a) shows the EBL stamp of the square wells pattern (instead of discs). These EBL stamps were used for the nanotransfer process using the same protocol of depositing 70 nm Ag. A small region with an area of approximately $5\ \mu\text{m} \times 2\ \mu\text{m}$ of distinguished square nano-discs was transferred and can be viewed in Figure 3.14(b). The transfer of the square discs was a promising sign and the next step was to improve the efficiency of the process in order to transfer large areas for SERS application.

After several trials, the reproducibility of this approach was still not sufficient enough and the SEM images shown in Figure 3.15(a) confirmed that Ag was adhering to the traces of resist and nano-discs were not transferring because of an inefficient developing stage. The developing stage of the pattern is a critical step in the transfer process, since overdeveloping patterns will be washed off and underdeveloped patterns reflect a stamp with several defects that cannot be used for nTP. Evidence of this problem can be seen in Figure 3.15(a) where

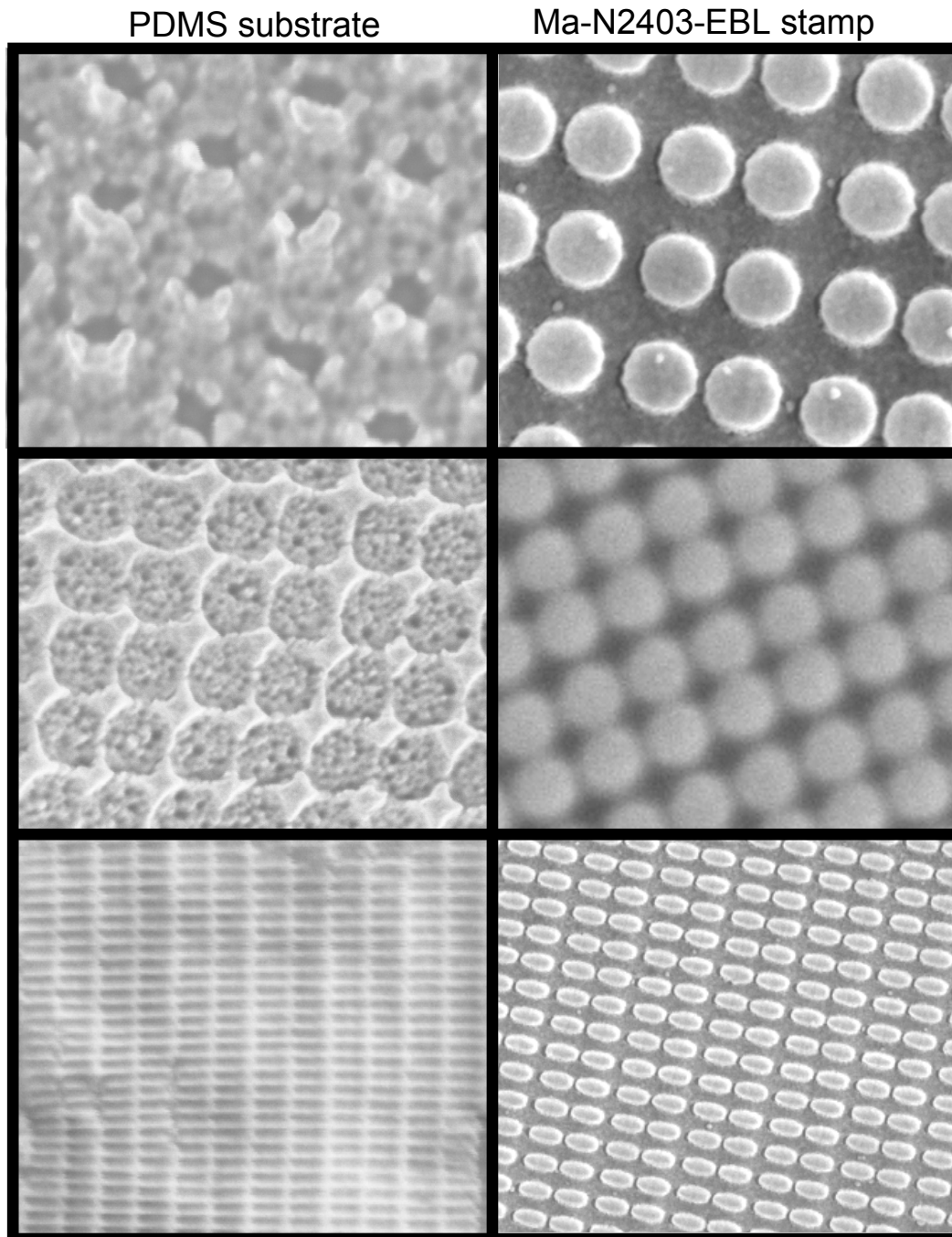


Figure 3.13(a) Scanning Electron Micrographs of the stamp and the PDMS substrate. Here, 15-20nm Al was used to cover ma-N2403 resist. The left column shows the PDMS substrate and the right column shows the resist stamp.

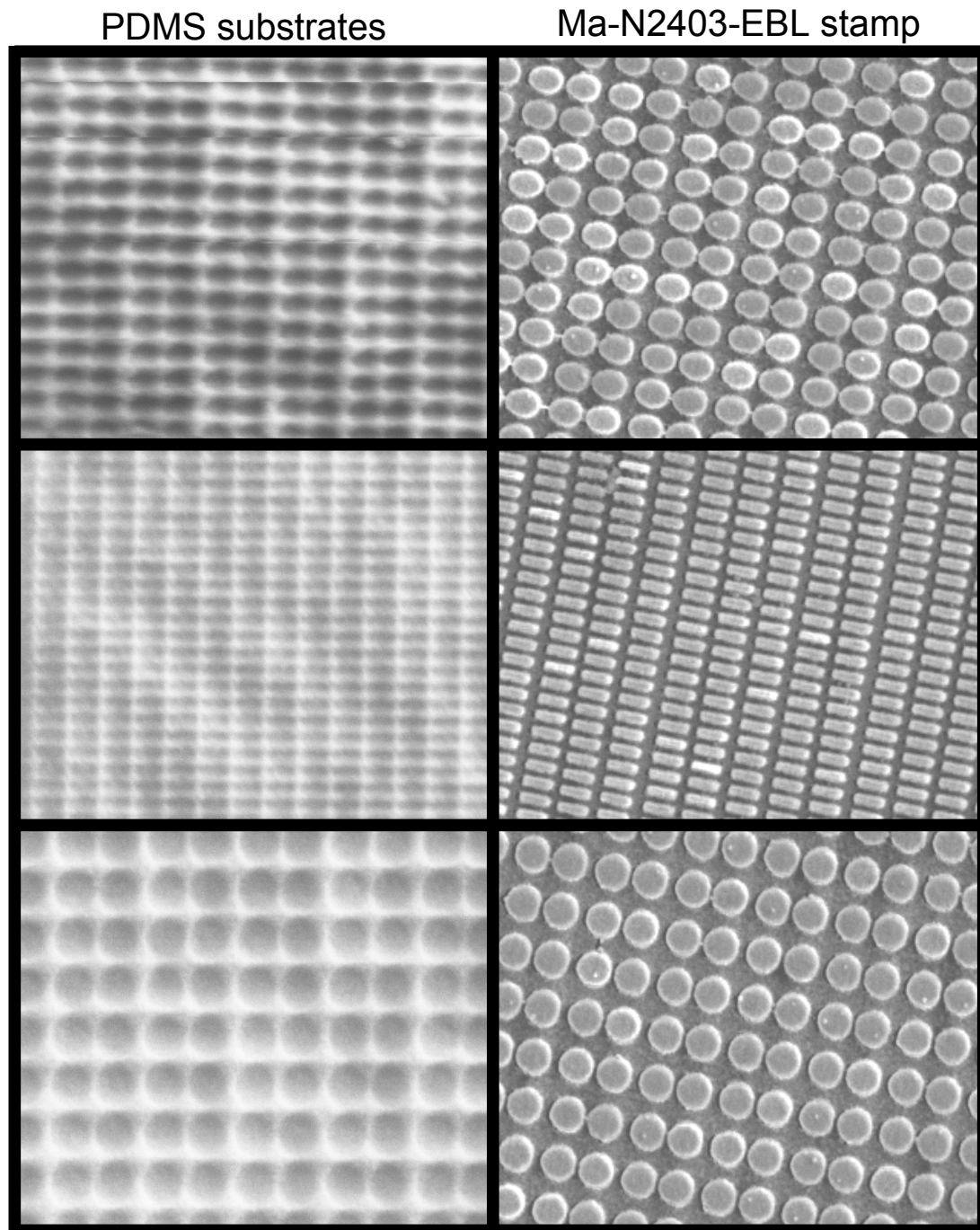
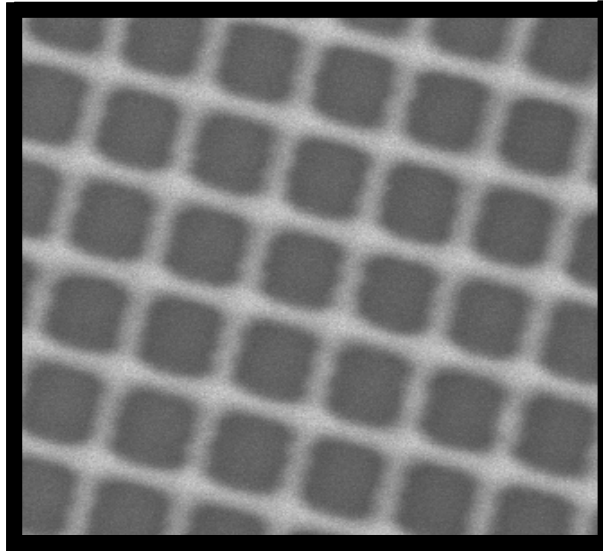


Figure 3.13(b) Scanning Electron Micrographs of the stamp and the PDMS substrate. Here, 15-20nm Al was used to cover ma-N2403 resist. The left column shows the PDMS substrate and the right column shows the resist stamp.

A



B

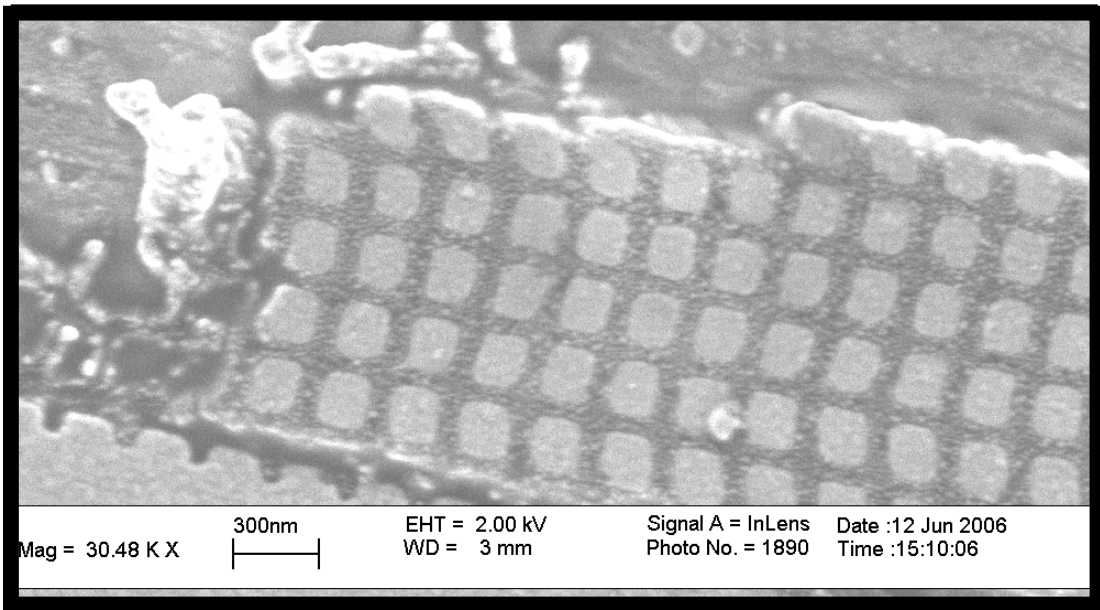


Figure 3.14 SEM micrographs of: (a) The negative ma-N2403-EBL stamp with square wells being created instead of discs. (b) The first nanotransfer trail with this stamp. This small area is where the Ag nano-discs were transferred onto the PDMS substrate.

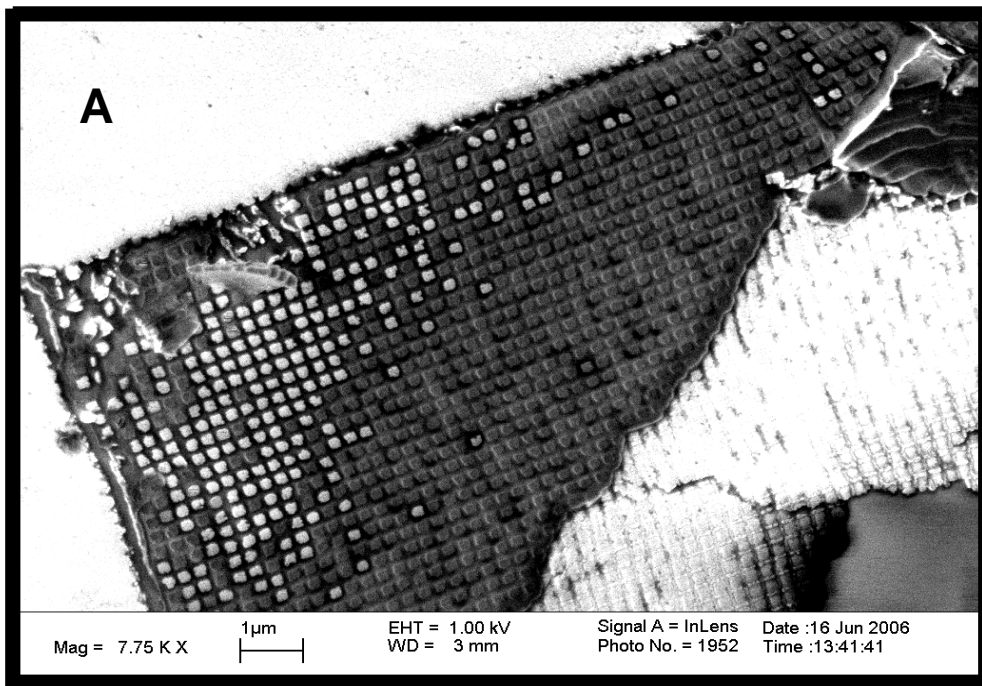


Figure 3.15 (a) SEM micrographs of PDMS substrate shows that some discs were transferred but not sufficient for SERS application (b) SEM micrographs of EBL stamp of ma-N2403 resist after developing the patterns.

traces of ma-N2403 resist are clear.

These results suggest that the next step should be covering the traces of ma-N2403 resist with Al. As such, 10 nm Al was first deposited to cover any traces of ma N2403 resist present in the wells and then 70 nm Ag was vapor deposited. Figure 3.16 clearly shows that wells were indeed transferred, as opposed to distinguished discs. This may have occurred because the Al particles were large in size and preferred the wells, instead the bottom of the wells. Based on the SEM, Al particles maybe agglomerating during the deposition step which could explain why Al-Ag are transferred as one unit, leading to Ag on the wells being transferred and not discs.

Since the previous approaches provided undesired results, a flowable, inorganic polymer, hydrogen silsesquioxane (HSQ) negative electron beam resist was used [79-82]. The decision to use this resist was motivated by two schemes for the chemical structure proposed in the literature. In the first scheme, HSQ is described by siloxane-based polymer with structural formula of $H_2(SiO)_3$. Every Si atom is bound to three oxygen (O) atoms and one hydrogen (H) atom, with the exception of the terminal Si atoms. In the terminal Si atoms, one of the O bonds is replaced by an OH bond. During curing of HSQ, the polymer crosslinks by condensation of Si-OH groups to Si-O-Si bonds. As a consequence, a three- dimensional network of ladder structures is formed. The second scheme describes HSQ as caged oligomer structures that open during curing and forms a network structure by either conversion to silica or by rearrangement reaction without any change in the stoichiometry. The general

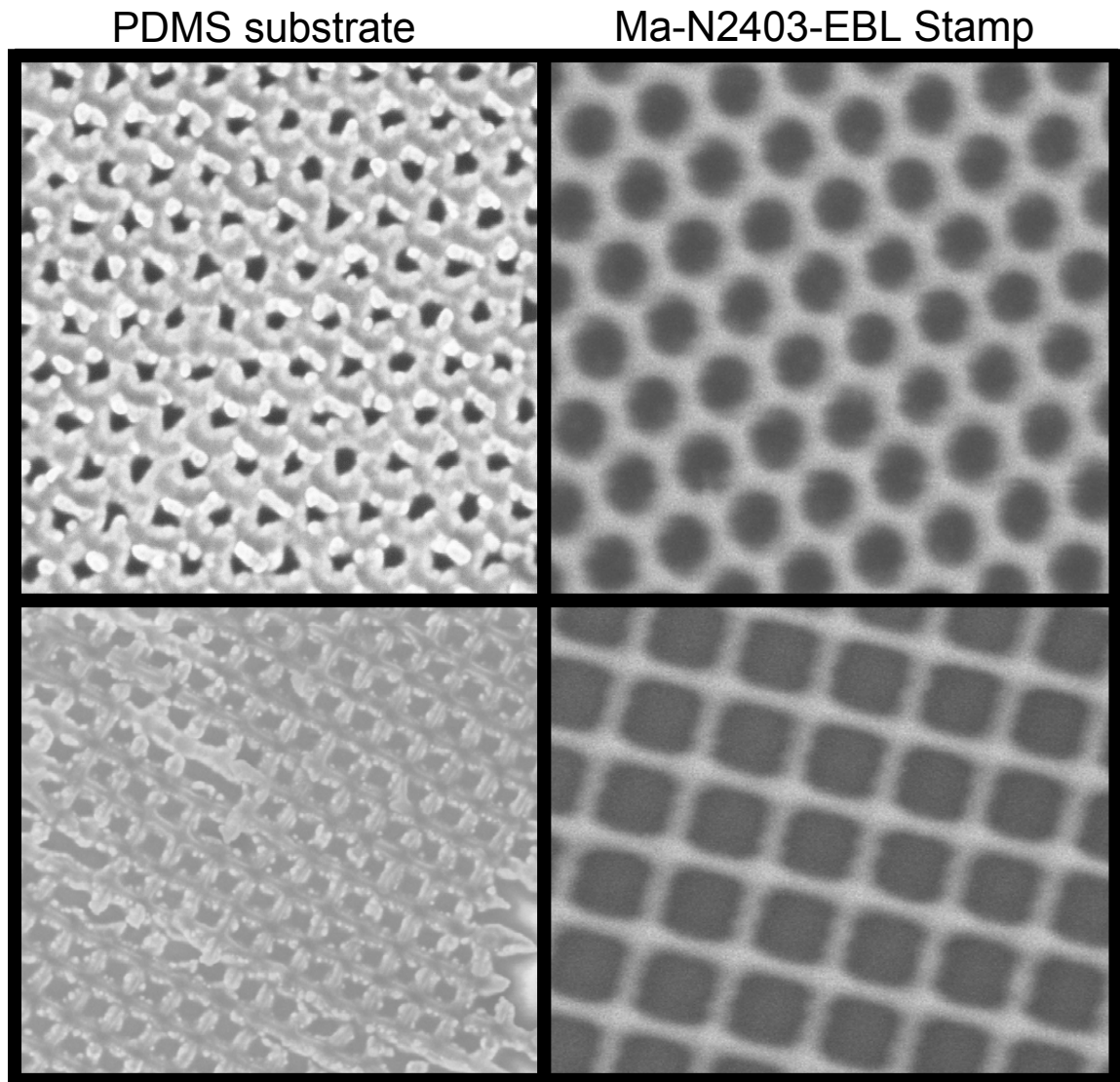


Figure 3.16 SEM micrographs of a nTP trial results with an EBL nano-wells stamp. Left column shows PDMS substrate after the nTP process, using 10nm Al to cover the traces of resist. Right column shows the EBL nano-wells stamp.

formula in this case is $(\text{HSiO}_{3/2})_{2n}$ [238-241]. These two descriptions of HSQ indicated that it would be a non-adhesive polymer that permitted the printing of Ag.

The first evaluation of the HSQ resist's effectiveness was an attempt to optimize the EBL exposure conditions such as the area exposure dose. In this trial, the thickness of the HSQ layer was 366 nm and the e-beam dose was ramped in the range of 700 to 1100 $\mu\text{C}/\text{cm}^2$. This yielded a series of patterns with approximately 3 μm spacing in x and y-directions and the wafer was divided into five areas with patterns that varied based on the different e-beam doses of 700, 800, 900, 1000, and 1100 $\mu\text{C}/\text{cm}^2$, respectively. SEM showed that different doses produced different patterns, but it was not clear whether the heights varied with the dose. Consequently, a preliminary nanotransfer printing was performed on the EBL pattern expose to 1100 $\mu\text{C}/\text{cm}^2$, under the assumption this dose would have pillars with the greatest height. As seen in Figure 3.17, SEM revealed a continuous film was transferred, instead of distinguished discs. These results provide evidence that HSQ resist is not an adhesive polymer; however, the transfer of the continuous film could be occurring because of the inadequate height of the pillars or because of the manner in which Ag particles interacted with the HSQ resist during vapor deposition. So Atomic Force Microscopy (AFM) was necessary to distinguish their height. The AFM results shown in Figure 3.18 confirmed that height of the pillars is approximately 15-20 nm, a height that is not adequate enough to transfer isolated pillars. The next experimental steps were to apply a higher EBL exposure dose and spin coat the silicon wafer with a thinner

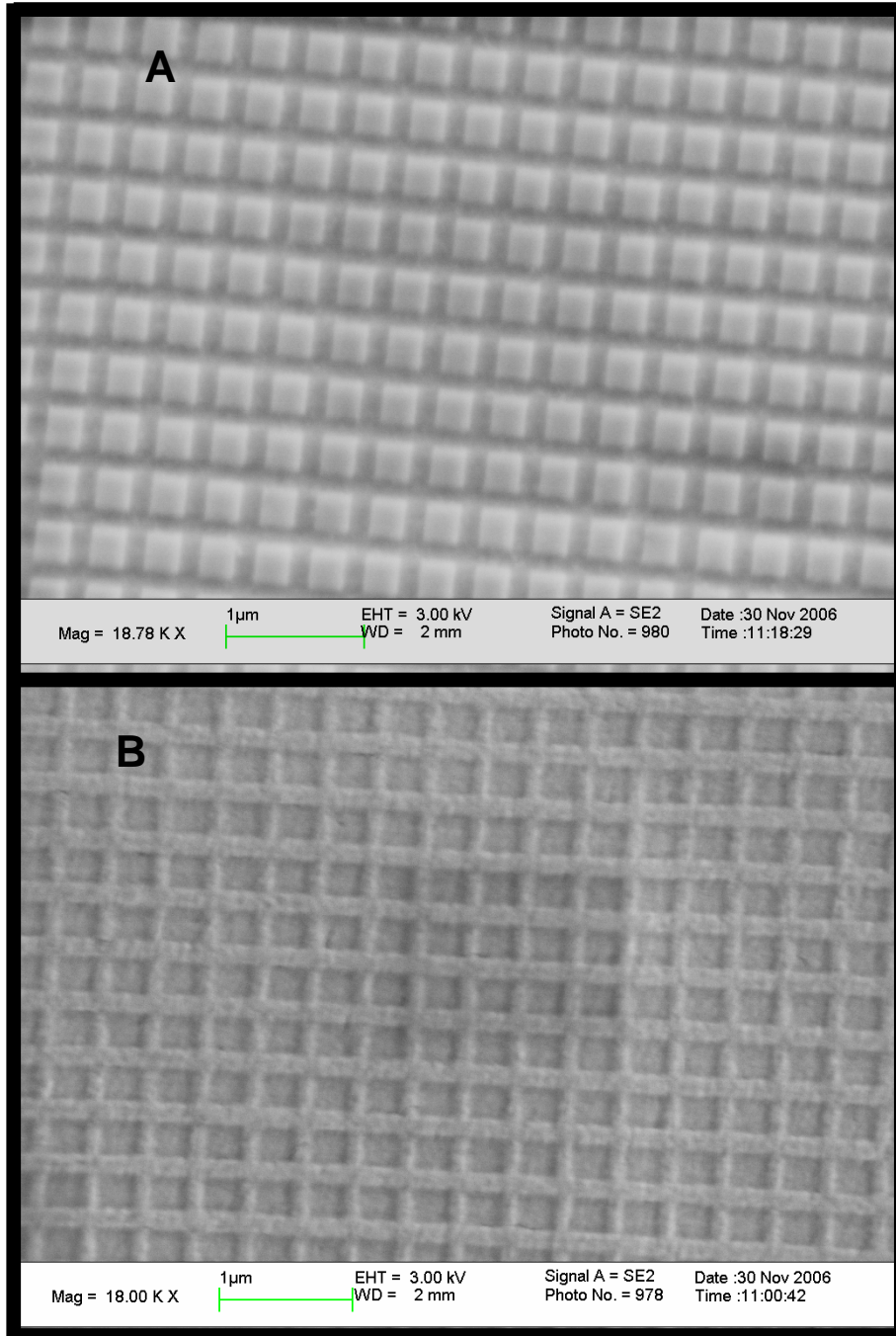


Figure 3.17(A) SEM micrographs of HSQ resist stamp that was exposed to 1100um/cm² EBL dose. (B) SEM micrographs of PDMS substrate exhibit a continuous transferred Ag film.

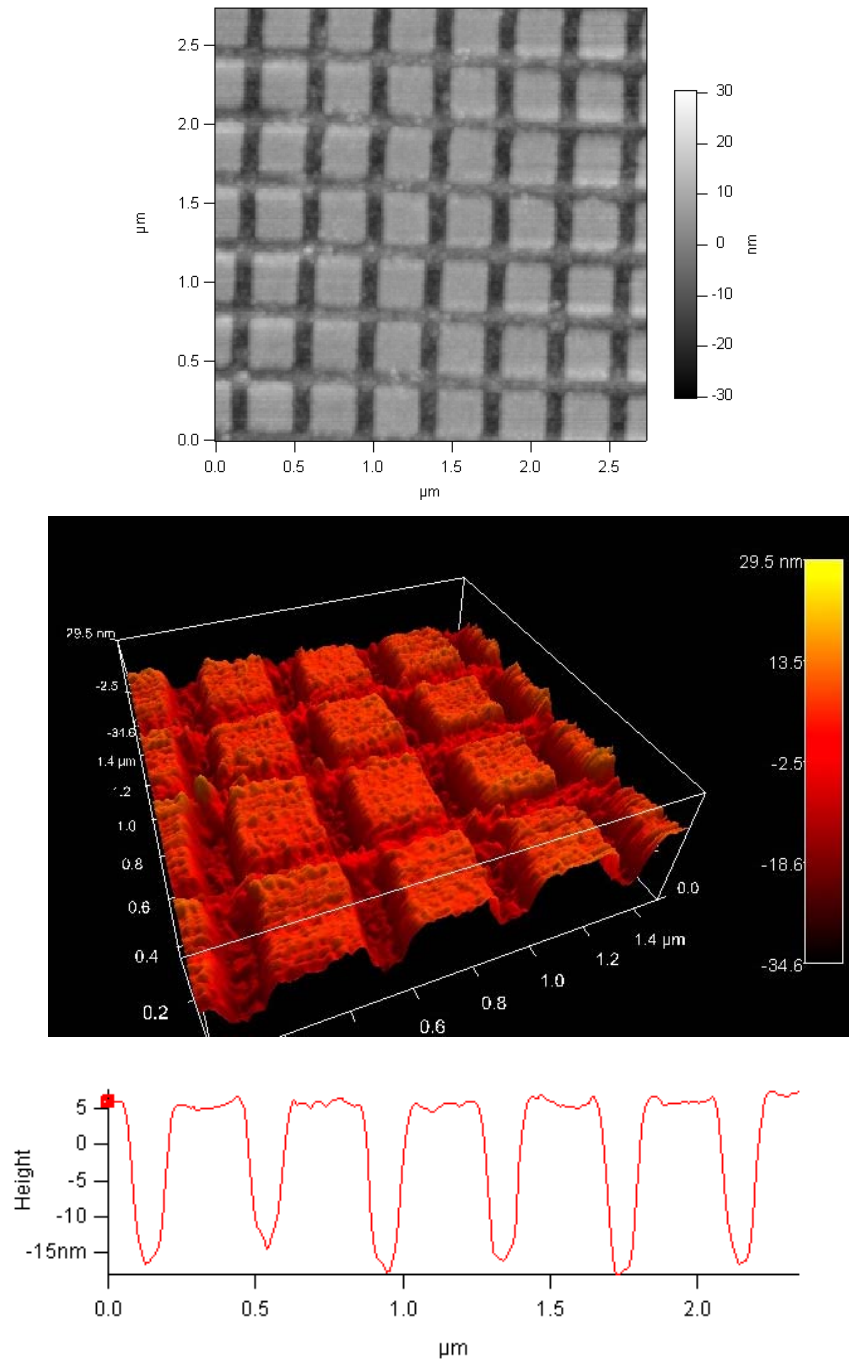


Figure 3.18 Atomic Force Microscopy (AFM) image of HSQ resist EBL stamp. Exposure dose was $1100\mu\text{C}/\text{cm}^2$. Top shows an area of $2.5\ \mu\text{m} \times 2.5\ \mu\text{m}$ that was mapped. Middle shows a three dimensional AFM image for the pattern. Bottom shows the height of the discs which was approximately 20 nm.

layer of HSQ resist to see if higher exposing resulted in higher pillars. The dose applied in this case was $1600 \mu\text{C}/\text{cm}^2$, while the thickness of the HSQ spin coat was 121 nm. The AFM results (please refer to Figure 3.19) revealed that the height of pillars is approximately 10 nm – initially, it was believed this height was a consequence of temperature during developing and the developer concentration.

The same experiment was repeated, with the exception of lowering the base dose applied to $700 \mu\text{C}/\text{cm}^2$. The AFM images seen in Figure 3.20 indicate the height of pillars as approximately 15-20 nm for this particular e-beam dose. Based on the height of these pillars, one can conclude that the patterns and the resist suffered from proximity effects from the electron beam. As mentioned in section 3.2, the proximity effect is one of the major limiting factors in EBL and it is manifested as the undesired blurring in the written circuit pattern from electron scattering in the resist; furthermore, the proximity effect imposes a severe limitation on the ultimate spatial resolution attainable by EBL.

In an effort to address the proximity effect, another base dose study was performed in which several lower doses were used to determine the optimum e-beam exposure dose. The exposure doses applied were 100, 150, 200, 250, and $500 \mu\text{C}/\text{cm}^2$, but all were developed at the same temperature $22.0 \text{ }^\circ\text{C}$ with same developer concentration. The measured height for each array is presented in Figures 3.21, 3.22, and 3.23 where the AFM images of the patterns and the measured height are shown. The greatest height accomplished was 80 nm when the exposure dose was in the range of 150 - $200 \mu\text{C}/\text{cm}^2$, a height that is not

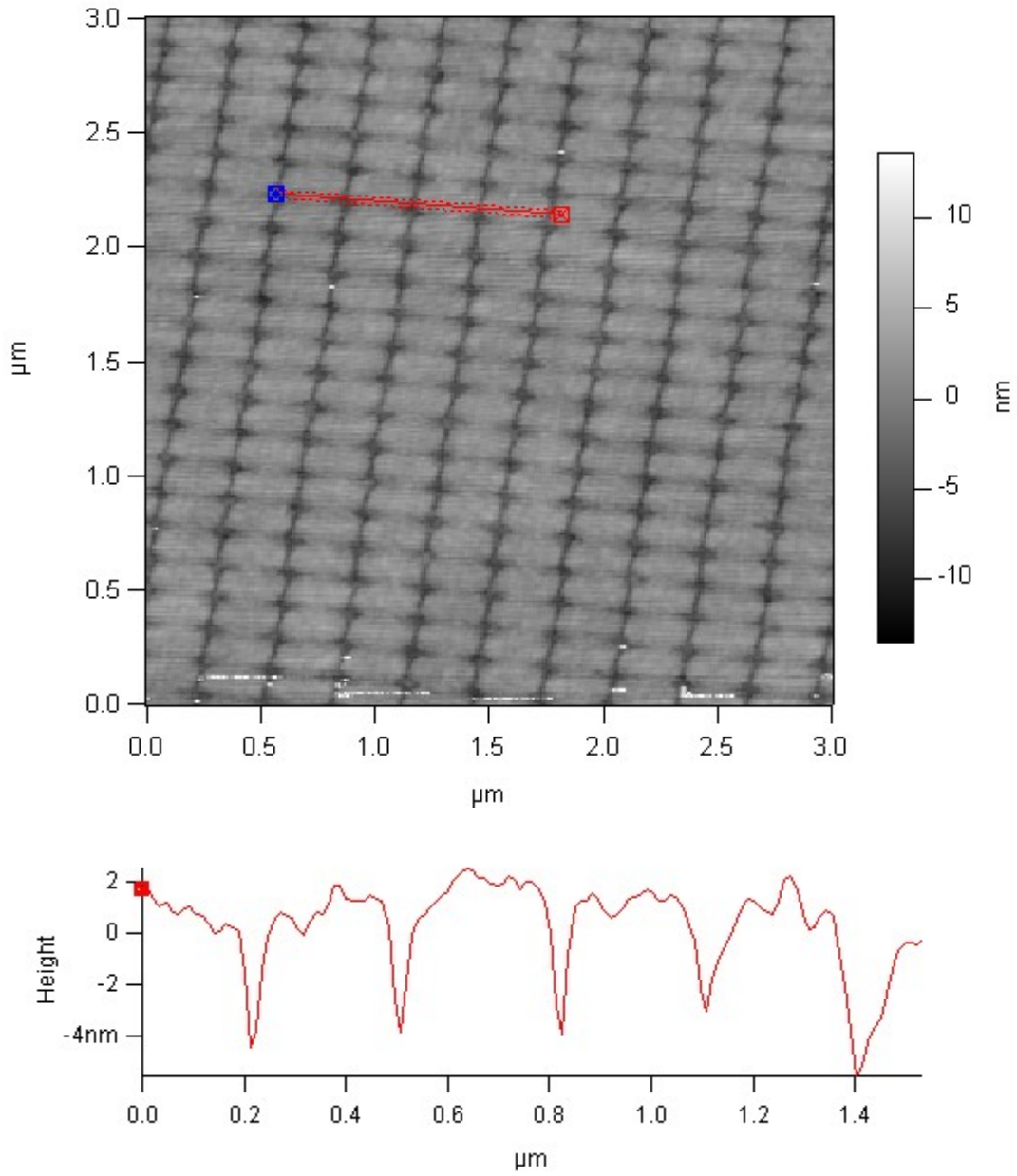


Figure 3.19 AFM image of HSQ resist EBL stamp. Exposure dose was $1600 \mu\text{C}/\text{cm}^2$. Top shows an area of $2.5 \mu\text{m} \times 2.5 \mu\text{m}$ that was mapped. Bottom shows the height of pillars which is approximately 10 nm.

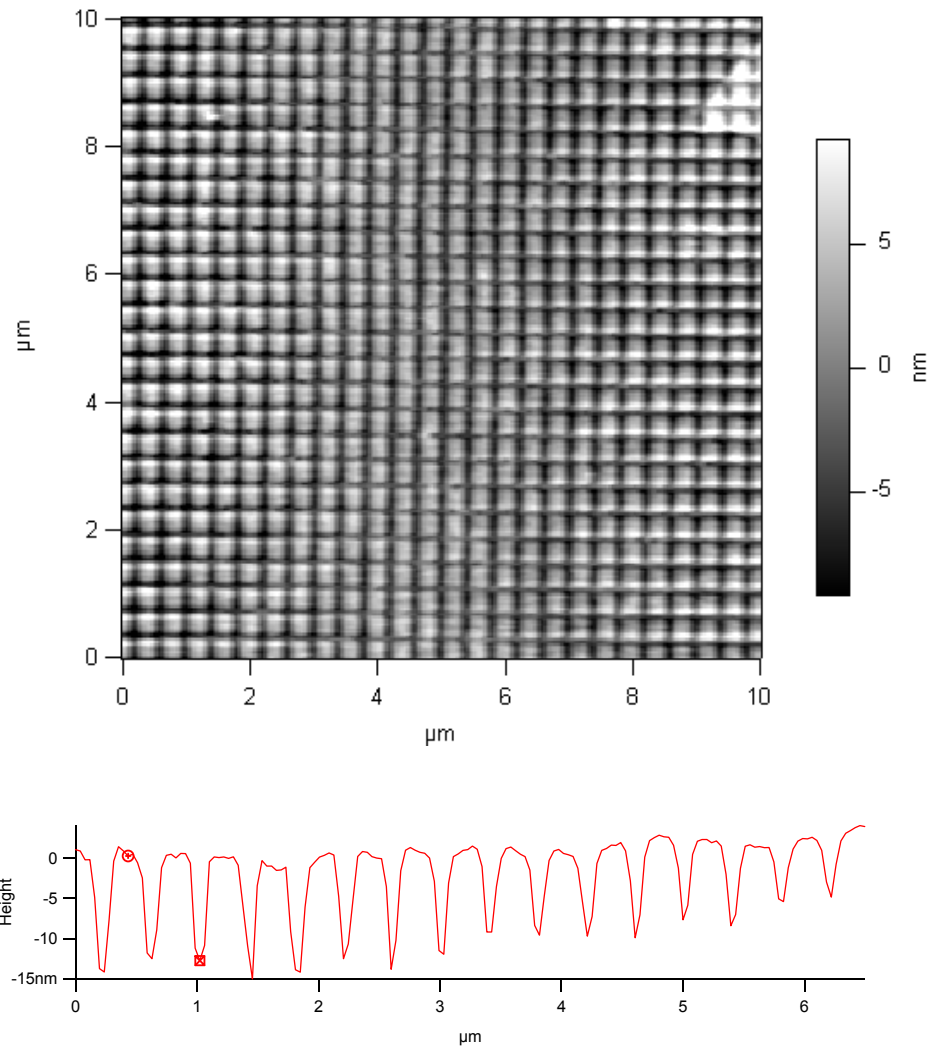


Figure 3.20 AFM image of HSQ resist stamp. Exposure dose was $700 \mu\text{C}/\text{cm}^2$ and the height of the pillars is approximately 15-20 nm.

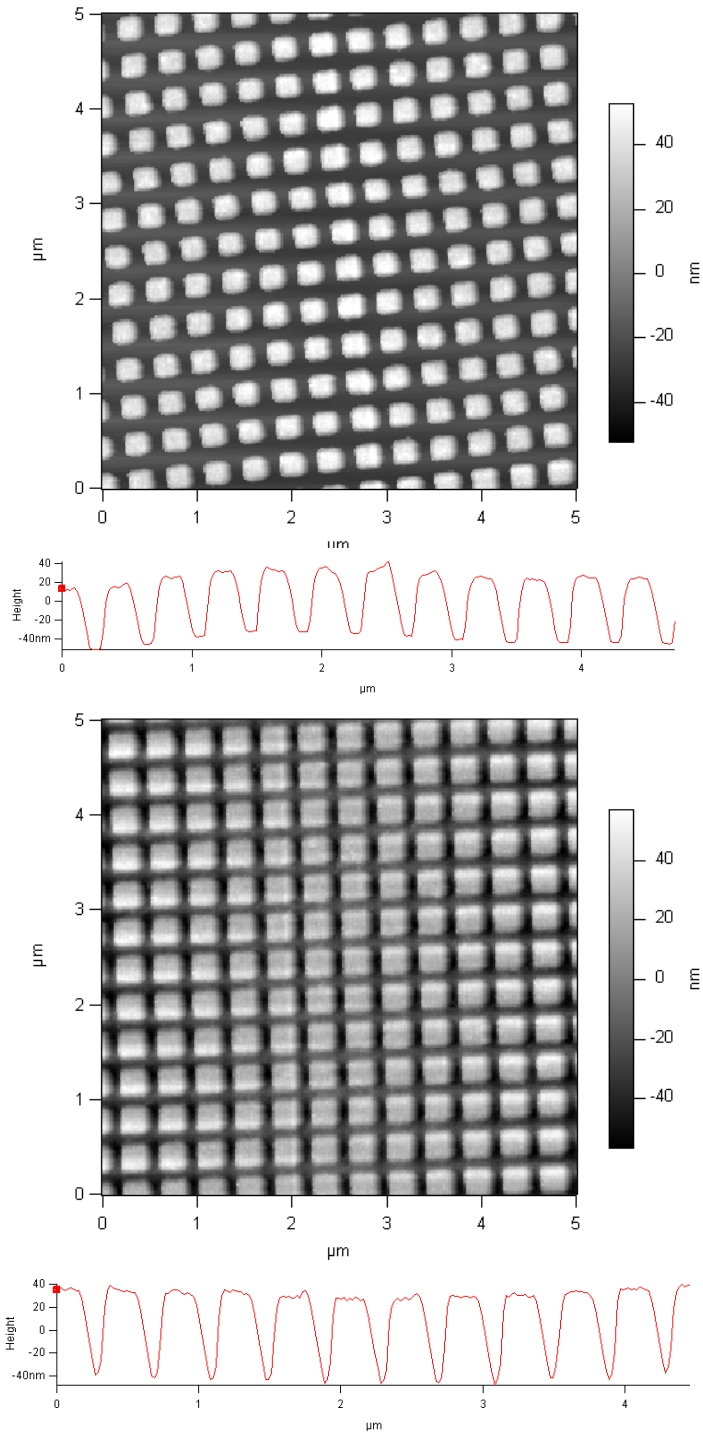


Figure 3.21 (Top) AFM image of HSQ resist stamp. Exposure dose was $100 \mu\text{C}/\text{cm}^2$ and the height of the pillars is approximately 60 nm. (Bottom) Exposure dose was $150 \mu\text{C}/\text{cm}^2$ and the thickness is approximately 80 nm.

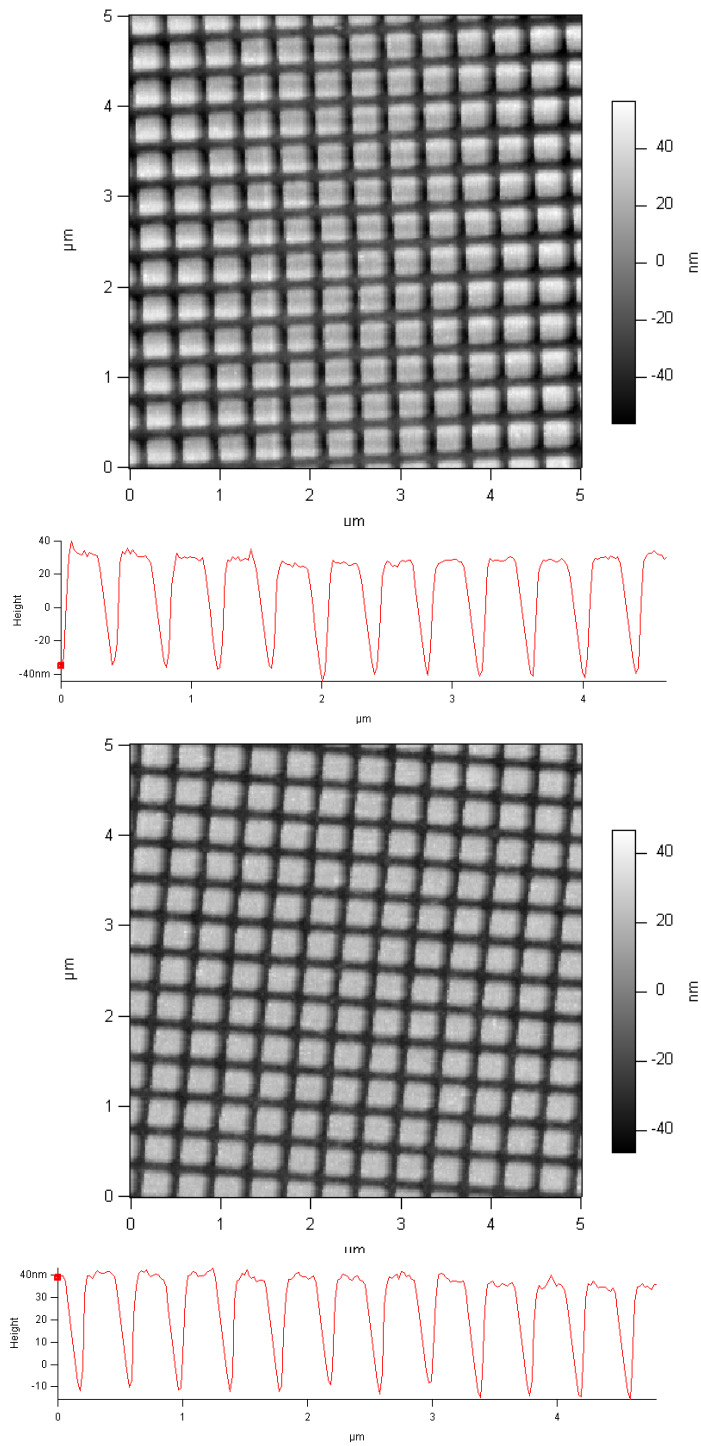


Figure 3.22 (Top) AFM image of HSQ resist stamp. Exposure dose was 200 $\mu\text{C}/\text{cm}^2$ and the height of the pillars is approximately 80 nm. (Bottom) Exposure dose was 250 $\mu\text{C}/\text{cm}^2$ and the thickness is approximately 50nm.

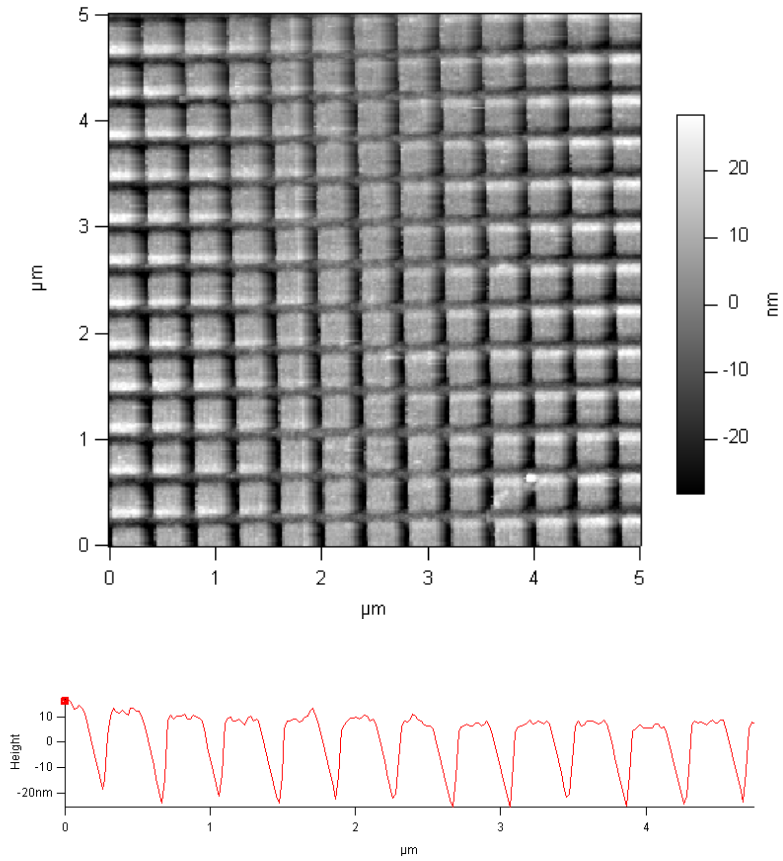


Figure 3.23 AFM image of HSQ resist stamp. Exposure dose was $500 \mu\text{C}/\text{cm}^2$ and the height of the pillars is approximately 30 nm.

sufficient enough to transfer isolated discs. Nonetheless, the EBL stamp with a pillar height of approximately 80 nm and $150 \mu\text{C}/\text{cm}^2$ dose was used for nanotransfer trial using 20 nm Ag. After nTP, SEM images seen in Figure 3.24 showed no evidence of transferred discs. The absence of transferred pillars could be explained by the interaction between Ag and the HSQ or a pillar height that is favorable to the formation of Ag continuous films during vapor deposition. Thus, it was concluded that under existing conditions of the HSQ resist and the desired feature size, transferring isolated Ag discs was not possible.

The last experimental attempt involved the use of various molecules to coat the adhesive surface of ma-N2403. Some of these phases were Heptakis(6-*O-tert*-butyldimethylsilyl-2,3-di-*O*-acetyl)- β -CD (H- β -CD) (was prepared using the method of Stoddart et al [237]) and 4-*tert*-Butylcalix[n]arene (Lancaster, Pelham, NH). These phases were chosen because they were studied in our group previously and were vapor deposited successfully [242-244].

The preliminary experiments were done in the macroscale and in the first attempt, 17-20 nm of each polymer were deposited onto two stamps that had ma-N2403 resist. 20 nm Ag were then deposited on these stamps and no discs were transferred. In the next trial, a different thickness (of the two phases) was used to determine if there were any effects on the nTP process. Initially, 30 nm of each phase were deposited on two ma-N2403 stamps, followed by 20 nm Ag. The results showed that a small region of the stamp coated with 30 nm H- β -CD had transferred. A 50 nm phase of H- β -CD was then deposited on ma-N2403 stamp, followed by 50 nm Ag. In this case, all the discs were transferred from the

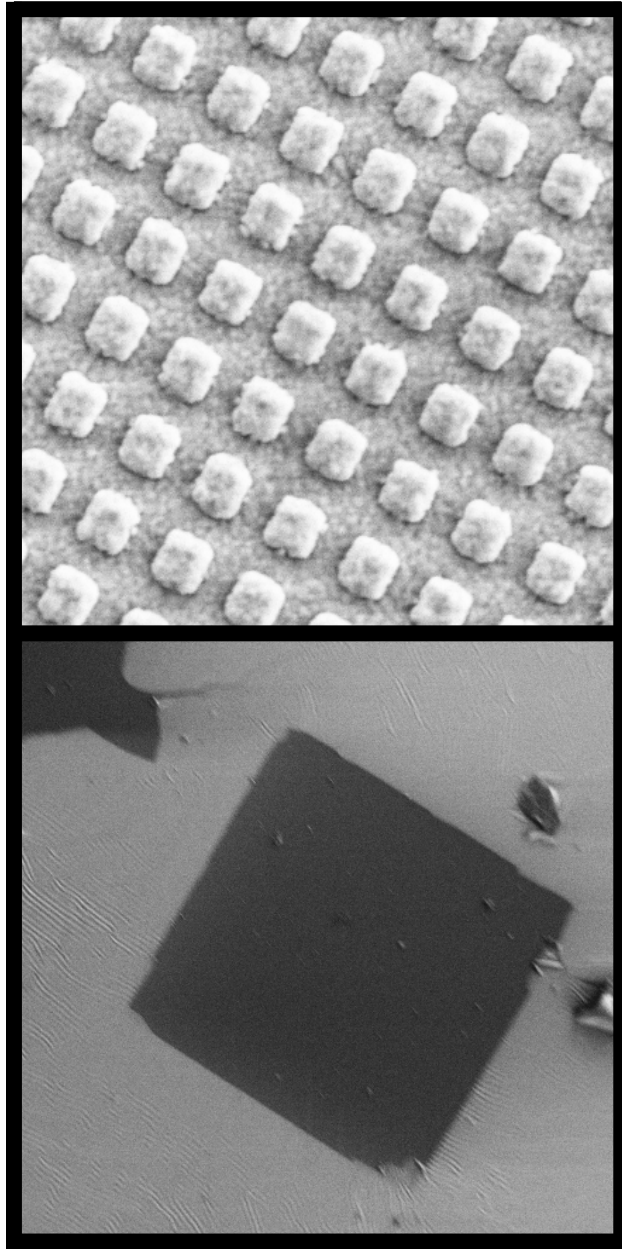


Figure 3.24 (Top) Shows SEM images of HSQ resist pattern where the exposure dose was $150 \mu\text{C}/\text{cm}^2$ and the height of the pillars is approximately 80 nm. (Bottom) Shows SEM image of PDMS substrate after the nanotransfer process and without any discs being transferred.

ma-N2403 stamp to PDMS substrate.

To examine the effect of the phase at the nanoscale, an ma-N2403 EBL stamp was vapor coated with 50 nm H- β -CD, followed by 50 nm Ag; the stamp was then used for the nTP process. Figure 3.25 shows the SEM images where Ag nano-discs transferred onto the PDMS substrate, though the discs were touching each other when the gaps between ellipses on the EBL stamp were 50 nm. Patterns that had a gap of approximately 300 nm were created with EBL and also tested for nTP process: results showed isolated nano-discs transferred to PDMS substrates and these discs can be seen in the SEM images in Figure 3.26(a). Preliminary SERS test show that these substrates are SERS active (please refer to Figure 3.26(b) when tested with 1×10^{-5} M Rhodamine 6G. Since the position of the discs is critical to ensuring there is no overlap, the next step in the experimental procedure is to refine the nTP process to eliminate contact between the discs transferred (by preparing EBL stamps with gaps of 100 and 200 nm between discs) and study their SERS performance and this is discussed in the following chapter.

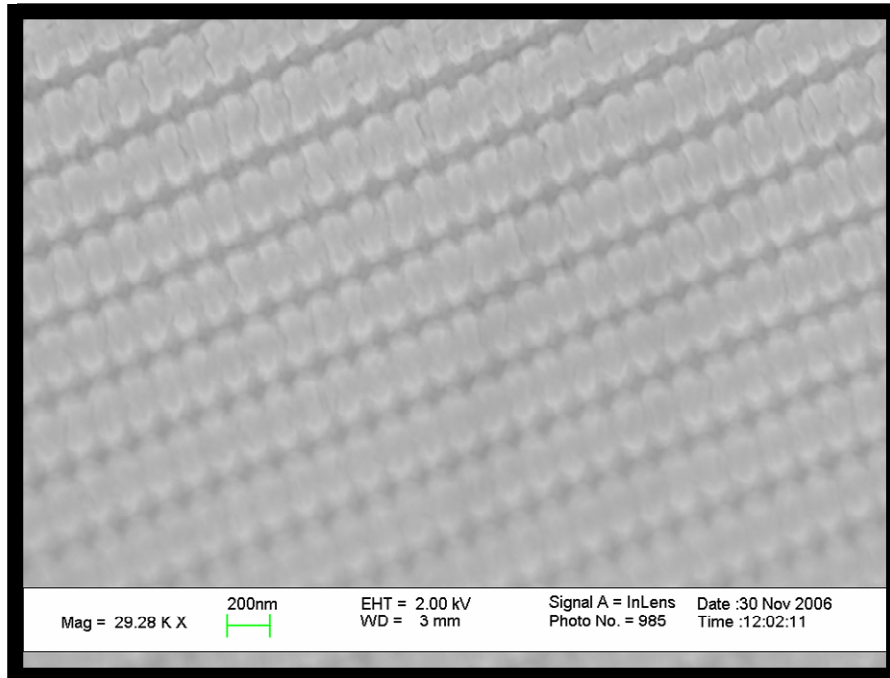


Figure 3.25 SEM micrographs image of PDMS substrate after the nTP trial. Ellipses, 100x250 nm in size were transferred from ma-N2403 stamp that was coated first with 50nm H-B-CD followed by 40nm Ag.

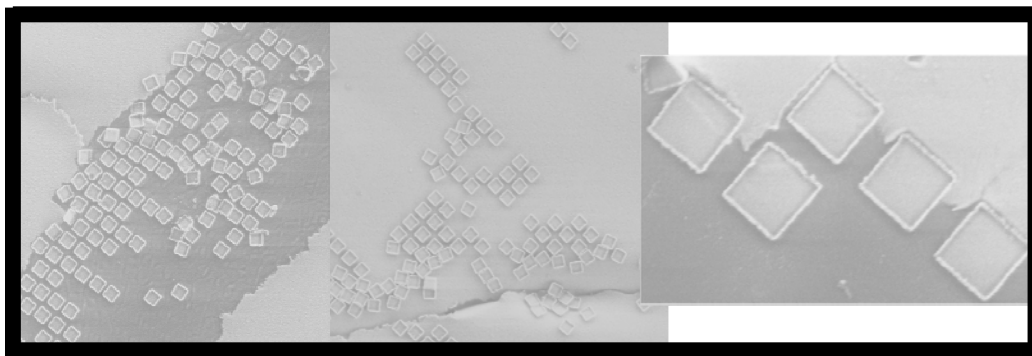
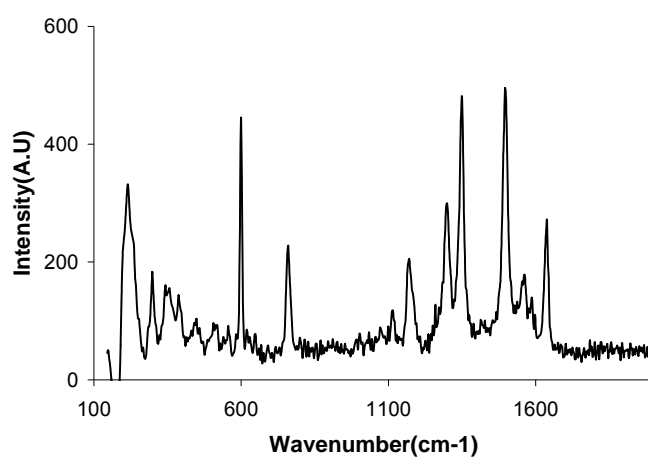
A**B**

Figure 3.26 (Top) Shows the SEM images of PDMS substrate after the nTP trial with the usage of H-B-CD to cover the adhesive resist. Squares, 100-500 nm in size were transferred to the PDMS substrate. (Bottom) Shows SERS spectrum of 1×10^{-5} M Rhodamine 6G.

CHAPTER 4

SERS Substrates Created Via Electron Beam Lithography and Nanotransfer Printing

4.1 Introduction

Over the past two decades, lithographic techniques based on printing, embossing, and molding have become essential to fabricate structures that have nanometer dimensions for research in material science, biology, chemistry, and physics [163,226,245]. These techniques have also been applied in manufacturing plastic electronics, biotechnology, and microfluidic devices. These techniques avoid many limitations of the conventional methods and were discussed in detail in chapter 3. Some advantages also to these methods include flexible patterning capabilities, experimental simplicity, and low cost [245]. Nanotransfer printing is a more recent high resolution stamping technique that involves transferring material from relief features on a stamp or mold to a substrate [226,227,231]. Metallic films or nanoparticle substrates are mainly produced by this method. The nTP method has the ability to pattern three-dimensional and multilayer structure, which is useful in many areas, such as fluidics and nanophotonics. With nTP, the stamp can either be rigid when created with EBL and RIE [226] or an elastomeric stamp prepared by casting a liquid polymer against a rigid master [245,246]. Nanotransfer printing is a fast process, additive in nature (material is only printed in locations where it is

needed), and enabled by interfacial chemical reactions when the stamp and substrate are brought into contact. In addition, the technique avoids exposing the substrate to high temperature or/and harsh materials such as organic solvents or basic and acidic solutions [163]. Preparing noble metallic nano-disc substrates by this method are of significant potential in SERS.

The observation of SERS by molecules in close proximity to roughened metal surfaces has motivated interest in the technique for chemical and biological applications [247]. In the last two decades, SERS has evolved into a very sensitive spectroscopic technique, providing single molecule sensitivity with enhancement factors as high as 10^{12} - 10^{15} in highly specialized cases [7,54,248-251]. In addition, SERS spectra provide detailed structural information and high selectivity [30,90]. Despite all of these advantages, SERS has limitations in analytical figures of merit, such as reproducibility and dynamic range. The causes of SERS enhancement continue to be an active research topic. However, two mechanisms are well discussed in the literature [7,19,46,252,253]. The more general mechanism is based on an electromagnetic effect wherein the local electromagnetic field at or near laser irradiated noble metal particle surfaces is enhanced as a result of localized surface plasmon excitation leading to more intense Raman scattering from molecules near or adsorbed onto the particle surfaces [50,254]. The electromagnetic mechanism renders SERS intensities strongly sensitive to surface structure, particle size, shape, composition, spatial arrangement, and dielectric environment [31]. The other mechanism is a

chemical effect which involves specific interactions or coupling between analyte molecules and the metal particles [73].

As discussed in chapter 1, several different techniques have been developed to create or fabricate functional noble-metal SERS substrates. The most commonly used substrates are disorganized media such as metal colloidal films [255,256], metal-island films on glass [60,257,258], electrochemically roughened silver electrodes [259,260], or polymer nanoparticle surfaces [261,262]. However, limitations in all these techniques include the complexity of these irregular surfaces, reproducibility from one experiment to another, and heterogeneity of the surface, which make elucidating details of the mechanisms of SERS a difficult task. Recent research has led to the preparation of metal particles with tunable shapes and sizes using chemical reactions in solution-wet chemistry such as rods [74,263,264], cubes [17,38], and disks [265]. Another method to prepare more uniform and controllable SERS substrates is nanosphere lithography, where regular structures with truncated tetrahedral shapes are produced [89]. Among the lithographic techniques, EBL with RIE allows for the optimization of the periodic structure, shape and spacing [45,92-97,266]. However, EBL techniques are associated with high preparation cost and scale-up issues.

Previous studies in our research group showed interesting SERS responses for a direct EBL technique where densely packed polymeric arrays of pillars with different shape, spacing, and arrangements were fabricated and metallized via physical vapor deposition to create metal nano-discs on top of the

pillars [267]. Here, for the first time we have used nTP to transfer Ag patterns from the resist stamp onto an elastomer PDMS substrate to fabricate reproducible, uniform ordered arrays of metallic nanostructures for SERS research. *Thus, the motivation for this approach is to increase the density of components, scale up production, and improve cost effectiveness and performance.* The flexibility of this nanofabrication technique enables the rapid generation of several substrates that contain patterns with a variety of geometries. Thus, we can rapidly examine a fairly large number of substrate designs for SERS. In this work the most efficient EBL stamps for nTP can be obtained by coating the stamp with H- β -CD as a metal releasing phase. The capability to transfer isolated metal nano-discs is verified with SEM. The SERS response of metallic nano-discs of various shapes and sizes on the original stamp is compared to the corresponding nTP created substrates, with similar trends observed. Specifically, by using the nTP technique and PDMS as a pliable substrate that can be physically manipulated, one can alter the gaps between the transferred Ag nano-discs. Moreover, by stamping-and-repeating, several SERS-active substrates or greater area can be produced using the same EBL-fabricated stamp.

4.2 Experimental

Surface Enhanced Raman Spectroscopy Instrumentation: The SERS spectra were acquired using a LabRam Spectrograph from JY-Horiba. The instrument set-up has been described in detail in chapter1. In general, the

instrument uses an Olympus BX-40 microscope with a 10X (0.25 NA, ∞) objective that delivers up to 9 mW of the 632.8 nm line from an electrically cooled He-Ne laser. The laser spot size in these studies was approximately 20-25 μm . All spectra were acquired in a 180° scattering geometry with a 2936 cm^{-1} spectral window. In this work, all sample acquisition times were set to 1 second.

Preparation of the stamp substrates: A set of two-dimensional models of squares, triangles, and elliptical nano-arrays were designed in AutoCAD 2005. Pattern size varies between 100-300 nm in the lateral dimension with an inter-particle spacing of 100 or 200 nm (see Table 1 for details). Following that, each drawing was converted to GDS-II format by using the LinkCAD conversion program. The files were transferred and programmed into the EBL computer. A 300 nm film of ma-N 2403, a methacrylate-based negative e-beam resist, was uniformly applied to the surface of a new 2" wafer (Wafer World, FL) by spin coating at 3000 rpm for 30 s. The coated wafer was then baked at 90°C in a conventional oven for 60 seconds and placed into the EBL system. Film thickness of the ma-N 2403 resist was estimated from a chart provided by the manufacturer and is based on spin rate.

A Jeol JBX-6000 FS/E electron beam lithography system with a 50keV thermal field-emission gun was used for the nanofabrication of the stamp. The ma-N 2403 resist film was exposed to a beam of 170 $\mu\text{C}/\text{cm}^2$, yielding an array of nano-patterns. Each array is approximately 40x40 μm in size with 500 μm spacing in the x direction and 100 μm spacing in the y direction between each uniquely patterned array. Once exposed, the ma-N 2403 patterns were

developed in alkaline ma-D 332 developer for 6 s and rinsed in deionized water (18MΩ Barnstead E-Pure) for 3 min. After development, the ma-N 2403 patterns were carefully dried using a low-flow stream of N₂ gas.

The stamps were then prepared for nanotransfer printing as follows by first using an in-house made physical vapor deposition system to vapor deposit H-β-CD and Cal-4. This system uses a light source for heating and operates at roughly 10⁻² torr. Average mass thickness and deposition rates were measured for each film with a Maxtec quartz-crystal microbalance (QCM) that is mounted adjacent to the arrays. Details on this procedure can be found in prior reports [242-244]. A Physical Vapor Deposition chamber from Cooke Vacuum Products, Inc. was then used to vapor deposit Ag. Samples were mounted 25 cm above and normal to the effusive source. The ma-N 2403 arrays were first coated with different thickness of H-β-CD (the CD was prepared using the method of Stoddart et al [237]) and Cal-4 (Lancaster, Pelham, NH). Next the arrays were coated with 50 nm of 99.99% Ag (Alfa Aesar, MA) under high vacuum conditions (1x10⁻⁶ torr). Once prepared, stamps were stored in a vacuum dessicator in the dark prior to use (see Table 1 for substrate specifications). To re-use the stamp, traces of Ag was etched out by placing the stamp in an aqueous solution of 0.2% w/v HAuCl₄ for 6 min. The stamp was then rinsed with copious amounts of water after etching. After drying the stamp, 20 nm H-β-CD was deposited followed by 50 nm Ag and the stamp was re-used for nTP.

Preparation of the SERS substrate: A 2" Si wafer was cleaned with ethanol (HPLC, Fisher). PDMS was prepared by the addition of Sylgard 184 curing

agent (Dow Corning) and its elastomer in a 1:10 mass to mass ratio. The two compounds were combined and then degassed under high vacuum for 15 min. PDMS was spin coated at 200 rpm for 30 s, then cured in the oven at 70 °C for one hour to create the film. PDMS was stored at room temperature until completely cured. The PDMS film was peeled off the wafer, and the side facing the Si wafer was treated with UV-Ozone for 3 min in a UVO-cleaner (Jelight Co., Inc., Irvine, CA). It was then treated with 1×10^{-5} M 3MPTMS, (95%, Aldrich, with acetone as the solvent) for 24 hrs. Following that, the PDMS film was rinsed with deionized water (18M Ω Barnstead E-Pure) for 1min. The stamps were placed on top of the treated PDMS under a metal block that provided roughly 75 g/cm² pressure and left in a vacuum dessicator held at 10^{-4} torr in the dark for 1 hr to transfer the patterns.

All SEM images were collected using a LEO 1525 scanning electron microscope with a field-emission gun operating at 22 kV, 2 kV for the stamp and PDMS, respectively. Images were obtained in secondary electron detection mode. These operating conditions were applied to reduce the sample damage and the build up of charge while producing high-resolution images of stamp and the PDMS substrate surfaces.

Sample preparation: The test analyte solutions used in these studies were 1×10^{-6} M Rhodamine 6G (98+%, Allied Chemicals), 1×10^{-8} M crystal violet (Fisher), and 1×10^{-9} M Mitoxantrone dihydrochloride (sigma) and all were prepared in deionized water (18M Ω Barnstead E-Pure).

Data acquisition and analysis: The substrates were placed at the bottom of a plastic Petri dish, filled with a 2 mL aliquot of each sample solution. The maximum SERS signal was obtained by fine-focusing the microscope objective of the Raman spectrometer and the spectroscopic data was collected by moving the stage at 10 μm intervals (1 spectral acquisition per step) over a 1600 μm^2 area. All Ag substrates were irradiated with 4.1 mW of the 632.8 line of a He-Ne laser for 1 second. Average spectra were collected on 3 arrays of the same pattern. The average of these spectra for each pattern was used for the interpretation of the analytical data. For the elliptical nano-discs arrays, spectra were collected with the polarization vector of the laser being parallel to the long axis of the disc.

4.3 Results and Discussion

Description of the technique: Nanotransfer printing involves four different components or operations: a stamp which can be rigid or elastomeric with relief features of the desired pattern, a technique or method to deposit a thin film of material onto the raised features of the stamp, a means of bringing the stamp into physical contact with the substrate, and in many cases a surface chemistry to prevent adhesion of deposited material to the stamp and promote its adhesion to the substrate [163,245]. The rigid stamp is often fabricated by patterning an e-beam resist on a Si substrate and etching the exposed regions of the substrate with an anisotropic reactive ion etch, then removing the resist [245]. Here, in contrast with usual nTP approaches to fabricate nanometal arrays [226,227,231],

our method is simply based on direct use of the EBL stamp without any further processes. After preparing the stamp using ma-N 2403 negative photoresist and EBL, H- β -CD is thermally evaporated onto the stamp to function as a releasing layer. This is necessary because the resist used here to create the pillars is a methacrylate-based negative e-beam resist and, as with most, is characterized as being an adhesive polymer [268,269]. Subsequent to the formation of a releasing layer, the stamp is metallized with Ag (the most common SERS metal) via physical vapor deposition to create isolated metal nanoparticles (nano-discs). These isolated metal nano-discs are transferred onto PDMS to create nanocomposite substrates with regular periodic morphologies. Placing the metal coated stamp on top of PDMS with minimum applied pressure leads to close, conformal contact between the raised regions of the stamp and the PDMS substrate. Peeling the substrate and stamp apart transfers the Ag from the raised regions of the stamp to the substrate. The transferring process relies on a common condensation reaction and self-assembled monolayer chemistry [231]. This technique enables successful metallic transferring without the need to combine EBL with any other techniques [226]. A schematic drawing of the fabrication process is shown in Figure 4.1 and the nano-disc shapes and dimensions are provided in Table 4.1.

Optimization and performance: Parameters that were optimized for the nTP process include the following: type of the phase used to cover the resist and behave as a releasing layer for Ag, thickness of the phase, and thickness of Ag. Transfer pressure was found not to be critical in our work since the elasticity and

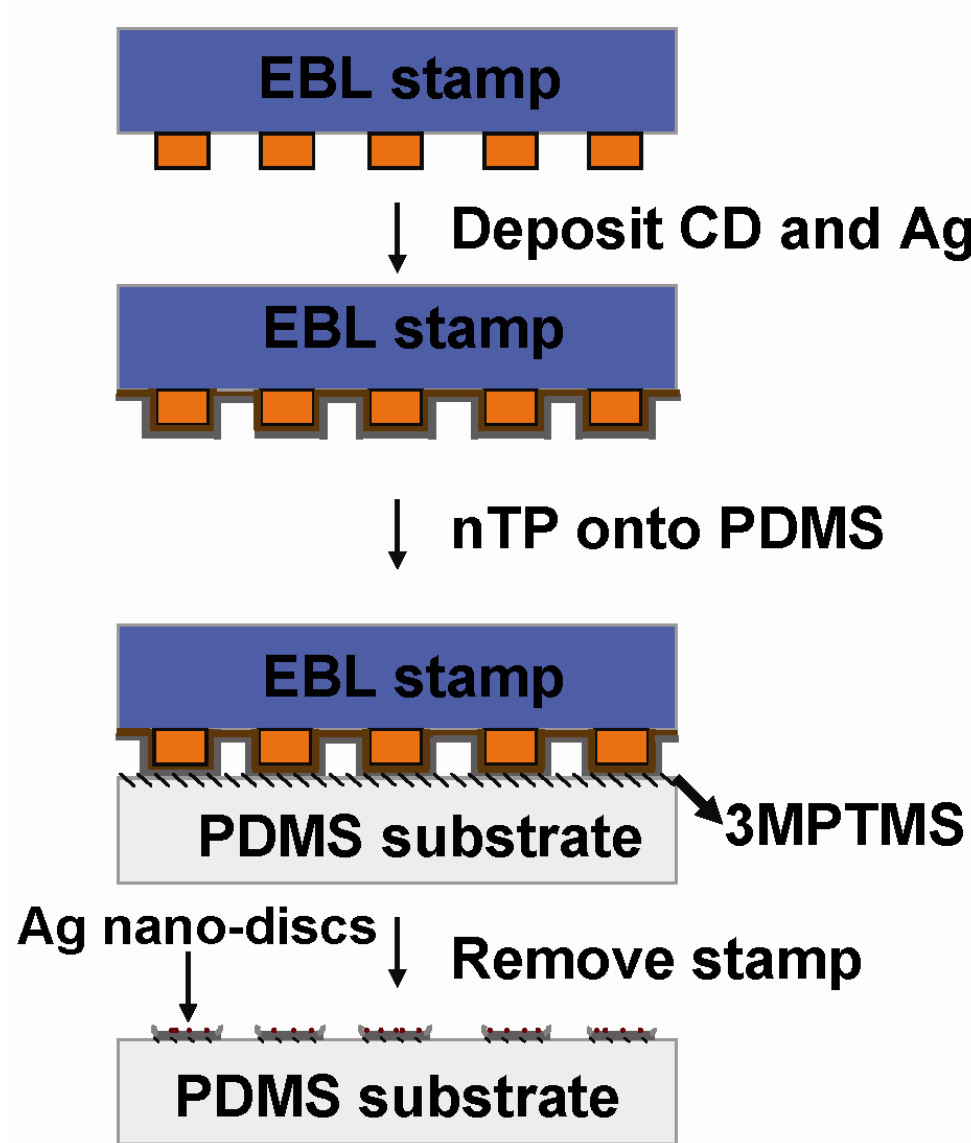












Figure 4.1 Schematic illustration of procedures for using nTP to fabricate nano-disc SERS substrates.

Table 4.1 EBL-created patterns and dimensions.

Pattern	L (nm)	W (nm)	H (nm)	Gap (nm)	Shape
S200_1	200	200	50	100	
S200_2	200	200	50	200	
S300_1	300	300	50	100	
S300_2	300	300	50	200	
E63_1	300	150	50	100	
E63_2	300	150	50	200	
E65_1	300	250	50	100	
E65_2	300	250	50	200	
T100_1	100	100	50	100	
T200_1	200	200	50	100	

mechanical properties of the PDMS substrate ensure close contact at the stamp/substrate interface with minimum pressure being applied. All studies presented here were done with roughly 75 g/cm^2 contact pressure. The first step was to test and compare the releasing efficacy of different phases such as H- β -CD and 4-*tert*-Butylcalix[4]arene (Cal-4).

Figure 4.2A and B represent SEM images of the transferred nano-discs using layers of 50 nm H- β -CD and 50 nm Cal-4 releasing phases, respectively. This results show that the H- β -CD phase, which had been synthesized for molecular recognition in sensing [270], is more efficient for the nTP process than simple Cal-4. This may be a result of the greater hydrophobic nature of the cyclodextrin and weaker adhesion to metal, or its ability to break apart during the transfer process. The effect of the thickness of H- β -CD phase for the nTP process was investigated. Thicknesses of 20, 35, and 50 nm were deposited on three separate EBL stamps and Ag thickness was kept constant at 50 nm. SEM images showed that the best performance for the nTP process is yielded when the thickest, 50 nm, H- β -CD phase is applied (compare Figure 4.2A with 4.2C). This amount seems to be large for a releasing layer, which may be an indication that the e-beam resist and H- β -CD create a mixed layer before a distinct layer of the CD is eventually formed. Although an extensive investigation was not conducted it is likely that numerous compatible phases with properties such as this particular cyclodextrin can be found. Ag was deposited on the EBL stamp at thicknesses of 20, 35, and 50 nm. In each case stamps were first coated with 50 nm H- β -CD phase. Upon the nTP process, SEM images showed that 50 nm Ag

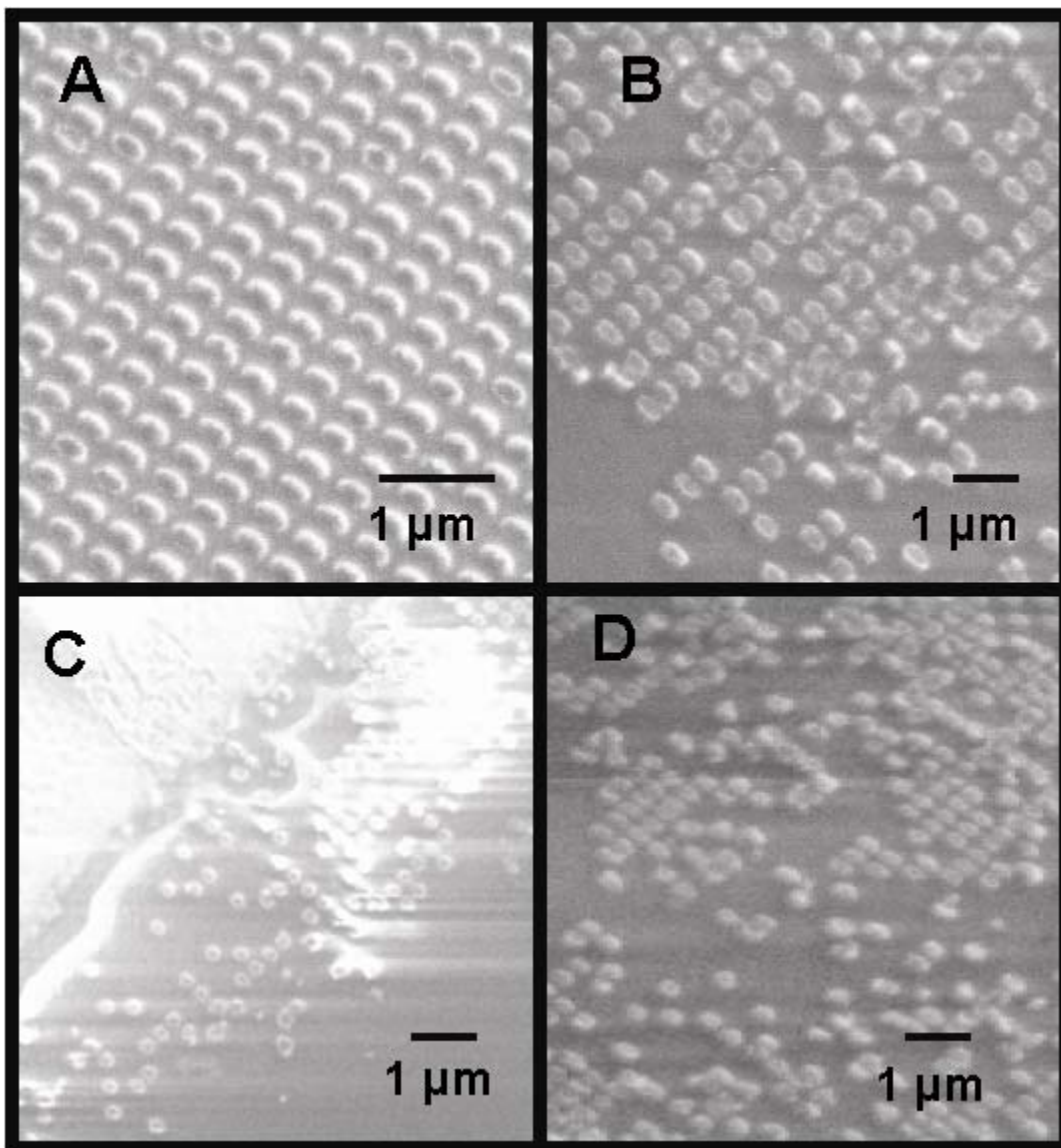


Figure 4.2 Scanning electron micrographs of the E63_1 pattern (A) nano-disc arrays transferred from a stamp under optimal conditions; 50 nm H- β -CD followed by 50 nm Ag and (B-D) nano-disc arrays transferred from a stamp under non optimal conditions; (B) 50nm Cal-4 followed by 50 nm Ag, (C) 20 nm H- β -CD followed by 50nm Ag, (D) 50 nm H- β -CD followed by 20 nm Ag.

gave the most promising results with minimum defects in the nTP process. Figure 4.2D shows the PDMS substrate with minimum numbers of nano-discs being transferred when only 20 nm Ag was deposited. With further study, conditions to create nano-discs of a range of thicknesses and releasing coating phases would be beneficial.

For three different patterns, Figure 4.3 shows SEM images of the stamp after the deposition of 50 nm H- β -CD and 50 nm Ag (left column). Similarly, SEM images of the stamp after the nTP process and the PDMS substrate with the transferred Ag nano-discs are shown in the middle column and the right column, respectively. It can be seen that the Ag that is vapor deposited in the interstices between the pillars is not transferred and only the nano-discs are printed. The appearance of a contrast at the edges of the nano-discs is probably an indication that a portion of the Ag on the sides of the e-beam pillars is also transferred. Low resolution SEMs (not shown) indicate that the entire 40 x 40 μ M EBL pattern is transferred as shown in Figure 4.3.

Altering the space or the gap between nanometallic particles has been shown in experimental studies to have a significant impact on the optical properties and SERS signal [247,96,271], and in modeling work predicted to have very dramatic effects [46,48,55]. With EBL alone, resolution is limited by the electron beam and the resist properties and may not permit closing the gap adequately to produce extremely hot (high field) spots between nanoparticles. Conversely, combining EBL and nTP provides the unique capability to alter the morphology and the interparticle gap of the Ag nano-discs by stretching and

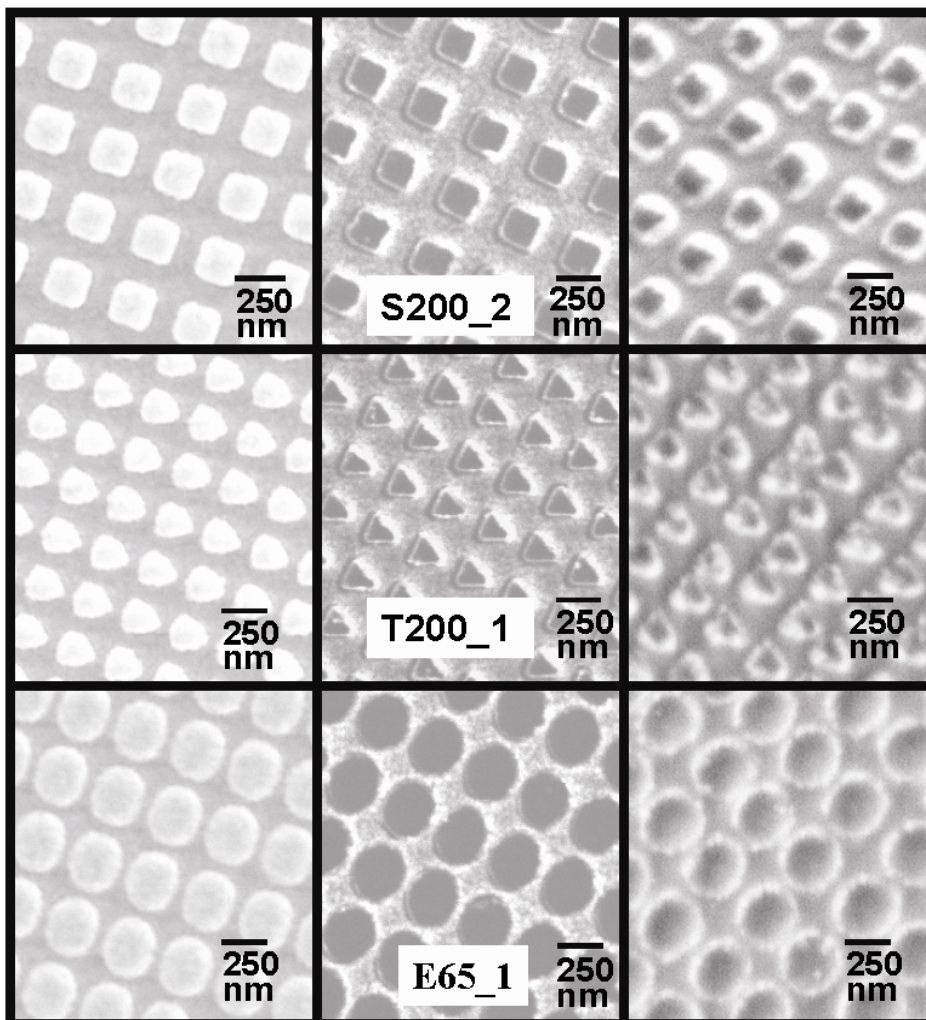


Figure 4.3 Scanning electron micrographs of a 50 nm H-β-CD followed by 50 nm thick Ag evaporated on the stamp (left column), stamp after nTP (middle column), and PDMS substrates showing integrity of the nanotransfer printing (right column). All micrographs were collected at a 15K magnification.

relaxing the PDMS substrate. In this way, substrates with the structural dimensions required for optimum SERS enhancement may be attainable. A preliminary result for this is shown in Figure 4.4 where after the nTP process, the PDMS substrate was mechanically stretched slowly (in one direction) up to 145% of the original post-cured length. The micrographs in the figure indicate that gaps between nano-discs are in proportion to the degree of stretch; thus surface morphology can be controlled by nTP onto pliable PDMS substrates. The approach to close the gap would be to nTP onto stretched polymer and then relax. PDMS is one of the most common elastomers for research and in our studies has been stretched and relaxed over the range 100%-to-150%. However, polymers such as Kraton G, Polystyrene-Poly(ethylene-butylene)-polystyrene, can be manipulated several fold in dimensional changes without rupture [272,273].

SERS Response and Comparison Studies: In the past, our group has demonstrated the potential advantages of using metal-polymer nanocomposites as random morphology substrates for SERS [62]. Moreover, we have further exploited the advantages of EBL to create nanostructured polymer (e-beam resist) surfaces with a variety of shapes, sizes and orientations [267]. Herein, we evaluated the performance of nTP-based SERS substrates and compared them to the original EBL nano-discs. One should note that the thickness of the Ag nano-discs surfaces used herein are greater than the optimum thickness for silver island on smooth glass ~ 8 nm, silver deposited on PDMS ~ 18.5 nm [61],

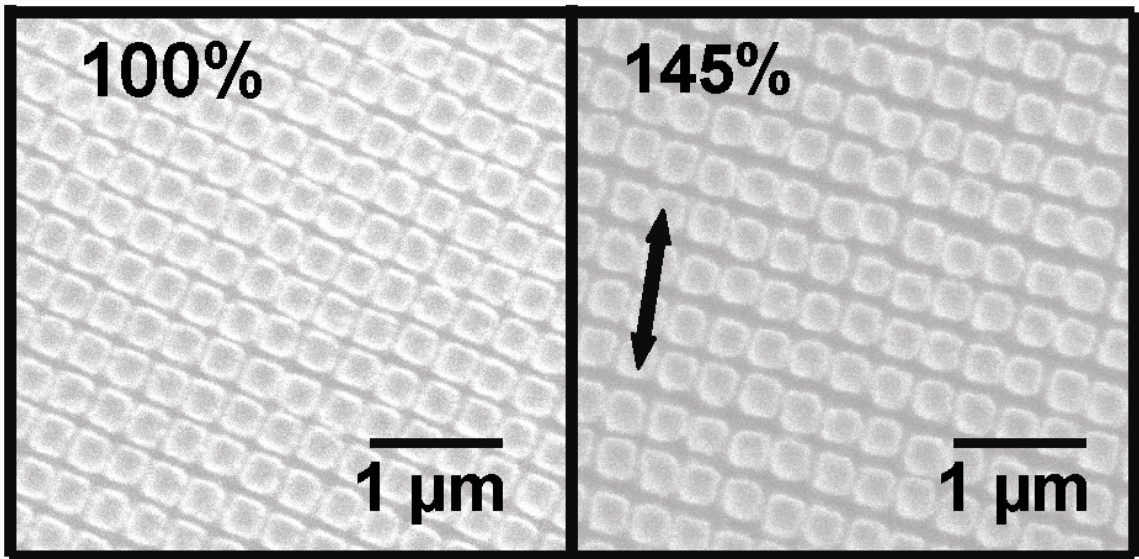


Figure 4.4 Scanning electron micrographs of the (A) S200_1 nano-disc arrays transferred from a stamp and after being stretched. The arrow denotes the stretching direction.

and silver deposited in our prior work on EBL nano-discs ~ 20 nm [267]. The optimum thickness for regular periodic nano-discs will depend, however, on the other dimensions, dielectric properties of the medium, and the excitation wavelength.

Figure 4.5 shows R6G spectra of the original and nanotransferred E63_1 Ag discs. One possible explanation for the modest drop in the signal in the figure is that some of the H- β -CD is probably transferred with the Ag nano discs, thus influencing dielectric properties and the partitioning of the R6G onto the Ag surface. Different disc shapes (squares, ellipses, and triangles), dimensions, and gap sizes were compared using the magnitude of the R6G SERS band area centered at 767 cm^{-1} . The results for this comparison study are shown in Figure 4.6. Each bar in these graphs corresponds to the average of 16 data points within a given array and the average of 3 different arrays of a given pattern. For the square discs (Figure 4.6A), the original and nTP discs SERS responses are following the same trend.

Previous studies in our group have shown that arrays of elliptical nano-discs have interesting SERS results [66,267]. To examine their performance for the nTP process, we fabricated close-packed arrays of these discs with two lateral dimensions 300:250 nm and 300:150 nm (long axis:short axis). The gaps were changed from 100 nm to 200 nm for each pattern. The results in Figure 6B show an increase in the R6G SERS signal when the lateral dimensions change from 300:150 nm to 300:250 nm and the gap decreases from 200 to 100 nm. These results are consistent with our previous data and calculations [66]. Both

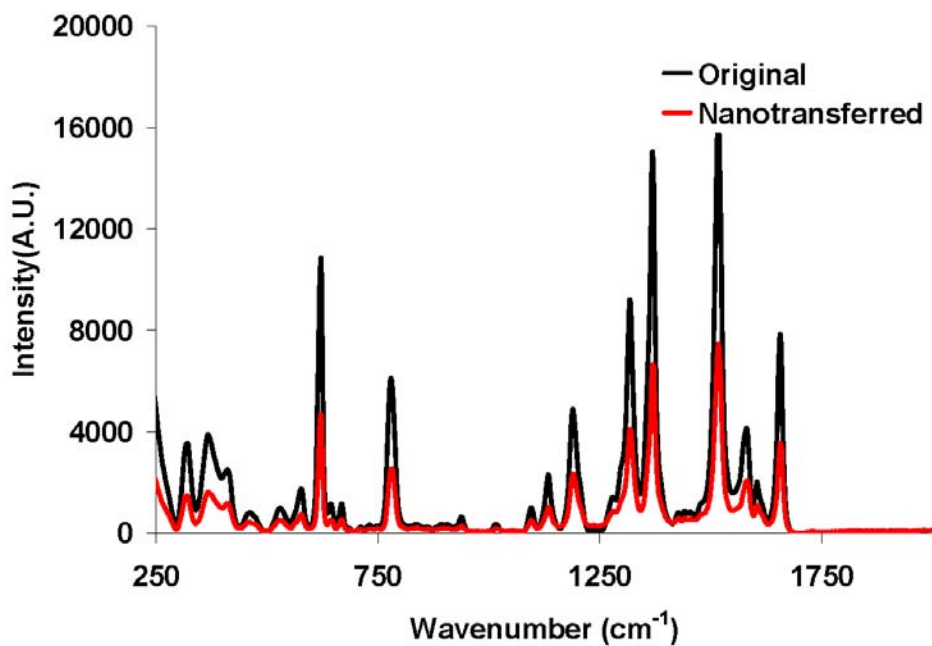


Figure 4.5 Comparison of R6G (1×10^{-6} M) SERS spectra for E63_1 pattern from a stamp (50 nm Ag discs) (black) and upon nTP of the nano-disc array onto PDMS (red).

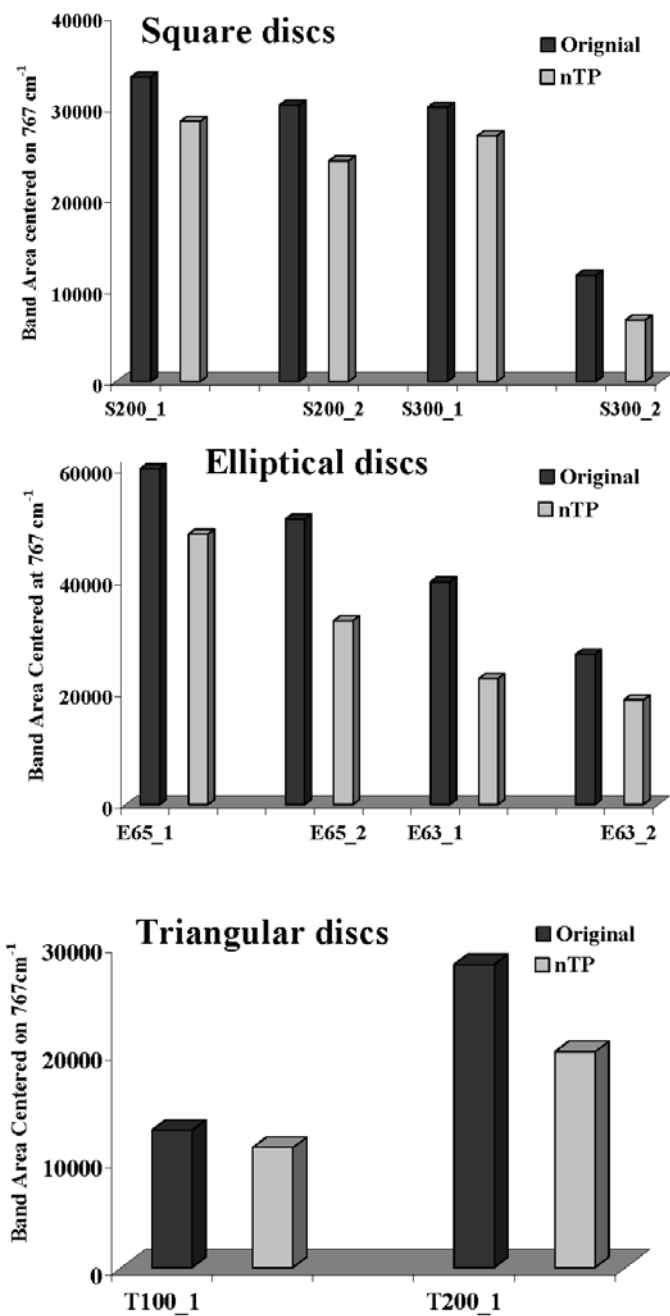


Figure 4.6 Comparison of the 767 cm^{-1} band area SERS signal of R6G ($1 \times 10^{-6}\text{ M}$) for stamp and nTP substrate as a function of the geometric pattern.

the elliptical and triangular patterns compared well in terms of trends (original vs nTP based signals). However, as with the smaller 100 nm squares, the smaller 100 nm triangles did not develop well in the EBL stage. Considering that each step in the nano-disc preparation protocol (EBL, vapor depositions, actual nTP) can be expected to distort the structures originally computationally created, it is reassuring that reasonably good consistency in SERS response trends are observed. We have acquired optical extinction spectra in previous work as an additional means of optical characterization [61]. However, the small sizes of our patterns makes the acquisition of optical extinction spectra somewhat difficult and since we were able to demonstrate the integrity of the nTP process with SEM and SERS experiments, no attempt was made to acquire such spectra.

The EBL approach can be used to create regular arrays of many different morphologies [267], but the main disadvantage of EBL is the high operational cost, particularly when creating large areas of substrate. As a result, nTP can be the basis for economical nanofabrication of SERS substrates when the same EBL stamp can be reused multiple times to create extended nano-disc arrays. SERS responses were investigated for the first, second, and third nTP using the same stamp by collecting the spectra for R6G each printing of the T200_1 pattern (see Figure 4.7). The RSD for the average SERS band area of the 767 cm^{-1} band of 1×10^{-6} M R6G was determined to be 13% between the three stamping trials. Thus, we have demonstrated for the first time an ability to use a stamp-and-repeat protocol to address the scaling limitation in creating EBL-based SERS substrates.

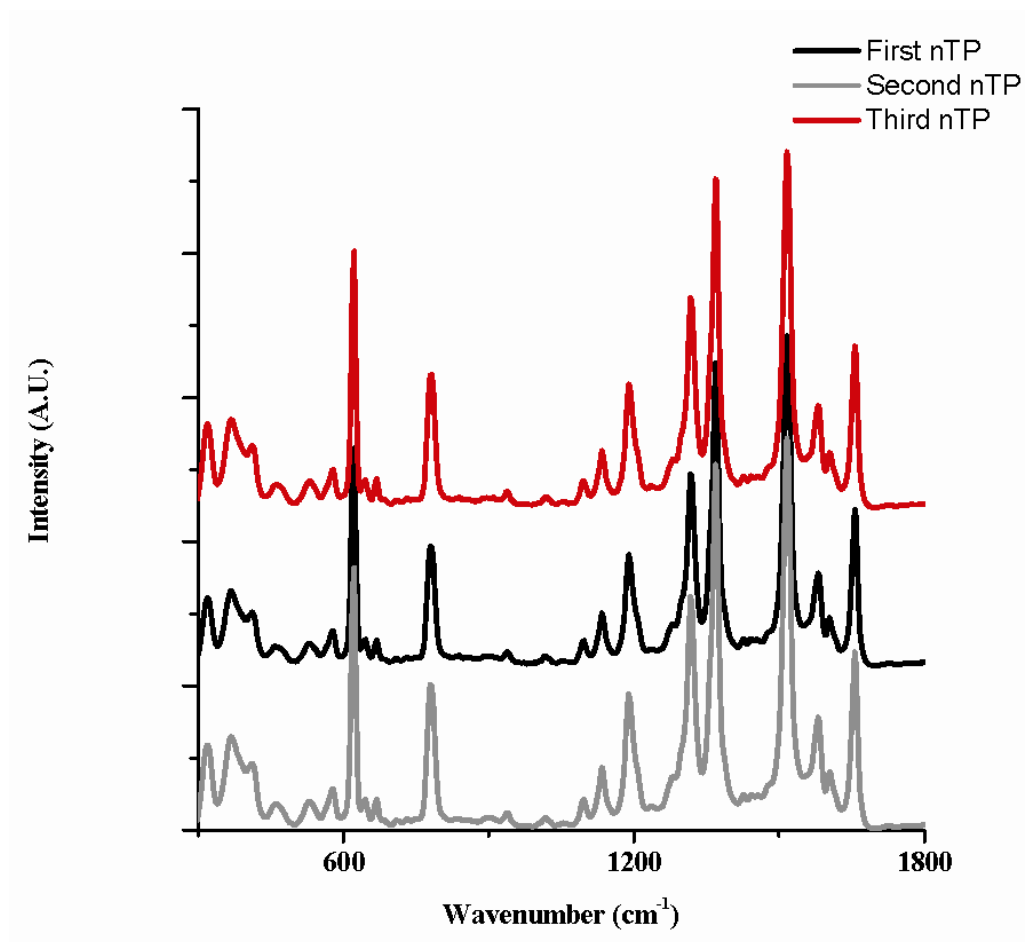


Figure 4.7 SERS spectra of R6G (1×10^{-6} M) using the same nano-disc nTP stamp onto three different PDMS substrates.

Sensitivity is an important figure of merit for SERS. Herein, the nTP substrates were tested for sensitivity by obtaining spectra near the detection limit for crystal violet dye (non-resonant SERS case) and for Mitoxantrone, (absorption maximum at ~ 650 nm [86] rendering this a resonance SERS case). Figure 4.8 shows the spectra of 1×10^{-8} M crystal violet and 1×10^{-9} M Mitoxantrone that demonstrate good sensitivity for these analytes using the nTP-created substrates. In Chapter 2, using Ag colloid SERS substrates and these analytes, the drug Mitoxantrone yielded about three orders of magnitude better detectability than crystal violet. We attribute this change in apparent selectivity to the dual function of the H- β -CD. Specifically, it acts both as a releasing agent and as a metal overcoating layer that exhibits molecular recognition properties which influence the partitioning of the analytes to the metal surface.

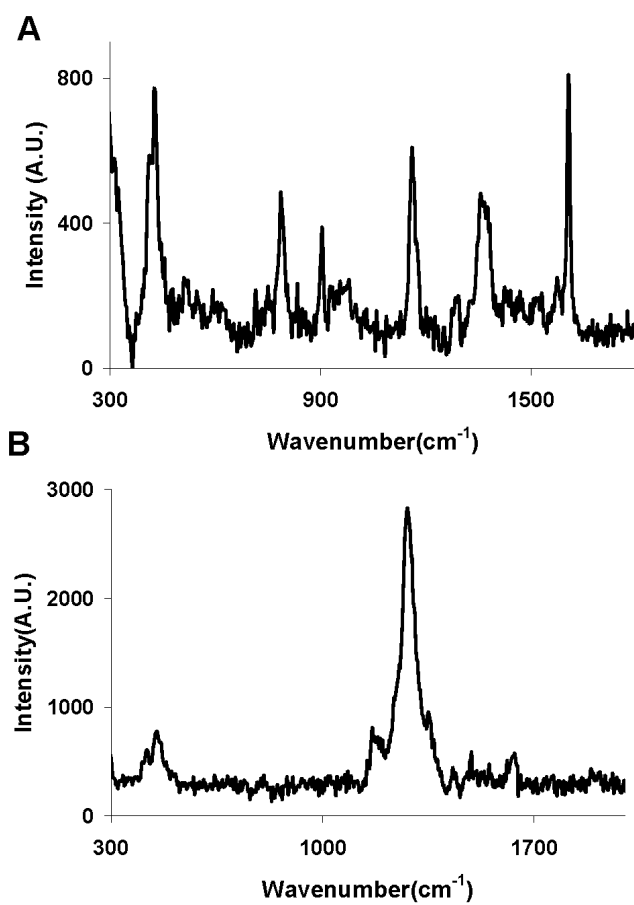


Figure 4.8 Spectra of crystal violet (A) and Mitoxantrone (B) at 10^{-8} M and 10^{-9} M, respectively.

CHAPTER 5

Concluding Remarks

SERS is a plasmonic phenomenon where molecules at or near nanostructural feature surfaces of a noble metal experience a dramatic increase in the magnitude of the electromagnetic field resulting in a high Raman intensity. The use of SERS for analytical applications is an expanding field since SERS is a powerful tool for obtaining valuable information about the chemical structure and composition of molecules. The combination of laser trapping with Raman microscopy has enabled the spatial localized study of different chemical species in single micrometre-sized and nanometre-sized volume [34,86].

However, it is not always possible to use SERS for routine applications. The reproducibility of the signal for a given substance and/or technique is questionable; sometimes signal is lost, random peaks or bands appear, bands are shifted, and signal intensity changes [77,87]. These complications will become even more problematic when trace detection level and sensitivity are required. Therefore, developing a practical, cheap, and reproducible homogeneous SERS substrate and techniques for its application with optimal enhancement are and will continue to be the major task for SERS application in quantitative analysis. Some of the typical requirements in order for SERS to be a quantitative analytical technique are: reproducibility of the results, linearity of the response, clear technique or method for sample preparation, and adequate

molecular selectivity [274]. Unfortunately, it is not easy to meet all of these requirements for SERS in many realistic applications. In the preceding chapters, two approaches were presented to develop technique and substrate that addressed and rectify the drawbacks of SERS. This chapter provides some conclusions and comments on the future of SERS as an analytical technique.

The use of the MMF-SERS approach helps to achieve a highly reproducible experimental geometry. Utilizing a very high numerical aperture microscope objective with a confocal-based Raman spectrometer, high sensitivity was achieved. Moreover, the long working distance of this objective coupled with an appreciable channel depth obviated normal alignment issues expected with translational multiplexing. Rapid evaluation of the effects of anion activators and the type of colloid employed on SERS performance were used to demonstrate the efficiency and applicability of the MMF approach. SERS spectra of various pesticides were also obtained. Calibration curves of crystal violet (non-resonant enhanced) and mitoxantrone (resonant enhanced) were generated, and the major SERS bands of these analytes were observable down to concentrations in the low-nM and sub-pM ranges, respectively. While conventional random morphology colloids were used in most of these studies, unique cubic nanoparticles of Ag were synthesized with different sizes and studied using visible wavelength optical extinction spectrometry, scanning electron microscopy, and the SERS-MMF approach.

The continuous irradiation of sample under SERS conditions can induce permanent damage to the substrate surface. However, the passive pumping

method is used to deliver sample and detection is performed under flowing conditions. This serves to minimize or eliminate photothermal and photochemical effects on SERS response. This approach considerably improves the efficiency of the analysis by allowing the rapid and efficient interrogation of the substrate. The MMF-SERS approach has been demonstrated with desirable analytical figures of merit that include high sensitivity, good reproducibility, calibration capabilities, and information-rich spectra for qualitative work. It can be employed easily for different kinds of samples, and is more convenient for analytical applications. In addition, the high-throughput aspects of the platform are shown to facilitate optimization studies and versatile environmental screening. Some of the variables that are or can be studied include: the effect of solution pH on SERS spectra, surface properties of different colloidal particles, laser power and excitation wavelength, and the influence of electrolytic anions on SERS spectra.

The unconventional nanofabrication methods extensively used for microelectronics purposes have been used in this work to prepare SERS substrate. Different approaches have been attempted for direct nanotransfer printing of metallic nanoparticles from an *EBL stamp to scale-up the production* of arrays of silver particles of different shape and size. Different phases and methods have been tested to overcome the adhesive nature of the EBL resist. Heptakis(6-*O-tert*-butyldimethylsilyl-2,3-di-*O*-acetyl)- β -Cyclodextrin (H- β -CD) has shown to be effective for transferring Ag nano-discs for SERS applications.

The performance of Ag nano-discs patterns developed by EBL and nTP have also been studied and evaluated. It is observed that there are optimum conditions for the Ag and H- β -CD thickness. With this cost-effective approach, mechanical or physical manipulations of the pliable PDMS substrates allow for control of the gaps between metallic nanostructures with intriguing implications for creating high performing SERS substrates. Although the SERS signal of the nTP nano-discs are seen to be slightly lower than the signal of the original EBL nano-discs, they follow the similar trends as disc shapes and dimensions are changed. Overall, the SERS signal of the transferred silver nano-discs onto PDMS substrate demonstrate nTP as a promising nanofabrication method to fabricate extended structures of SERS substrates and as an effective means to overcome the high cost of EBL. It is hoped that EBL with nanotransfer printing will produce substrates with uniform distribution of the enhanced field across the metal surface.

Although progress has been made in the collection of SERS spectra from the nano-composite substrate, further studies are still required to improve the sensitivity, reproducibility, and selectivity of the total technique. This work represents the first steps toward developing Ag nano-discs patterns with controlled inter-particles spacing to prepare SERS substrates that have “hot particles” with giant enhancement.

Future studies involving SERS detection and applications should be focused on designing universal substrates for SERS. By having one or few numbers of SERS substrates, experimental conditions, during the acquisition of

the SERS spectra, can be controlled, and as a result the compilations of a SERS spectral library that takes these experimental conditions into account will be possible and will be a huge asset in the daily use of SERS in real world applications. Future work should also involve creating nTP-SERS substrates and studying the inter-particle spacing effect on SERS signal, combining EBL and RIE to develop a permanent stamp that can generate more than one hundred nTP-SERS substrates, and using nTP-SERS substrates for environmental and biological applications.

REFERENCES

- (1) Raman, C. V. K., K.S., *Nature* **1928**, 121, 501.
- (2) Long, D. A., *The Raman effect: a unified treatment of the theory of Raman scattering by molecules*. Wiley: Chichester ; New York, **2002**; Chapters 1-3.
- (3) McCreery, R. L., *Raman spectroscopy for chemical analysis*. John Wiley & Sons: New York, **2000**; Chapters 1-3.
- (4) Edwards, H. G. M.; Lewis, I. R., *Handbook of Raman spectroscopy: from the research laboratory to the process line*. Marcel Dekker: New York, **2001**; Chapter1-2.
- (5) Browne, W. R.; McGarvey, J. J., *The Raman effect and its application to electronic spectroscopies in metal-centered species: Techniques and investigations in ground and excited states*. *Coord. Chem. Rev.* **2007**, 251, (3+4), 454-473.
- (6) Skoog, D. A.; Nieman, T. A.; Holler, F. J., *Principles of instrumental analysis*. 5th ed.; Saunders College Pub. ;Harcourt Brace College Publishers: Philadelphia Orlando, Fla., **1998**; Chapter7,18.
- (7) Kneipp, K.; Kneipp, H., *Single molecule Raman scattering*. *Appl. Spectrosc.* **2006**, 60, (12), 322A.
- (8) Higuchi, S.; Aiko, O.; Tanaka, S., *Determination of trace amounts of some phenylamide pesticides by resonance Raman spectrometry*. *Analytica Chimica Acta* **1980**, 116, (1), 1-6.
- (9) Spiro, T. G.; Czernuszewicz, R. S., *Resonance Raman spectroscopy*. *Phys. Methods Bioinorg. Chem.* **2000**, 59-119.
- (10) Dines, T. J., *Resonance Raman spectroscopy in surface chemistry*. *Spectrosc. Eur.* **1996**, 8, (1), 27-31.
- (11) Dijkstra, R. J.; Ariese, F.; Gooijer, C.; Brinkman, U. A. T., *Raman spectroscopy as a detection method for liquid-separation techniques*. *TrAC, Trends Anal. Chem.* **2005**, 24, (4), 304-323.
- (12) Pitt, G. D.; Batchelder, D. N.; Bennett, R.; Bormett, R. W.; Hayward, I. P.; Smith, B. J. E.; Williams, K. P. J.; Yang, Y. Y.; Baldwin, K. J.; Webster, S., *Engineering aspects and applications of the new Raman instrumentation*. *IEE Proc.: Sci., Meas. Technol.* **2005**, 152, (6), 241-318.
- (13) Viets, C.; Hill, W., *Laser Power Effects in SERS Spectroscopy at Thin Metal Films*. *Journal of Physical Chemistry B* 2001, 105, (27), 6330-6336.
- (14) LaPlant, F.; Ben-Amotz, D., *Design and construction of a microscope-based Raman system*. *Rev. Sci. Instrum.* **1995**, 66, (6), 3537-44.
- (15) Fleischmann, M.; Hendra, P. J.; McQuillan, A. J., *Raman spectra of pyridine adsorbed at a silver electrode*. *Chem. Phys. Lett.* **1974**, 26, (2), 163-6.
- (16) Jeanmaire, D. L.; Van Duyne, R. P., *Surface Raman spectroelectrochemistry. Part I. Heterocyclic, aromatic, and aliphatic amines adsorbed on the anodized silver electrode*. *J. Electroanal. Chem. Interfacial Electrochem.* **1977**, 84, (1), 1-20.
- (17) Tian, Z.-Q.; Yang, Z.-L.; Ren, B.; Li, J.-F.; Zhang, Y.; Lin, X.-F.; Hu, J.-W.; Wu, D.-Y., *Surface-enhanced Raman scattering from transition metals*

- with special surface morphology and nanoparticle shape. *Faraday Discuss.* **2006**, 132, (Surface Enhanced Raman Spectroscopy), 159-170.
- (18) Haynes, C. L. M., A.D.; Van Duyne, R.P., Surface-Enhanced Raman Spectroscopy. *Analytical Chemistry* 2005, September 2005, 338 A-346 A.
 - (19) Haynes, C. L.; Yonzon, C. R.; Zhang, X.; Van Duyne, R. P., Surface-enhanced Raman sensors: Early history and the development of sensors for quantitative biowarfare agent and glucose detection. *J. Raman Spectrosc.* **2005**, 36, (6/7), 471-484.
 - (20) Haynes, C. L.; Yonzon, C. R.; Zhang, X.; Van Duyne, R. P., Surface-enhanced Raman sensors: Early history and the development of sensors for quantitative biowarfare agent and glucose detection. *J. Raman Spectrosc.* **2005**, 36, (6/7), 471-484.
 - (21) Leopold, N.; Baena, J. R.; Bolboaca, M.; Cozar, O.; Kiefer, W.; Lendl, B., Raman, IR, and surface-enhanced Raman spectroscopy of papaverine. An automated setup for in situ synthesis of the silver substrate and recording of the SER spectra. *Vib. Spectrosc.* **2004**, 36, (1), 47-55.
 - (22) Vo-Dinh, T., SERS chemical sensors and biosensors: new tools for environmental and biological analysis. *Sens. Actuators, B* **1995**, B29, (1-3), 183-9.
 - (23) Stokes, D. L.; Vo-Dinh, T., Development of an integrated single-fiber SERS sensor. *Sens. Actuators, B: Chem.* **2000**, B69, (1-2), 28-36.
 - (24) Wang, Y.; Li, Y.-S.; Zhang, Z.; An, D., Surface-enhanced Raman scattering of some water insoluble drugs in silver hydrosols. *Spectrochimica Acta, Part A: Mol. Biomol. Spectrosc.* **2003**, 59A, (3), 589-594.
 - (25) Xu, H.; Bjerneld, E. J.; Kall, M.; Borjesson, L., Spectroscopy of single hemoglobin molecules by surface enhanced Raman scattering. *Phys. Rev. Lett.* **1999**, 83, (21), 4357-4360.
 - (26) Pal, T.; Anantha Narayanan, V.; Stokes, D. L.; Vo-Dinh, T., Surface-enhanced Raman detection of nicotinamide in vitamin tablets. *Analytica Chimica Acta* **1998**, 368, (1-2), 21-28.
 - (27) Wang, Y.; Li, Y.-S.; Wu, J.; Zhang, Z.; An, D., Surface-enhanced Raman spectra of some anti-tubercle bacillus drugs. *Spectrochimica Acta, Part A: Molecular and Biomolecular Spectroscopy* 2000, 56A, (14), 2637-2644.
 - (28) Xu, H.; Kall, M., Polarization-dependent surface-enhanced Raman spectroscopy of isolated silver nanoaggregates. *Chemphyschem* **2003**, 4, (9), 1001-5.
 - (29) Pinzaru, S. C.; Pavel, I.; Leopold, N.; Kiefer, W., Identification and characterization of pharmaceuticals using Raman and surface-enhanced Raman scattering. *J. Raman Spectrosc.* **2004**, 35, (5), 338-346.
 - (30) Vo-Dinh, T.; Allain, L. R.; Stokes, D. L., Cancer gene detection using surface-enhanced Raman scattering (SERS). *J. Raman Spectrosc.* **2002**, 33, (7), 511-516.
 - (31) Zhang, X.; Yonzon, C. R.; Young, M. A.; Stuart, D. A.; Van Duyne, R. P., Surface-enhanced Raman spectroscopy biosensors: excitation

- spectroscopy for optimisation of substrates fabricated by nanosphere lithography. *IEE Proc.: Nanobiotechnol.* **2005**, 152, (6), 195-206.
- (32) Felidj, N.; Aubard, J.; Levi, G., Review of certain approaches in the characterization of surface enhanced Raman scattering substrates. *Trends Phys. Chem.* **1999**, 7, 103-113.
- (33) Kambhampati, P.; Child, C. M.; Foster, M. C.; Campion, A., On the chemical mechanism of surface enhanced Raman scattering: Experiment and theory. *J. Chem. Phys.* **1998**, 108, (12), 5013-5026.
- (34) Kneipp, K.; Kneipp, H.; Itzkan, I.; Dasari, R. R.; Feld, M. S., Surface-enhanced Raman scattering and biophysics. *J. Phys.: Condens. Matter* **2002**, 14, (18), R597-R624.
- (35) Kneipp, K.; Kneipp, H.; Itzkan, I.; Dasari, R. R.; Feld, M. S., Ultrasensitive chemical analysis by Raman spectroscopy. *Chem. Rev.* **1999**, 99, (10), 2957-2975.
- (36) Tian, Z.-Q.; Ren, B.; Wu, D.-Y., Surface-Enhanced Raman Scattering: From Noble to Transition Metals and from Rough Surfaces to Ordered Nanostructures. *J. Phys. Chem. B* **2002**, 106, (37), 9463-9483.
- (37) Moskovits, M., Surface-enhanced spectroscopy. *Rev. Modern Phys.* **1985**, 57, (3, Pt. 1), 783-826.
- (38) McLellan, J. M.; Siekkinen, A.; Chen, J.; Xia, Y., Comparison of the surface-enhanced Raman scattering on sharp and truncated silver nanocubes. *Chem. Phys. Lett.* **2006**, 427, (1-3), 122-126.
- (39) Michaels, A. M.; Nirmal, M.; Brus, L. E., Surface Enhanced Raman Spectroscopy of Individual Rhodamine 6G Molecules on Large Ag Nanocrystals. *J. Am. Chem. Soc.* **1999**, 121, (43), 9932-9939.
- (40) Ambjornsson, T.; Mukhopadhyay, G.; Apell, S. P.; Kall, M., Resonant coupling between localized plasmons and anisotropic molecular coatings in ellipsoidal metal nanoparticles. *Phys. Rev. B: Condens. Matter Mater. Phys.* **2006**, 73, (8), 1-10.
- (41) Xu, H.; Kall, M., Surface-Plasmon-Enhanced Optical Forces in Silver Nanoaggregates. *Phys. Rev. Lett.* **2002**, 89, (24), 246802/1-246802/4.
- (42) Johansson, P.; Xu, H.; Kall, M., Surface-enhanced Raman scattering and fluorescence near metal nanoparticles. *Phys. Rev. B: Condens. Matter Mater. Phys.* **2005**, 72, (3), 1-17.
- (43) Chen, S.; Webster, S.; Czerw, R.; Xu, J.; Carroll, D. L., Morphology effects on the optical properties of silver nanoparticles. *J. Nanosci. Nanotechnol.* **2004**, 4, (3), 254-259.
- (44) Kottmann, J. P.; Martin, O. J. F.; Smith, D. R.; Schultz, S., Dramatic localized electromagnetic enhancement in plasmon resonant nanowires. *Chem. Phys. Lett.* **2001**, 341, (1,2), 1-6.
- (45) Kahl, M.; Voges, E., Analysis of plasmon resonance and surface-enhanced Raman scattering on periodic silver structures. *Phys. Rev. B: Condens. Matter Mater. Phys.* **2000**, 61, (20), 14078-14088.
- (46) Schatz, G. C.; Young, M. A.; Van Duyne, R. P., Electromagnetic mechanism of SERS. *Top. Appl. Phys.* **2006**, 103, 19-46.

- (47) Vo-Dinh, T., Surface-enhanced Raman spectroscopy using metallic nanostructures. *TrAC, Trends Anal. Chem.* **1998**, 17, (8+9), 557-582.
- (48) Hinde, R. J.; Sepaniak, M. J.; Compton, R. N.; Nordling, J.; Lavrik, N., Surface-enhanced resonance Raman scattering of adsorbates under liquid nitrogen. *Chem. Phys. Lett.* **2001**, 339, (3,4), 167-173.
- (49) Campion, A.; Kambhampati, P., Surface-enhanced Raman scattering. *Chem. Soc. Rev.* **1998**, 27, (4), 241-250.
- (50) Kneipp, K.; Wang, Y.; Dasari, R. R.; Feld, M. S., Approach to single molecule detection using surface-enhanced resonance Raman scattering (SERRS): a study using rhodamine 6G on colloidal silver. *Appl. Spectrosc.* **1995**, 49, (6), 780-4.
- (51) Zou, S.; Schatz, G. C., Coupled plasmonic plasmon/photonic resonance effects in SERS. *Topics Appl. Phys.* **2006**, 103, (Surface-Enhanced Raman Scattering), 67-86.
- (52) Zou, S.; Schatz, G. C., Combining micron-size glass spheres with silver nanoparticles to produce extraordinary field enhancements for surface-enhanced Raman scattering applications. *Israel J. Chem.* **2006**, 46, (3), 293-297.
- (53) Qin, L.; Zou, S.; Xue, C.; Atkinson, A.; Schatz, G. C.; Mirkin, C. A., Designing, fabricating, and imaging Raman hot spots. *Proceedings National Academy Sciences* **2006**, 103, (36), 13300-13303.
- (54) Otto, A., What is observed in single molecule SERS, and why? *J. Raman Spectrosc.* **2002**, 33, (8), 593-598.
- (55) Hao, E.; Schatz, G. C., Electromagnetic fields around silver nanoparticles and dimers. *J. Chem. Phys.* **2004**, 120, (1), 357-366.
- (56) Zhang, X.; Hicks, E. M.; Zhao, J.; Schatz, G. C.; Van Duyne, R. P., Electrochemical Tuning of Silver Nanoparticles Fabricated by Nanosphere Lithography. *Nano Lett.* **2005**, 5, (7), 1503-1507.
- (57) Doering, W. E.; Nie, S., Single-Molecule and Single-Nanoparticle SERS: Examining the Roles of Surface Active Sites and Chemical Enhancement. *J. Phys. Chem. B* **2002**, 106, (2), 311-317.
- (58) Radicic, W. N.; Ni, E. V.; Tombrello, C.; Fountain, A. W., III, Characterizing the spectral reproducibility of quartz-bound Au nanoparticle substrates for surface-enhanced Raman spectroscopy. *Proc. SPIE-Int. Soc. Opt. Eng.* **2006**, 6218, (Chemical and Biological Sensing VII), 1-9.
- (59) Drachev, V. P.; Thoreson, M. D.; Nashine, V.; Khaliullin, E. N.; Ben-Amotz, D.; Davissson, V. J.; Shalaev, V. M., Adaptive silver films for surface-enhanced Raman spectroscopy of biomolecules. *J. Raman Spectrosc.* **2005**, 36, (6/7), 648-656.
- (60) Reilly, T. H., III; Corbman, J. D.; Rowlen, K. L., Vapor Deposition Method for Sensitivity Studies on Engineered Surface-Enhanced Raman Scattering-Active Substrates. *Anal. Chem.* **2007**, 79, (13), 5078-5081.
- (61) Giesfeldt, K. S.; Connatser, R. M.; De Jesus, M. A.; Lavrik, N. V.; Dutta, P.; Sepaniak, M. J., Studies of the optical properties of metal-pliable polymer composite materials. *Appl. Spectrosc.* **2003**, 57, (11), 1346-1352.

- (62) Alak, A. M.; Vo Dinh, T., Silver-coated fumed silica as a substrate material for surface-enhanced Raman scattering. *Anal. Chem.* **1989**, 61, (7), 656-60.
- (63) Giesfeldt, K. S.; Connatser, R. M.; De Jesus, M. A.; Dutta, P.; Sepaniak, M. J., Gold-polymer nanocomposites. Studies of their optical properties and their potential as SERS substrates. *J. Raman Spectrosc.* **2005**, 36, (12), 1134-1142.
- (64) Tolaieb, B.; Constantino, C. J. L.; Aroca, R. F., Surface-enhanced resonance Raman scattering as an analytical tool for single molecule detection. *Analyst* **2004**, 129, (4), 337-341.
- (65) De Jesus, M. A.; Giesfeldt, K. S.; Sepaniak, M. J., Improving the analytical figures of merit of SERS for the analysis of model environmental pollutants. *J. Raman Spectrosc.* **2004**, 35, (10), 895-904.
- (66) Oran, J. M. Hinde., R. J.; Abu Hatab, N.; and Sepaniak, M. J., Nanofabricated Periodic Arrays of Silver Elliptical Discs as SERS Substrates. *Appl. Spectrosc.* **2007**.
- (67) Roark, S. E. R., K.L., Thin Ag films: influence of substrate and postdeposition treatment on morphology and optical properties. *Anal. Chem.* **1994**, 66, 261-270.
- (68) Zou, X.; Dong, S., Surface-Enhanced Raman Scattering Studies on Aggregated Silver Nanoplates in Aqueous Solution. *J. Phys. Chem. B* **2006**, 110, (43), 21545-21550.
- (69) Cinta Pinzaru, S.; Leopold, N.; Pavel, I.; Kiefer, W., Raman, SERS and theoretical studies of papaverine hydrochloride and its neutral species. *Spectrochimica Acta, Part A: Mol. Biomol. Spectrosc.* **2004**, 60A, (8-9), 2021-2028.
- (70) Seballos, L.; Olson, T. Y.; Zhang, J. Z., Effects of chromophore orientation and molecule conformation on surface-enhanced Raman scattering studied with alkanolic acids and colloidal silver nanoparticles. *J. Chem. Phys.* **2006**, 125, (23), 1-6.
- (71) Zhang, A.; Fang, Y., Influence of adsorption orientation of methyl orange on silver colloids by Raman and fluorescence spectroscopy: pH effect. *Chem. Phys.* **2006**, 331, (1), 55-60.
- (72) Fang, J.; Zhong, C.; Mu, R., The study of deposited silver particulate films by simple method for efficient SERS. *Chem. Phys. Lett.* **2005**, 401, (1-3), 271-275.
- (73) Kneipp, K.; Kneipp, H., Surface-enhanced raman scattering on silver nanoparticles in different aggregation stages. *Israel J. Chem.* **2006**, 46, (3), 299-305.
- (74) Orendorff, C. J.; Gearheart, L.; Jana, N. R.; Murphy, C. J., Aspect ratio dependence on surface enhanced Raman scattering using silver and gold nanorod substrates. *Phys. Chem. Chem. Phys.* **2006**, 8, (1), 165-170.
- (75) Orendorff, C. J.; Gole, A.; Sau, T. K.; Murphy, C. J., Surface-Enhanced Raman Spectroscopy of Self-Assembled Monolayers: Sandwich

- Architecture and Nanoparticle Shape Dependence. *Anal. Chem.* **2005**, *77*, (10), 3261-3266.
- (76) Evanoff, D. D., Jr.; Chumanov, G., Synthesis and optical properties of silver nanoparticles and arrays. *ChemPhysChem* **2005**, *6*, (7), 1221-1231.
- (77) Aroca, R., Surface-enhanced vibrational spectroscopy. Wiley: Chichester; Hoboken, NJ, **2006**; Chapters 3-6.
- (78) Evanoff, D. D., Jr.; Chumanov, G., Size-controlled synthesis of nanoparticles. 1. Silver-only aqueous suspensions via hydrogen reduction. *J. Phys. Chem. B* **2004**, *108*, (37), 13948-13956.
- (79) Evanoff, D. D., Jr.; Chumanov, G., Size-Controlled Synthesis of Nanoparticles. 2. Measurement of Extinction, Scattering, and Absorption Cross Sections. *J. Phys. Chem. B* **2004**, *108*, (37), 13957-13962.
- (80) Sau, T. K.; Murphy, C. J., Room temperature, high-yield synthesis of multiple shapes of gold nanoparticles in aqueous solution. *J. Amer. Chem. Soci.* **2004**, *126*, (28), 8648-8649.
- (81) Lee, C. J.; Kim, H. J.; Karim, M. R.; Lee, M. S., Surface-enhanced Raman spectroscopy of ethephone adsorbed on silver surface. *Bull. Korean Chem. Soc.* **2006**, *27*, (4), 545-548.
- (82) Aubard, J.; Bagnasco, E.; Pantigny, J.; Ruasse, M. F.; Levi, G.; Wentrup-Byrne, E., An Ion-Exchange Reaction as Measured by Surface-Enhanced Raman Spectroscopy on Silver Colloids. *J. Phys. Chem.* **1995**, *99*, (18), 7075-81.
- (83) Li, Y. S.; Cheng, J.; Wang, Y., Surface-enhanced Raman spectra of dyes and organic acids in silver solutions: chloride ion effect. *Spectrochimica Acta, Part A: Mol. Biomol. Spectrosc.* **2000**, *56A*, (11), 2067-2072.
- (84) Campbell, M.; Lecomte, S.; Smith, W. E., Effect of different mechanisms of surface binding of dyes on the surface-enhanced resonance Raman scattering obtained from aggregated colloid. *J. Raman Spectrosc.* **1999**, *30*, (1), 37-44.
- (85) Bengter, H.; Tengroth, C.; Jacobsson, S. P., New light on Ag-colloid preparation for surface-enhanced FT-Raman spectroscopy: the role of aggregation. *J. Raman Spectrosc.* **2005**, *36*, (11), 1015-1022.
- (86) Cunningham, D.; Littleford, R. E.; Smith, W. E.; Lundahl, P. J.; Khan, I.; McComb, D. W.; Graham, D.; Laforest, N., Practical control of SERRS enhancement. *Faraday Discuss.* **2006**, *132*, (Surface Enhanced Raman Spectroscopy), 135-145.
- (87) Cinta, S.; Vogel, E.; Maniu, D.; Aluas, M.; Iliescu, T.; Cozar, O.; Kiefer, W., SERS mechanisms of the Vitamin PP on different Au and Ag surfaces. *J. Mol. Structure* **1999**, *482-483*, 679-684.
- (88) Zhang, j. F., Y., Surface-enhanced Raman scattering of p-hydroxybenzoic acid in pure Ag colloids produced by laser ablation. *Colloids and Surfaces A: Physicochem. Eng. Aspects* **2005**, *266*, 38-43.
- (89) Zhang, X.; Yonzon, C. R.; Van Duyne, R. P., Nanosphere lithography fabricated plasmonic materials and their applications. *J. Mater. Research* **2006**, *21*, (5), 1083-1092.

- (90) Zhang, X.; Shah, N. C.; Van Duyne, R. P., Sensitive and selective chem/bio sensing based on surface-enhanced Raman spectroscopy (SERS). *Vib. Spectrosc.* **2006**, 42, (1), 2-8.
- (91) Haynes, C. L.; Van Duyne, R. P., Nanosphere Lithography: A Versatile Nanofabrication Tool for Studies of Size-Dependent Nanoparticle Optics. *J. Phys. Chem. B* **2001**, 105, (24), 5599-5611.
- (92) Sackmann, M.; Bom, S.; Balster, T.; Materny, A., Nanostructured gold surfaces as reproducible substrates for surface-enhanced Raman spectroscopy. *J. Raman Spectrosc.* **2007**, 38, (3), 277-282.
- (93) Yu, Q.; Golden, G., Probing the Protein Orientation on Charged Self-Assembled Monolayers on Gold Nanohole Arrays by SERS. *Langmuir* **2007**, 23, (17), 8659-8662.
- (94) Billot, L.; Lamy de la Chapelle, M.; Grimault, A. S.; Vial, A.; Barchiesi, D.; Bijeon, J. L.; Adam, P. M.; Royer, P., Surface enhanced Raman scattering on gold nanowire arrays: Evidence of strong multipolar surface plasmon resonance enhancement. *Chem. Phys. Lett.* **2006**, 422, (4-6), 303-307.
- (95) Hicks, E. M.; Zou, S.; Schatz, G. C.; Spears, K. G.; Van Duyne, R. P.; Gunnarsson, L.; Rindzevicius, T.; Kasemo, B.; Kaell, M., Controlling Plasmon Line Shapes through Diffractive Coupling in Linear Arrays of Cylindrical Nanoparticles Fabricated by Electron Beam Lithography. *Nano Lett.* **2005**, 5, (6), 1065-1070.
- (96) Gunnarsson, L.; Bjerneld, E. J.; Xu, H.; Petronis, S.; Kasemo, B.; Kall, M., Interparticle coupling effects in nanofabricated substrates for surface-enhanced Raman scattering. *Appl. Phys. Lett.* **2001**, 78, (6), 802-804.
- (97) Kahl, M.; Voges, E.; Kostrewa, S.; Viets, C.; Hill, W., Periodically structured metallic substrates for SERS. *Sens. Actuators, B: Chem.* **1998**, B51, (1-3), 285-291.
- (98) Whitesides, G. M.; Ostuni, E.; Takayama, S.; Jiang, X.; Ingber, D. E., Soft lithography in biology and biochemistry. *Annu. Rev. Biomed. Eng.* **2001**, 3, 335-373.
- (99) Whitesides, G. M., The origins and the future of microfluidics. *Nature* **2006**, 442, (7101), 368-373.
- (100) Xia, N.; Hunt, T. P.; Mayers, B. T.; Alsberg, E.; Whitesides, G. M.; Westervelt, R. M.; Ingber, D. E., Combined microfluidic-micromagnetic separation of living cells in continuous flow. *Biomed. Microdevices* **2006**, 8, (4), 299-308.
- (101) DeMello Andrew, J., Control and detection of chemical reactions in microfluidic systems. *Nature* **2006**, 442, (7101), 394-402.
- (102) Chen, X.; Wu, H.; Mao, C.; Whitesides, G. M., A prototype two-dimensional capillary electrophoresis system fabricated in poly(dimethylsiloxane). *Anal. Chem.* **2002**, 74, (8), 1772-1778.
103. McClain, M. A.; Culbertson, C. T.; Jacobson, S. C.; Allbritton, N. L.; Sims, C. E.; Ramsey, J. M., Microfluidic devices for the high-throughput chemical analysis of cells. *Anal. Chem.* **2003**, 75, (21), 5646-5655.

- (104) Chen, G.; McCandless, G. T.; McCarley, R. L.; Soper, S. A., Integration of large-area polymer nanopillar arrays into microfluidic devices using in situ polymerization cast molding. *Lab Chip* **2007**, *7*, (11), 1424-1427.
- (105) Weibel, D. B.; Whitesides, G. M., Applications of microfluidics in chemical biology. *Curr. Opin. Chem. Biol.* **2006**, *10*, (6), 584-591.
- (106) Wang, R. Y.; Segalman, R. A.; Majumdar, A., Room temperature thermal conductance of alkanedithiol self-assembled monolayers. *Appl. Phys. Lett.* **2006**, *89*, (17), 1-3.
- (107) Broyles, B. S.; Jacobson, S. C.; Ramsey, J. M., Sample filtration, concentration, and separation integrated on microfluidic devices. *Anal. Chem.* **2003**, *75*, (11), 2761-2767.
- (108) McDonald, J. C.; Whitesides, G. M., Poly(dimethylsiloxane) as a Material for Fabricating Microfluidic Devices. *Acc. Chem. Res.* **2002**, *35*, (7), 491-499.
- (109) Siegel, A. C.; Bruzewicz, D. A.; Weibel, D. B.; Whitesides, G. M., Microsolidics: fabrication of three-dimensional metallic microstructures in poly(dimethylsiloxane). *Adv. Mater.* **2007**, *19*, (5), 727-733.
- (110) McDonald, J. C.; Metallo, S. J.; Whitesides, G. M., Fabrication of a configurable, single-use microfluidic device. *Anal. Chem.* **2001**, *73*, (23), 5645-5650.
- (111) Soper, S. A.; Henry, A. C.; Vaidya, B.; Galloway, M.; Wabuye, M.; McCarley, R. L., Surface modification of polymer-based microfluidic devices. *Anal. Chim. Acta* **2002**, *470*, (1), 87-99.
- (112) Shadpour, H.; Hupert, M. L.; Patterson, D.; Liu, C.; Galloway, M.; Stryjewski, W.; Goettert, J.; Soper, S. A., Multichannel Microchip Electrophoresis Device Fabricated in Polycarbonate with an Integrated Contact Conductivity Sensor Array. *Anal. Chem.* **2007**, *79*, (3), 870-878.
- (113) Sinville, R.; Soper, S. A., High resolution DNA separations using microchip electrophoresis. *J. Sep. Sci.* **2007**, *30*, (11), 1714-1728.
- (114) Musyimi, H. K.; Guy, J.; Narcisse, D. A.; Soper, S. A.; Murray, K. K., Direct coupling of polymer-based microchip electrophoresis to online MALDI-MS using a rotating ball inlet. *Electrophoresis* **2005**, *26*, (24), 4703-4710.
- (115) Monti, G.; De Napoli, L.; Mainolfi, P.; Barone, R.; Guida, M.; Marino, G.; Amoresano, A., Monitoring food quality by microfluidic electrophoresis, gas chromatography, and mass spectrometry techniques: Effects of aquaculture on the sea bass (*Dicentrarchus labrax*). *Anal. Chem.* **2005**, *77*, (8), 2587-2594.
- (116) Llopis, S. L.; Osiri, J.; Soper, S. A., Surface modification of poly(methyl methacrylate) microfluidic devices for high-resolution separations of single-stranded DNA. *Electrophoresis* **2007**, *28*, (6), 984-993.
- (117) Hashimoto, M.; Barany, F.; Xu, F.; Soper, S. A., Serial processing of biological reactions using flow-through microfluidic devices: Coupled PCR/LDR for the detection of low-abundant DNA point mutations. *Analyst* **2007**, *132*, (9), 913-921.

- (118) El-Ali, J.; Sorger, P. K.; Jensen, K. F., Cells on chips. *Nature* **2006**, 442, (7101), 403-411.
- (119) Ramsey, J. D.; Jacobson, S. C.; Culbertson, C. T.; Ramsey, J. M., High-efficiency, two-dimensional separations of protein digests on microfluidic devices. *Anal. Chem.* **2003**, 75, (15), 3758-3764.
- (120) Price, A. K.; Culbertson, C. T., Chemical Analysis of Single Mammalian Cells with Microfluidics. *Anal. Chem.* **2007**, 79, (7), 2614-2621.
- (121) Fleischmann, M.; Hendra, P. J.; and McQuillan, A. J.; Raman spectra of pyridine adsorbed at a silver electrode. *Chem. Phys. Lett.* **2006**, 26, (2), 163-6.
- (122) Kneipp, K.; Haka, A.S.; Kneipp, H.; Badizadegan, K.; Yoshizawa, N.; Boone, C.; Shafer-Peltier, K.E.; Motz, J.T.; Dasari, R.R.; and Feld, M.S.; Surface-enhanced Raman spectroscopy in single living cells using gold nanoparticles";. *Appl. Spectrosc.* **2002**, 56, (2), 150-154.
- (123) Yan, F.; and Tuan, V.-D.; Surface-enhanced Raman scattering detection of chemical and biological agents using a portable Raman integrated tunable sensor. *Sens. Actuators, B: Chem.* **2007**, B121, (1), 61-66.
- (124) Faulds, K.; Fruk, L.; Robson, D. C.; Thompson, D.G.; Enright, A.; Ewen Smith, W.; and Graham, D.; A new approach for DNA detection by SERRS. *Faraday Discuss.* **2006**, 132, 261-268.
- (125) Alvarez-Ros, M. C.; Sanchez-Cortes, S.; Francioso, O.; and Garcia-Ramos, J. V.; Adsorption and chemical modification of gallic acid on silver nanoparticles studied by Raman spectroscopy: Effect of anions and cationic pesticide paraquat. *Can. J. Anal. Sci. Spectrosc.* **2003**, 48, (2), 132-138.
- (126) Spencer, K. M.; Sylvia, J. M.; Clauson, S. L.; Bertone, J. F.; and Christesen, S. D.; Surface-enhanced Raman for monitoring toxins in water. *Proc. SPIE-Int. Soc. Opt. Eng.* **2004**, 5268, 340-348.
- (127) Bertone, J. F.; Cordeiro, K. L.; Sylvia, J. M.; and Spencer, K. M.; A nanoengineered sensor to detect vibrational modes of warfare agents/explosives using surface-enhanced Raman scattering. *Proc. SPIE-Int. Soc. Opt. Eng.* **2004**, 5403, 387-394.
- (128) Kim, K.; Lee, H. S.; and Kim, N. H.; Silver-particle-based surface-enhanced resonance Raman scattering spectroscopy for biomolecular sensing and recognition. *Anal. Bioanal. Chem.* **2007**, 388, (1), 81-88.
- (129) Kumar, G. V. P.; Shruthi, S.; Vibha, B.; Reddy, B. A. A.; Kundu, T. K.; Narayana, C.; Hot Spots in Ag Core-Au Shell Nanoparticles Potent for Surface-Enhanced Raman Scattering Studies of Biomolecules. *J. Phys. Chem. C* **2007**, 111, (11), 4388-4392.
- (130) Bao, L.; Mahurin, S. M.; Haire, R. G.; Dai, S.; Silver-Doped Sol-Gel Film as a Surface-Enhanced Raman Scattering Substrate for Detection of Uranyl and Neptunyl Ions. *Anal. Chem.* **2003**, 75, (23), 6614-6620.
- (131) Otto, A.; On the electronic contribution to single molecule surface enhanced Raman spectroscopy. *Indian J. Phys. B*, **2003**, 77B, (1), 63-73.

- (132) Le Ru, E. C.; Etchegoin, P. G.; Meyer, M.; Enhancement factor distribution around a single surface-enhanced Raman scattering hot spot and its relation to single molecule detection. *J. Chem. Phys.* **2006**, 125, 4701-4713.
- (133) Goulet, P. J. G.; Aroca, R. F.; Distinguishing individual vibrational fingerprints: Single-molecule surface-enhanced resonance Raman scattering from one-to-one binary mixtures in Langmuir-Blodgett monolayers. *Anal. Chem.* **2007**, 79, (7), 2728-2734.
- (134) Jensen, L.; and Schatz, G. C.; Resonance Raman Scattering of Rhodamine 6G as Calculated Using Time-Dependent Density Functional Theory. *J. Phys. Chem. A*, **2006**, 110, (18), 5973-5977.
- (135) Lee, P. C.; Meisel, D., Adsorption and surface-enhanced Raman of dyes on silver and gold sols. *Journal of Physical Chemistry* **1982**, 86, (17), 3391-5.
- (136) Canamares, M. V.; Garcia-Ramos, J. V.; Gomez-Varga, J. D.; Domingo, C.; Sanchez-Cortes, S., Comparative Study of the Morphology, Aggregation, Adherence to Glass, and Surface-Enhanced Raman Scattering Activity of Silver Nanoparticles Prepared by Chemical Reduction of Ag⁺ Using Citrate and Hydroxylamine. *Langmuir* **2005**, 21, (18), 8546-8553.
- (137) Fang, J.; Zhong, C.; Mu, R., The study of deposited silver particulate films by simple method for efficient SERS. *Chem. Phys. Lett.* **2005**, 401, (1-3), 271-275.
- (138) Liang, E. J.; Ye, X. L.; Kiefer, W., Interaction of halide and halate ions with colloidal silver and their influence on surface-enhanced Raman scattering of pyridine with near-infrared excitation. *Vib. Spectrosc.* **1997**, 15, (1), 69-78.
- (139) Iliescu, T.; Cinta, S.; Astilean, S.; Bratu, I., pH influence on the Raman spectra of PP vitamin in silver sol. *J. Mol. Structure* **1997**, 410-411, 193-196.
- (140) Bengter, H.; Tengroth, C.; Jacobsson, S. P., New light on Ag-colloid preparation for surface-enhanced FT-Raman spectroscopy: the role of aggregation. *J. Raman Spectrosc.* **2005**, 36, (11), 1015-1022.
- (141) Liang, E. J.; Engert, C.; Kiefer, W., Surface-enhanced Raman spectroscopy of p-aminobenzoic acid with excitation in the visible and near infrared spectral region. *Vib. Spectrosc.* **1993**, 6, (1), 79-85.
- (142) Aubard, J.; Bagnasco, E.; Pantigny, J.; Ruasse, M. F.; Levi, G.; Wentrup-Byrne, E., An Ion-Exchange Reaction as Measured by Surface-Enhanced Raman Spectroscopy on Silver Colloids. *J. Phys. Chem.* **1995**, 99, (18), 7075-81.
- (143) Li, Y. S.; Cheng, J.; Wang, Y., Surface-enhanced Raman spectra of dyes and organic acids in silver solutions: chloride ion effect. *Spectrochimica Acta, Part A: Mol. Biomol. Spectrosc.* **2000**, 56A, (11), 2067-2072.
- (144) Seballos, L.; Olson, T. Y.; Zhang, J. Z., Effects of chromophore orientation and molecule conformation on surface-enhanced Raman scattering

- studied with alkanolic acids and colloidal silver nanoparticles. *J. Chem. Phys.* **2006**, 125, (23), 234706/1-234706/6.
- (145) Whitesides, G. M.; Stroock, A. D., Flexible methods for microfluidics. *Phys. Today* **2001**, 54, (6), 42-48.
- (146) Whitesides, G. M., Revolutions in chemistry. *Chem. & Engineer. News* **2007**, 85, (13), 12-17.
- (147) Ng, J. M. K.; Gitlin, I.; Stroock, A. D.; Whitesides, G. M., Components for integrated poly(dimethylsiloxane) microfluidic systems. *Electrophoresis* **2002**, 23, (20), 3461-3473.
- (148) Siegel, A. C.; Bruzewicz, D. A.; Weibel, D. B.; Whitesides, G. M., Microsolidics: fabrication of three-dimensional metallic microstructures in poly(dimethylsiloxane). *Advan. Mater.* **2007**, 19, (5), 727-733.
- (149) De Jesus, M. A.; Giesfeldt, K. S.; Sepaniak, M. J., Use of a sample translation technique to minimize adverse effects of laser irradiation in surface-enhanced Raman spectrometry. *Appl. Spectrosc.* **2003**, 57, (4), 428-438.
- (150) Lee, S.; Choi, J.; Chen, L.; Park, B.; Kyong, J. B.; Seong, G. H.; Choo, J.; Lee, Y.; Shin, K.-H.; Lee, E. K.; Joo, S.-W.; Lee, K.-H., Fast and sensitive trace analysis of malachite green using a surface-enhanced Raman microfluidic sensor. *Anal. Chimica Acta* **2007**, 590, (2), 139-144.
- (151) Lee, D.; Lee, S.; Seong, G. H.; Choo, J.; Lee, E. K.; Gweon, D.-G.; Lee, S., Quantitative analysis of methyl parathion pesticide in a polydimethylsiloxane microfluidic channel using confocal surface-enhanced Raman spectroscopy. *Appl. Spectrosc.* **2006**, 60, (4), 373-377.
- (152) Walker, G. M.; Beebe, D. J., A passive pumping method for microfluidic devices. *Lab on a Chip* **2002**, 2, (3), 131-134.
- (153) Connatser, R. M.; Riddle, L. A.; Sepaniak, M. J., Metal-polymer nanocomposites for integrated microfluidic separations and surface enhanced Raman spectroscopic detection. *J. Separa. Sci.* **2004**, 27, (17-18), 1545-1550.
- (154) Sun, Y.; Xia, Y., Shape-Controlled Synthesis of Gold and Silver Nanoparticles. *Science* **2002**, 298, (5601), 2176-2179.
- (155) Oldenburg, S. J.; Jackson, J. B.; Westcott, S. L.; Halas, N. J., Infrared extinction properties of gold nanoshells. *Appl. Phys. Lett.* **1999**, 75, (19), 2897-2899.
- (156) Hunyadi, S. E.; Murphy, C. J., Bimetallic silver-gold nanowires: fabrication and use in surface-enhanced Raman scattering. *J. Mater. Chem.* **2006**, 16, (40), 3929-3935.
- (157) Pavel, I.; Szeghalmi, A.; Moigno, D.; Cinta, S.; Kiefer, W., Theoretical and pH dependent surface enhanced Raman spectroscopy study on caffeine. *Biopolymers* **2002**, 72, (1), 25-37.
- (158) Cunningham, D.; Littleford, R. E.; Smith, W. E.; Lundahl, P. J.; Khan, I.; McComb, D. W.; Graham, D.; Laforest, N., Practical control of SERRS enhancement. *Faraday Discuss.* **2006**, 132, (Surface Enhanced Raman Spectroscopy), 135-145.

- (159) Nabiev, I.; Baranov, A.; Chourpa, I.; Beljebbar, A.; Sockalingum, G. D.; Manfait, M., Does Adsorption on the Surface of a Silver Colloid Perturb Drug/DNA Interactions? Comparative SERS, FT-SERS, and Resonance Raman Study of Mitoxantrone and Its Derivatives. *J. Phys. Chem.* **1995**, *99*, (5), 1608-13.
- (160) McLaughlin, C.; MacMillan, D.; McCardle, C.; Smith, W. E., Quantitative Analysis of Mitoxantrone by Surface-Enhanced Resonance Raman Scattering. *Anal. Chem.* **2002**, *74*, (13), 3160-3167.
- (161) <http://www.epa.gov/oscpmont/oscpendo/index.htm>
- (162) Bhushan, B., Springer Handbook of Nanotechnology, 2nd Revised and Extended Edition. **2007**; 279-297.
- (163) Xia, Y.; Rogers, J. A.; Paul, K. E.; Whitesides, G. M., Unconventional methods for fabricating and patterning nanostructures. *Chem. Rev.* **1999**, *99*, (7), 1823-1848.
- (164) Schiff, H.; David, C.; Gobrecht, J.; D'Amore, A.; Simoneta, D.; Kaiser, W.; Gabriel, M., Quantitative analysis of the molding of nanostructures. *J. Vac. Sci. Technol., B* **2000**, *18*, (6), 3564-3568.
- (165) Stewart, M. D.; Patterson, K.; Somervell, M. H.; Willson, C. G., Organic imaging materials: a view of the future. *J. Phys. Org. Chem.* **2000**, *13*, (12), 767-774.
- (166) Willson, C. G.; Trinquet, B. C., The evolution of materials for the photolithographic process. *J. Photopolym. Sci. Technol.* **2003**, *16*, (4), 621-627.
- (167) Geissler, M.; Xia, Y., Patterning: Principles and some new developments. *Advan. Mater.* **2004**, *16*, (15), 1249-1269.
- (168) Gates, B. D.; Xu, Q.; Love, J. C.; Wolfe, D. B.; Whitesides, G. M., Unconventional nanofabrication. *Annual Rev. Mater. Research* **2004**, *34*, 339-372.
- (169) Yasin, S.; Hasko, D. G.; Ahmed, H., Fabrication of <5 nm width lines in poly(methyl methacrylate) resist using a water:isopropyl alcohol developer and ultrasonically-assisted development. *Appl. Phys. Lett.* **2001**, *78*, (18), 2760-2762.
- (170) Hu, W.; Sarveswaran, K.; Lieberman, M.; Bernstein, G. H., Sub-10 nm electron beam lithography using cold development of poly(methyl methacrylate). *J. Vac. Sci. Technol., B: Microelectron. Nanometer Struct.--Process., Meas., Phenom.* **2004**, *22*, (4), 1711-1716.
- (171) Groves, T. R.; Pickard, D.; Rafferty, B.; Crosland, N.; Adam, D.; Schubert, G., Maskless electron beam lithography: prospects, progress, and challenges. *Microelectron. Eng.* **2002**, *61-62*, 285-293.
- (172) Anbumony, K.; Lee, S. Y., True three-dimensional proximity effect correction in electron-beam lithography. *J. Vac. Sci. Technol., B: Microelectron. Nanometer Struct.--Process., Meas., Phenom.* **2006**, *24*, (6), 3115-3120.

- (173) Bolorizadeh, M.; Joy, D. C., Effects of fast secondary electrons to low-voltage electron beam lithography. *J. Micro/Nanolithogr., MEMS, MOEMS* **2007**, 6, (2), 1-7.
- (174) Gadegaard, N.; McCloy, D., Direct stamp fabrication for NIL and hot embossing using HSQ. *Microelectron. Eng.* **2007**, 84, (12), 2785-2789.
- (175) Martiradonna, L.; Quattieri, A.; Stomeo, T.; Carbone, L.; Cingolani, R.; De Vittorio, M., Lithographic nano-patterning of colloidal nanocrystal emitters for the fabrication of waveguide photonic devices. *Sens. Actuators, B* **2007**, B126, (1), 116-119.
- (176) Parekh, V. A.; Ruiz, A.; Ruchhoeft, P.; Brankovic, S.; Litvinov, D., Close-Packed Noncircular Nanodevice Pattern Generation by Self-Limiting Ion-Mill Process. *Nano Lett.* **2007**, 7, (10), 3246-3248.
- (177) Wu, C.-S.; Lin, C.-F.; Lin, H.-Y.; Lee, C.-L.; Chen, C.-D., Polymer-based photonic crystals fabricated with single-step electron-beam lithography. *Adv. Mater.* **2007**, 19, (19), 3052-3056.
- (178) Schiff, H.; David, C.; Gabriel, M.; Gobrecht, J.; Heyderman, L. J.; Kaiser, W.; Koppel, S.; Scandella, L., Nanoreplication in polymers using hot embossing and injection molding. *Microelectron. Eng.* **2000**, 53, (1-4), 171-174.
- (179) Tseng, A. A.; Notargiacomo, A., Nanoscale fabrication by nonconventional approaches. *J. Nanosci. Nanotechnol.* **2005**, 5, (5), 683-702.
- (180) Truskett, V. N.; Watts, M. P. C., Trends in imprint lithography for biological applications. *Trends Biotechnol.* **2006**, 24, (7), 312-317.
- (181) Gates, B. D., Nanofabrication with molds and stamps. *Mater. Today* **2005**, 8, (2), 44-49.
- (182) Resnick, D. J.; Mancini, D. P.; Sreenivasan, S. V.; Willson, G., Release layers for contact and imprint lithography. *Semicond. Int.* **2002**, 25, (6), 71-72,74,76,78,80.
- (183) Zhang, T.; Kobrin, B.; Wanebo, M.; Nowak, R.; Yi, R.; Chinn, J.; Bender, M.; Fuchs, A.; Otto, M., Vapor deposited release layers for nanoimprint lithography. *Proc. SPIE-Int. Soc. Opt. Eng.* **2006**, 6151, (Pt. 1, Emerging Lithographic Technologies X), 1-6.
- (184) Stewart, M. D.; Johnson, S. C.; Sreenivasan, S. V.; Resnick, D. J.; Willson, C. G., Nanofabrication with step and flash imprint lithography. *J. Microlithogr., Microfabr., Microsyst.* **2005**, 4, (1), 1-6.
- (185) Gates, B. D.; Xu, Q.; Stewart, M.; Ryan, D.; Willson, C. G.; Whitesides, G. M., New Approaches to Nanofabrication: Molding, Printing, and Other Techniques. *Chem. Rev.* **2005**, 105, (4), 1171-1196.
- (186) Colburn, M.; Grot, A.; Choi, B. J.; Amistoso, M.; Bailey, T.; Sreenivasan, S. V.; Ekerdt, J. G.; Grant Willson, C., Patterning nonflat substrates with a low pressure, room temperature, imprint lithography process. *J. Vac. Sci. Technol., B* **2001**, 19, (6), 2162-2172.
- (187) Ruchhoeft, P.; Colburn, M.; Choi, B.; Nounu, H.; Johnson, S.; Bailey, T.; Darmle, S.; Stewart, M.; Ekerdt, J.; Sreenivasan, S. V.; Wolfe, J. C.; Willson, C. G., Patterning curved surfaces: Template generation by ion

- beam proximity lithography and relief transfer by step and flash imprint lithography. *J. Vac. Sci. Technol., B* **1999**, 17, (6), 2965-2969.
- (188) Resnick, D. J.; Dauksher, W. J.; Mancini, D.; Nordquist, K. J.; Ainley, E.; Gehoski, K.; Baker, J. H.; Bailey, T. C.; Choi, B. J.; Johnson, S.; Sreenivasan, S. V.; Ekerdt, J. G.; Willson, C. G., High resolution templates for step and flash imprint lithography. *J. Microlithogr., Microfabr., Microsyst.* **2002**, 1, (3), 284-289.
- (189) Xu, F.; Stacey, N. A.; Watts, M.; Truskett, V.; McMackin, I.; Choi, J.; Schumaker, P.; Thompson, E.; Babbs, D.; Sreenivasan, S. V.; Willson, C. G.; Schumaker, N., Development of imprint materials for the Step and Flash Imprint Lithography process. *Proc. SPIE-Int. Soc. Opt. Eng.* **2004**, 5374, (Pt. 1, Emerging Lithographic Technologies VIII), 232-241.
- (190) Mancini, D. P.; Gehoski, K. A.; Ainley, E.; Nordquist, K. J.; Resnick, D. J.; Bailey, T. C.; Sreenivasan, S. V.; Ekerdt, J. G.; Willson, C. G., Hydrogen silsesquioxane for direct electron-beam patterning of step and flash imprint lithography templates. *J. Vac. Sci. Technol., B* **2002**, 20, (6), 2896-2901.
- (191) Choi, K.-B.; Lee, J. J., Passive compliant wafer stage for single-step nano-imprint lithography. *Rev. Sci. Instrum.* **2005**, 76, (7), 1-6.
- (192) Ooe, H.; Morimatsu, M.; Yoshikawa, T.; Kawata, H.; Hirai, Y., Three-dimensional multilayered microstructure fabricated by imprint lithography. *J. Vac. Sci. Technol., B: Microelectron. Nanometer Struct.--Process., Meas., Phenom.* **2005**, 23, (2), 375-379.
- (193) Zhang, W.; Chou, S. Y., Fabrication of 60-nm transistors on 4-in. wafer using nanoimprint at all lithography levels. *Appl. Phys. Lett.* **2003**, 83, (8), 1632-1634.
- (194) Chou, S. Y.; Krauss, P. R.; Renstrom, P. J., Imprint of sub-25 nm vias and trenches in polymers. *Appl. Phys. Lett.* **1995**, 67, (21), 3114-16.
- (195) Jung, G. Y.; Ganapathiappan, S.; Ohlberg, D. A. A.; Olynick, D. L.; Chen, Y.; Tong, W. M.; Williams, R. S., Fabrication of a 34 micro e 34 Crossbar Structure at 50 nm Half-pitch by UV-based Nanoimprint Lithography. *Nano Lett.* **2004**, 4, (7), 1225-1229.
- (196) Lan, H.; Ding, Y.; Liu, H.; Lu, B., Review of the wafer stage for nanoimprint lithography. *Microelectron. Eng.* **2007**, 84, (4), 684-688.
- (197) Li, H.-W.; Huck, W. T. S., Ordered Block-Copolymer Assembly Using Nanoimprint Lithography. *Nano Letters* 2004, 4, (9), 1633-1636.
- (198) Yang, K.-Y.; Hong, S.-H.; Lee, H.; Choi, J.-W., Fabrication of nano-sized gold dot array using bi-layer nano imprint lithography. *Mater. Sci. Forum* 2006, 510-511, (Eco-Materials Processing & Design VII), 446-449.
- (199) Kehagias, N.; Zelsmann, M.; Sotomayor Torres, C. M., Polymer optical devices made by reverse and 3D nanoimprint lithography. *Proc. SPIE-Int. Soc. Opt. Eng.* **2005**, 5825, (Optoelectronics, Photonic Devices, and Optical Networks), 654-660.
- (200) Chou, S. Y.; Krauss, P. R.; Renstrom, P. J., Nanoimprint lithography. *J. Vac. Sci. Technol., B* **1996**, 14, (6), 4129-4133.

- (201) Scheer, H. C.; Schulz, H., A contribution to the flow behavior of thin polymer films during hot embossing lithography. *Microelectron. Eng.* **2001**, 56, (3-4), 311-332.
- (202) Sotomayor Torres, C. M.; Zankovych, S.; Seekamp, J.; Kam, A. P.; Clavijo Cedeno, C.; Hoffmann, T.; Ahopelto, J.; Reuther, F.; Pfeiffer, K.; Bleidiessel, G.; Gruetzner, G.; Maximov, M. V.; Heidari, B., Nanoimprint lithography: an alternative nanofabrication approach. *Mater. Sci. Eng., C* **2003**, C23, (1-2), 23-31.
- (203) Schiff, H.; Park, S.; Gobrecht, J., Nanoimprint - molding resists for lithography. *J. Photopolym. Sci. Technol.* **2003**, 16, (3), 435-438.
- (204) Scheer, H. C.; Schulz, H.; Hoffmann, T.; Sotomayor Torres, C. M., Problems of the nanoimprinting technique for nanometer scale pattern definition. *J. Vac. Sci. Technol., B* **1998**, 16, (6), 3917-3921.
- (205) Scheer, H. C.; Bogdanski, N.; Wissen, M.; Konishi, T.; Hirai, Y., Polymer time constants during low temperature nanoimprint lithography. *J. Vac. Sci. Technol., B: Microelectron. Nanometer Struct.--Process., Meas., Phenom.* **2005**, 23, (6), 2963-2966.
- (206) Bailey, T.; Smith, B.; Choi, B. J.; Colburn, M.; Meissl, M.; Sreenivasan, S. V.; Ekerdt, J. G.; Willson, C. G., Step and flash imprint lithography: Defect analysis. *J. Vac. Sci. Technol., B* **2001**, 19, (6), 2806-2810.
- (207) Chen, L.; Deng, X.; Wang, J.; Takahashi, K.; Liu, F., Defect control in nanoimprint lithography. *J. Vac. Sci. Technol., B: Microelectron. Nanometer Struct.--Process., Meas., Phenom.* **2005**, 23, (6), 2933-2938.
- (208) McAlpine, M. C.; Friedman, R. S.; Lieber, C. M., Nanoimprint Lithography for Hybrid Plastic Electronics. *Nano Lett.* **2003**, 3, (4), 443-445.
- (209) Li, M.; Wang, J.; Zhuang, L.; Chou, S. Y., Fabrication of circular optical structures with a 20 nm minimum feature size using nanoimprint lithography. *Appl. Phys. Lett.* **2000**, 76, (6), 673-675.
- (210) Rogers, J. A.; Nuzzo, R. G., Recent progress in soft lithography. *Mater. Today* **2005**, 8, (2), 50-56.
- (211) Delamarche, E.; Schmid, H.; Michel, B.; Biebuyck, H., Stability of molded polydimethylsiloxane microstructures. *Adv. Mater.* **1997**, 9, (9), 741-746.
- (212) Kumar, A.; Biebuyck, H. A.; Whitesides, G. M., Patterning Self-Assembled Monolayers: Applications in Materials Science. *Langmuir* **1994**, 10, (5), 1498-511.
- (213) Cao, T.; Xu, Q.; Winkleman, A.; Whitesides, G. M., Fabrication of thin, metallic films along the sidewalls of a topographically patterned stamp and their application in charge printing. *Small* **2005**, 1, (12), 1191-1195.
- (214) Kumar, A.; Whitesides, G. M., Features of gold having micrometer to centimeter dimensions can be formed through a combination of stamping with an elastomeric stamp and an alkanethiol "ink" followed by chemical etching. *Appl. Phys. Lett.* **1993**, 63, (14), 2002-4.
- (215) Hidber, P. C.; Helbig, W.; Kim, E.; Whitesides, G. M., Microcontact printing of palladium colloids: micron-scale patterning by electroless deposition of copper. *Langmuir* **1996**, 12, (5), 1375-80.

- (216) Xia, Y.; Whitesides, G. M., Use of controlled reactive spreading of liquid alkanethiol on the surface of gold to modify the size of features produced by microcontact Printing. *J. Am. Chem. Soc.* **1995**, 117, (11), 3274-5.
- (217) Love, J. C.; Wolfe, D. B.; Chabinyc, M. L.; Paul, K. E.; Whitesides, G. M., Self-assembled monolayers of alkanethiolates on palladium are good etch resists. *J. Am. Chem. Soc.* **2002**, 124, (8), 1576-1577.
- (218) Xia, Y.; Zhao, X.-M.; Kim, E.; Whitesides, G. M., A Selective Etching Solution for Use with Patterned Self-Assembled Monolayers of Alkanethiolates on Gold. *Chem. Mater.* **1995**, 7, (12), 2332-7.
- (219) Jiang, W.; Garfunkel, E.; Zhitenev, N.; Abusch-Magder, D.; Tennant, D.; Bao, Z., Molecular conductance measurements through printed Au nanodots. *Appl. Phys. Lett.* **2006**, 89, (11), 113107/1-113107/3.
- (220) Crespo-Biel, O.; Dordi, B.; Maury, P.; Peter, M.; Reinhoudt, D. N.; Huskens, J., Patterned, Hybrid, Multilayer Nanostructures Based on Multivalent Supramolecular Interactions. *Chem. Mater.* **2006**, 18, (10), 2545-2551.
- (221) Yang, K.-I.; Cadwell, K.; Abbott, N. L., Contact printing of metal ions onto carboxylate-terminated self-assembled monolayers. *Adv. Mater.* **2003**, 15, (21), 1819-1823.
- (222) Pla-Roca, M.; Fernandez, J. G.; Mills, C. A.; Martinez, E.; Samitier, J., Micro/Nanopatterning of Proteins via Contact Printing Using High Aspect Ratio PMMA Stamps and NanoImprint Apparatus. *Langmuir* **2007**, 23, (16), 8614-8618.
- (223) Hsu, J. W. P., Soft lithography contacts to organics. *Mater. Today* 2005, 8, (7/8), 42-54.
- (224) Lee, B. H.; Cho, Y. H.; Lee, H.; Lee, K.-D.; Kim, S. H.; Sung, M. M., High-resolution patterning of aluminum thin films with a water-mediated transfer process. *Adv. Mater.* **2007**, 19, (13), 1714-1718.
- (225) Wang, R. Y.; Segalman, R. A.; Majumdar, A., Room temperature thermal conductance of alkanedithiol self-assembled monolayers. *Appl. Phys. Lett.* **2006**, 89, (17), 1-3.
- (226) Loo, Y.-L.; Willett, R. L.; Baldwin, K. W.; Rogers, J. A., Additive, nanoscale patterning of metal films with a stamp and a surface chemistry mediated transfer process: Applications in plastic electronics. *Appl. Phys. Lett.* **2002**, 81, (3), 562-564.
- (227) Loo, Y.-L.; Hsu, J. W. P.; Willett, R. L.; Baldwin, K. W.; West, K. W.; Rogers, J. A., High-resolution transfer printing on GaAs surfaces using alkane dithiol monolayers. *J. Vac. Sci. & Technol., B* **2002**, 20, (6), 2853-2856.
- (228) Menard, E.; Bilhaut, L.; Zaumseil, J.; Rogers, J. A., Improved Surface Chemistries, Thin Film Deposition Techniques, and Stamp Designs for Nanotransfer Printing. *Langmuir* **2004**, 20, (16), 6871-6878.
- (229) Schmid, H.; Wolf, H.; Allenspach, R.; Riel, H.; Karg, S.; Michel, B.; Delamarche, E., Preparation of metallic films on elastomeric stamps and

- their application for contact processing and contact printing. *Adv. Funct. Mater.* **2003**, 13, (2), 145-153.
- (230) Odom, T. W.; Love, J. C.; Wolfe, D. B.; Paul, K. E.; Whitesides, G. M., Improved pattern transfer in soft lithography using composite stamps. *Langmuir* **2002**, 18, (13), 5314-5320.
- (231) Loo, Y.-L.; Willett, R. L.; Baldwin, K. W.; Rogers, J. A., Interfacial Chemistries for Nanoscale Transfer Printing. *J. Am. Chem. Soc.* **2002**, 124, (26), 7654-7655.
- (232) Hur, S.-H.; Khang, D.-Y.; Kocabas, C.; Rogers, J. A., Nanotransfer printing by use of noncovalent surface forces: Applications to thin-film transistors that use single-walled carbon nanotube networks and semiconducting polymers. *Appl. Phys. Lett.* **2004**, 85, (23), 5730-5732.
- (233) Zaumseil, J.; Meitl, M. A.; Hsu, J. W. P.; Acharya, B. R.; Baldwin, K. W.; Loo, Y.-L.; Rogers, J. A., Three-Dimensional and Multilayer Nanostructures Formed by Nanotransfer Printing. *Nano Lett.* **2003**, 3, (9), 1223-1227.
- (234) Jeon, S.; Menard, E.; Park, J.-U.; Maria, J.; Meitl, M.; Zaumseil, J.; Rogers, J. A., Three-dimensional nanofabrication with rubber stamps and conformable photomasks. *Adv. Mater.* **2004**, 16, (15), 1369-1373.
- (235) Erbe, A.; Jiang, W.; Bao, Z.; Abusch-Magder, D.; Tennant, D. M.; Garfunkel, E.; Zhitenev, N., Nanoscale patterning in application to materials and device structures. *J. Vac. Sci. Technol., B* **2005**, 23, (6), 3132-3137.
- (236) Le Drogoff, B.; Cui, B.; Veres, T., Fast three-dimensional nanostructure fabrication by laser-assisted nanotransfer printing. *Appl. Phys. Lett.* **2006**, 89, (11), 1-3.
- (237) Rojas, M. T.; Koeniger, R.; Stoddart, J. F.; Kaifer, A. E., Supported Monolayers Containing Preformed Binding Sites. Synthesis and Interfacial Binding Properties of a Thiolated β -Cyclodextrin Derivative. *J. Am. Chem. Soc.* **1995**, 117, (1), 336-43.
- (238) Henschel, W.; Georgiev, Y. M.; Kurz, H., Study of a high contrast process for hydrogen silsesquioxane as a negative tone electron beam resist. *J. Vac. Sci. Technol., B* **2003**, 21, (5), 2018-2025.
- (239) Yang, C.-C.; Chen, W.-C., The structures and properties of hydrogen silsesquioxane (HSQ) films produced by thermal curing. *J. Mater. Chem.* **2002**, 12, (4), 1138-1141.
- (240) Van Delft, F. C. M. J. M.; Weterings, J. P.; van Langen-Suurling, A. K.; Romijn, H., Hydrogen silsesquioxane/novolak bilayer resist for high aspect ratio nanoscale electron-beam lithography. *J. Vac. Sci. Technol., B* **2000**, 18, (6), 3419-3423.
- (241) Word, M. J.; Adesida, I.; Berger, P. R., Nanometer-period gratings in hydrogen silsesquioxane fabricated by electron beam lithography. *J. Vac. Sci. Technol., B* **2003**, 21, (6), L12-L15.

- (242) Lavrik, N. V.; Tipple, C. A.; Sepaniak, M. J.; Datskos, P. G., Enhanced chemi-mechanical transduction at nanostructured interfaces. *Chem. Phys. Lett.* **2001**, 336, (5,6), 371-376.
- (243) Culha, M.; Lavrik, N. V.; Schell, F. M.; Tipple, C. A.; Sepaniak, M. J., Characterization of volatile, hydrophobic cyclodextrin derivatives as thin films for sensor applications. *Sens. Actuators, B* **2003**, B92, (1-2), 171-180.
- (244) Dutta, P.; Senesac, L. R.; Lavrik, N. V.; Datskos, P. G.; Sepaniak, M. J., Response signatures for nanostructured, optically-probed, functionalized microcantilever sensing arrays. *Sens. Lett.* **2004**, 2, (3, 4), 238-245.
- (245) Menard, E.; Rogers, J. A. *Stamping Techniques for Micro- and Nanofabrication*. Springer Handb. Nanotechnol. (2nd Ed.) 2007, 279-297.
- (246) Lee, B. H.; Cho, Y. H.; Lee, H.; Lee, K.-D.; Kim, S. H.; Sung, M. M. High-Resolution Patterning of Aluminum Thin Films with A Water-Mediated Transfer Process. *Adv. Mater.* 2007, 19, (13), 1714-1718.
- (247) Dieringer, J. A.; McFarland, A. D.; Shah, N. C.; Stuart, D. A.; Whitney, A. V.; Yonzon, C. R.; Young, M. A.; Zhang, X.; Van Duyne, R. P. Surface Enhanced Raman Spectroscopy: New Materials, Concepts, Characterization Tools, and Applications. *Faraday Discuss.* **2006**, 132, 9-26.
- (248) Bizzarri, A. R.; Cannistraro, S. Temporal Fluctuations in Single-Molecule SERS Spectra. *Topics in Appl. Phys.* **2006**, 103, 279-296.
- (249) Chen, K.; Vo-Dinh, T. Single-Molecule Detection Techniques for Monitoring Cellular Activity at the Nanoscale Level. *Nanotechnol. Bio. Med.* **2007**, 16/1-16/24.
- (250) Habuchi, S.; Hofkens, J. Single-Molecule Surface-Enhanced Resonance Raman Spectroscopy of the Enhanced Green Fluorescent Protein EGFP. *Topics Appl. Phys.* **2006**, 103, 297-312.
- (251) Kneipp, H.; Kneipp, K. Surface-Enhanced Hyper Raman Scattering in Silver Colloidal Solutions. *J. Raman Spectrosc.* **2005**, 36, (6/7), 551-554.
- (252) Kneipp, K.; Kneipp, H.; Bohr, H. G. Single-Molecule SERS Spectroscopy. *Topics Appl. Phys.* 2006, 103, 261-278.
- (253) Moskovits, M.; Tay, L.-L.; Yang, J.; Haslett, T. SERS and the Single Molecule. *Topics Appl. Phys.* **2002**, 82, 215-226.
- (254) Moskovits, M. Surface-Enhanced Raman Spectroscopy. A Brief Perspective. *Topics Appl. Phys.* **2006**, 103, 1-18.
- (255) Musick, M. D.; Keating, C. D.; Lyon, L. A.; Botsko, S. L.; Pena, D. J.; Holliday, W. D.; McEvoy, T. M.; Richardson, J. N.; Natan, M. J. Metal Films Prepared By Stepwise Assembly. 2. Construction and Characterization of Colloidal Au and Ag Multilayers. *Chem. Mater.* **2000**, 12, (10), 2869-2881.
- (256) Park, S.-H.; Im, J.-H.; Im, J.-W.; Chun, B.-H.; Kim, J.-H. Adsorption Kinetics of Au and Ag Nanoparticles on Functionalized Glass Surfaces. *Microchemical J.* **1999**, 63,(1), 71-91.

- (257) Lacy, W. B.; Olson, L. G.; Harris, J. M. Quantitative SERS Measurements on Dielectric-Overcoated Silver-Island Films by Solution-Deposition Control of Surface Concentrations. *Anal. Chem.* **1999**, 71, (13), 2564-2570.
- (258) Mulvaney, S. P.; He, L.; Natan, M. J.; Keating, C. D. Three-Layer Substrates for Surface-Enhanced Raman Scattering: Preparation and Preliminary Evaluation. *J. Raman Spectrosc.* **2003**, 34, (2), 163-171.
- (259) Li, J.; Fang, Y. An Investigation Of The Surface Enhanced Raman Scattering (SERS) From A New Substrate of Silver-Modified Silver Electrode by Magnetron Sputtering. *Spectrochim. Acta, Part A* **2007**, 66A, (4-5), 994-1000.
- (260) Murgida, D.; Hildebrandt, P. Surface-Enhanced Vibrational Spectroelectrochemistry: Electric Field Effects on Redox and Redox-Coupled Processes of Heme Proteins. *Topics Appl. Phys.* **2006**, 103, 313-334.
- (261) Pristiniski, D.; Tan, S.; Erol, M.; Du, H.; Sukhishvili, S. In Situ SERS Study of Rhodamine 6G Adsorbed on Individually Immobilized Ag Nanoparticles. *J. Raman Spectrosc.* **2006**, 37, (7), 762-770.
- (262) Qian, X. M.; Ansari, D.; Nie, S. A New Class of Nontoxic Nanoparticle Tags Based on Surface Enhanced Raman Scattering. *Proc. SPIE-Int. Soc. Opt. Eng.* **2007**, 6448, 1-12.
- (263) Yang, Y.; Xiong, L.; Shi, J.; Nogami, M. Aligned Silver Nanorod Arrays for Surface-Enhanced Raman Scattering. *Nanotechnology* **2006**, 17, (10), 2670-2674.
- (264) White, D. J.; Mazzolini, A. P.; Stoddart, P. R. Fabrication of A Range of SERS Substrates on Nanostructured Multicore Optical Fibres. *J. Raman Spectrosc.* **2007**, 38, (4), 377-382.
- (265) Lu, L.; Kobayashi, A.; Tawa, K.; Ozaki, Y. Silver Nanoplates with Special Shapes: Controlled Synthesis and Their Surface Plasmon Resonance and Surface-Enhanced Raman Scattering Properties. *Chem. Mater.* **2006**, 18, (20), 4894-4901.
- (266) Haynes, C. L.; McFarland, A. D.; Zhao, L.; Van Duyne, R. P.; Schatz, G. C.; Gunnarsson, L.; Prikulis, J.; Kasemo, B.; Kaell, M. Nanoparticle Optics: The Importance of Radiative Dipole Coupling in Two-Dimensional Nanoparticle Arrays. *J. Phys. Chem. B* **2003**, 107, (30), 7337-7342.
- (267) De Jesus, M. A.; Giesfeldt, K. S.; Oran, J. M.; Abu-Hatab, N. A.; Lavrik, N. V.; Sepaniak, M. J. Nanofabrication of Densely Packed Metal-Polymer Arrays for Surface-Enhanced Raman Spectrometry. *Appl. Spectrosc.* **2005**, 59, (12), 1501-1508.
- (268) Moszner, N.; Salz, U.; Zimmermann, J. Chemical Aspects of Self-Etching Enamel-Dentin Adhesives: A Systematic Review. *Dental Mater.* 2005, 21, (10), 895-910.
- (269) Whitaker, G.; Kincaid, B. J.; Raftery, D. P.; Van Hoof, N.; Regan, F.; Smyth, M. R.; Leonard, R. G. Potential of CE for the Determination of

- Inorganic and Acidic Anions in Cyanoacrylate Adhesives. *Electrophoresis* **2006**, 27, (22), 4532-4537.
- (270) Culha, M.; Schell, F. M.; Fox, S.; Green, T.; Betts, T.; Sepaniak, M. J. Evaluation of Newly Synthesized and Commercially Available Charged Cyclomaltooligosaccharides (Cyclodextrins) for Capillary Electrokinetic Chromatography. *Carbohydr. Res.* **2004**, 339, (2), 241-249.
- (271) Wang, H.; Levin, C. J.; Halas, N. J. Nanosphere Arrays With Controlled Sub-10-Nm Gaps as Surface-Enhanced Raman Spectroscopy Substrates. *J. Am. Chem. Soc.* **2005**, 127, (43), 14992-14993.
- (272) Jaziri, M.; Kallel, T. K.; Mbarek, S.; Elleuch, B. Morphology Development in Polyethylene/Polystyrene Blends: The Influence of Processing Conditions and Interfacial Modification. *Polym. Int.* 2005, 54, 1384-1391.
- (273) De Groot, H. Recent Developments of KRATON G Polymers for TPE-S Compounds. *TPE 2003, Int. Conf. New Oppor. Thermoplast. Elastomers*, 6th **2003**, 157-169.
- (274) Sackmann, M.; Materny, A., Surface enhanced Raman scattering (SERS) - a quantitative analytical tool? *J. Raman Spectrosc.* **2006**, 37, (1-3), 305-310.

VITA

Nahla Abu Hatab was born in Kuwait to parents who immigrated from Palestine in 1965. She lived in Kuwait, where she finished high school. She immigrated to Canada in 1994. She came to New Jersey in 1997 and entered Excess county college. She moved to Knoxville, Tennessee in August 2000 where she entered the University of Tennessee and she was awarded a Bachelor of Science in Chemistry 2002. She entered the doctoral program in chemistry at the University of Tennessee, Knoxville in December 2002. She officially received her doctoral degree in analytical chemistry in May, 2008.